ISRS

Signatures

Newsletter of the Indian Society of Remote Sensing –Ahmedabad Chapter

Volume: 22, No.4 November-December 2010

Special Issue on

Microwave Remote Sensing Applications

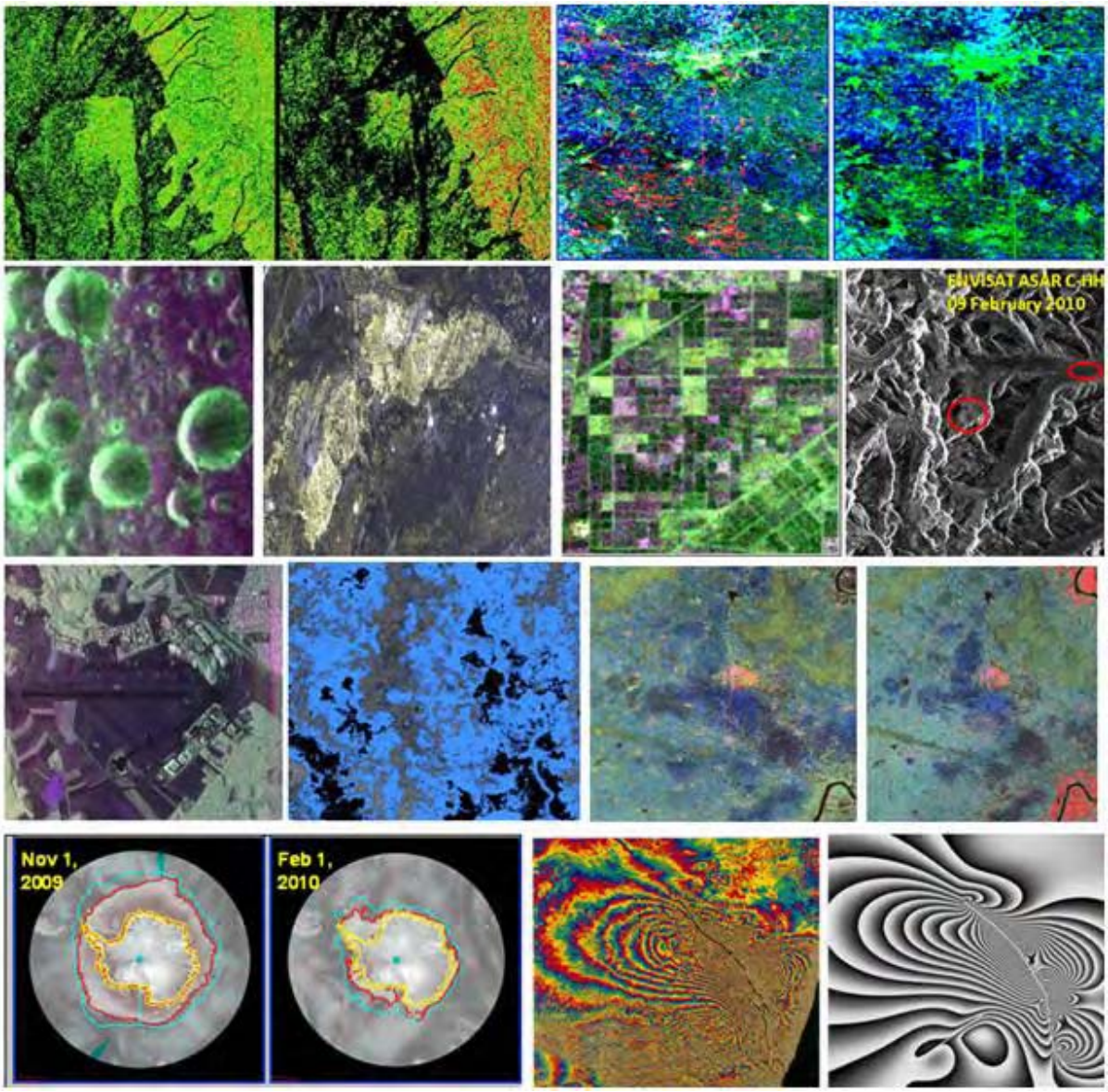

Polarimetric Radar vegetation index: C-band Radarsat-2 Data Dec 2008, L-band ALOS PALSAR Data Apr 2009; Polarimetric Decompositions of ALOS-PALSAR Data Linear Full – POL, RC – Hybrid, RGB: Double-Bounce, Volume, Surface; Chandrayaan-1 MiniSAR Image covering part of Lunar north pole; ALOS- PALSAR: L-band, FCC: HV HH HV for detection of subsurface features: Limestone; ALOS PALSAR, HH,HV and VV Classification for discrimination of vegetation types; ENVISAT ASAR data over Samundra Tapu glacier in Chenab basin; L band DLR E-SAR image; Extent of flood derived from DMSAR over part of Bihar in 2007; Early detection of rice crop by Polarimetric SAR data (before & after sowing); Sea ice cover as observed from Oceansat-2 OSCAT scatterometer data; Co-seismic deformation of Landers earthquake (left) with modeled interferogram from fault geometry (right)

Inside this Issue

Regular Columns

1. From the Chairman's Desk 3
2. Member News 4
3. Readers' Views 4
4. Chapter News:
   - An Interview with *Prof. Wolfgang-Martin Boerner*, Univ. of Illinois 5
   - Glimpses of Educational Excursion to Udaipur 88
   - A Brief Report on 11th Prof. Pisharoty Memorial Lecture by Prof. A K Singhvi, PRL 89
   - Forthcoming Chapter Activities 20
5. ISRS Updates November-December 2010 8
6. Forthcoming RS related Conferences 20 & 68
7. Snippets on Naturally & Historically Remote Sensing 45 & 48
8. Signing Off 90

General Articles

1. Synthetic Aperture Radars developed in ISRO, *Tapan Misra* 9
2. Onboard Signal Processing for ISRO's SAR Sensors, *R K Sharma, B S Kumar & N M Desai* 16
3. SAR Signal Processing & Data Products, *Santanu Chowdhury* 21

Theme Articles

4. A Tutorial on the Application Potential of SAR for Characterising Land Targets, *Parul Patel* 25
5. Microwave Remote Sensing Applications for Terrestrial and Lunar Surface, *Shiv Mohan* 41
6. Rice Crop Monitoring in India Using SAR Data: Current Status & Future Prospects Using RISAT Data, *M. Chakraborty et. al.* 46
7. Conjunctive use of RADARSAT and ENVISAT Data for Biophysical Parameter Retrieval Research: A Case Study in Bardhaman district, West Bengal, *Indrani Choudhury & M.Chakraborty* 49
8. Microwave Remote Sensing of Nalsarovar – A Notified Wetland, Gujarat, *TVR Murthy & Sushma Panigrahy* 54
9. Interpretation of ALOS – PULSAR Wide Beam Data over a Part of Kachchh for Lithological Discrimination and Study of Tectonic Processes, *T. J. Majumdar, F. Bhattacharyya & K. M. Sreejith* 59
10. Potential of Microwave Remote Sensing for Snow and Glacier Studies, *Sushil Kumar Singh* 64
11. Microwave Remote Sensing for Land Subsidence Studies: Differential Interferometry Technique, *Shweta Sharma* 69
12. Applications of SAR Interferometry in Crustal Deformation Studies, *K. M. Sreejith & A. S. Rajawat* 78
13. Ocean Observations System for India Using Active Microwave Remote Sensing Techniques, *Raj Kumar & Abhisek Chakraborty* 80
14. Active and Passive Microwave Remote Sensing of Polar Ice, *Sandip R Oza et. al.* 85

ISRS-AC Office Bearers

Shri D.R.M. Samudraiah,
Chairman
Prof. Anupam K. Singh,
Vice-Chairman
Smt. Parul Patel,
Secretary
Dr. Indrani C. Singh,
Jt. Secretary
Shri K.P. Bharucha,
Treasurer

ISRS-AC EC Members

Shri Kashyap N. Mankad
Smt. Arundhati Misra
Dr. Abha Chhabra
Dr. Rahul Nigam
Shri R.P. Prajapati

ISRS-AC Office

Room No. 4372,
Space Applications Centre (SAC),
ISRO, Ahmedabad-380015.
Email: **parul@sac.isro.gov.in**
Phone: +91 79 2691 4372

ISRS Headquarters

C/o Indian Institute of Remote Sensing, 4, Kalidas Road, Dehradun - 248 001, India.
Email: isrs@iirs.gov.in,
Fax: +91 135 2741 987
Web: www.isrsindia.org

From the Chairman's Desk

Dear Members,

I have great pleasure in reaching out to you all, the members and well-wishers of Indian Society of Remote Sensing – Ahmedabad Chapter once again through *Signatures*. I convey my greetings and best wishes to all of you. The previous issue of *Signatures* was well received by our members. In the intervening period since the last issue was released, we had two activities conducted by the Chapter some jointly with the local chapters of other professional Societies having a common interest in the geospatial sciences as well as by itself organizing the eleventh Prof. Pisharoty memorial lecture, with very good participation from members.

This issue of *Signatures* focuses on the theme: *Microwave Remote Sensing Applications*. *Signatures* Editorial Team has compiled a number of interesting articles of topical interest on this theme. Several sensor designers, software engineers, and application scientists from Space Applications Centre and other agencies have contributed to this special issue through their brief and vivid articles on the focal theme. This issue also contains an Interview with Prof. Wolfgang-Martin Boerner from the University of Illinois, USA, an expert in the area of Microwave Remote Sensing, when he visited Ahmedabad, apart from the regular Columns. I thank all the authors and Prof. WM Boerner for their contributions to *Signatures*.

The potential of any branch of technology is indicated by the participation from industry. Remote Sensing has a very good contribution from industry in the areas like onboard sub-systems development, ground sub-systems support, algorithm & software development and application proliferation. ISRS-AC is planning the next issue of *Signatures* on the theme- "Industry Contributions to Remote Sensing Activities". I request all members to organise getting industry contributions for the same.

I take this opportunity to invite all of you to actively contribute to the objectives of ISRS by taking part in the Chapter events and contributing to *Signatures.*

Wishing you all the very best,

DRM Samudraiah

Theme for the forthcoming issue of Signatures:

Jan – Apr 2011: Industry Contributions to Remote Sensing Activities

Member News

Awards

Dr. S.K. Pathan, GD-UPDG receiving Natioanl Geospatial Award for Excellence – 2009 from Dr. R.R. Navalgund, President, ISRS on 1st December, 2010 at Lonavala.
(The award carried a i) Medal, ii) Citation and iii) Cash prize of Rs.50,000)

Superannuation

Mr. K.M. Bhavsar
EPSA, SAC

Readers' Views on Signatures, Vol.22, No 3, Aug-Oct 2010

Quote: The Signatures Aug-Oct 2010 issue on " Non-imaging remote sensors for earth observations" is found to be very informative. *Unquote.* **– Dr. Indrani Choudhury**

Quote: The ISRS Newsletter has really come well. It has very useful and extensive information on non-imaging sensors (all at one place). Thanks for the efforts of editorial team. Keep it up. *Unquote.* - **Sh. B Gopala Krishna**

Quote: Congratulations to all team of ISRS who have contributed to bringing out such a nice, informative and very useful Newsletter Signatures(Aug-Oct2010).*Unquote.* **– Sh Himanshu Pandya**

Quote: This is an excellent newsletter. I am seeing it after a long time. There is a lot of improvement. New topics and areas are welcome. I suggest to include a small section which shows the work done by industries in the field of Remote Sensing. *Unquote.* **– Sh. Surednra Singh Pokharna (**Next issue is dedicated to this topic. – Eds)

Quote: I have read many articles with interest. Once again the Editorial Team deserves appreciation for their efforts to bring out a massive theme based special issue incorporating information packed articles displaying a wide variety of applications. And as I had mentioned earlier, the Newsletter has really taken a great professional look. Congrats to one and all for the elaborate effort. *Unquote.* **– Dr. Satyendra M. Bhandari**

An Interview with Prof. Wolfgang-Martin Boerner, University of Illinois, USA

Signatures: *Professor Boerner, ISRS-AC is very fortunate to have an interview session with a renowned professor like yourself. You have a wide range of research interests covering almost the entire spectrum of electromagnetic field theory and wave propagation and particularly in microwave imaging and remote sensing. How do you forecast the future of RS and its utility to mankind?*

WMB: I have a strong belief that entire microwave band of EM spectrum is also essential for monitoring the health of our earth. Optical Remote Sensing helps in understanding the surface properties of the objects, but to understand the internal/ inner features microwave sensing is essential because of their penetration ability through precipitation and vegetation covers, and so on. More so, active microwave radar and SAR remote sensing can be implemented at day and night and during severe weather patterns which will be increasing ever more.

Signatures: *What, in your opinion, are the current limiting factors in the application of microwave RS to human development? Is it the technology to build sensors and operate them onboard orbiting satellites; or the human interpretation capabilities or the capabilities of the processing and analysis software aids? Could you give your expert views?*

WMB: At present, the antenna for microwave RS is very complex involving wave guiding structures. With the future nanotechnological researches and electro-optical circuitry it can be overcome. There should also be highly improved regulations on availability of the necessary frequency bands to avoid interference with other sources and communication sensors. The Microwave guiding structure-plumbing is very complex and requires diligent fine-tuned calibration which is one of the critical issues. Proper and efficient algorithms have to be developed for utilization of data obtained from microwave sensors. Coding of the full polarimetric data has to be done to exploit the best usage. In case of SAR, mathematical processing, algorithm development and innovations are required in the application area to keep with the pace of sensor development.

Signatures: *With regard to microwave RS, what according to you are the current issues in its utility? What is the future of Microwave RS in your opinion?*

WMB: Microwave RS is very essential for the overall understanding of the target / systems. In the last 10 years, ERIM, JPL, German Aerospace, NOAA-NASA & JAXA-NICT have understood the inevitable need for it and had carried out many researches and advancements in this field. The Microwave holographic system for the understanding of degree of polarization, the techniques for attaining the fully polarimetric high resolution image data sets, although with narrow swath gave deep insight in understanding of the scattering mechanisms of isolated and complex distributed scatterer ensembles. Further, with the advances in the field of nanotechnology will help in miniaturization of the sensors. For example, future hybrid-electronic cars will have SAR crash-avoidance sensors. It can be made possible only if we all scientists working in this field unite and work together.

Signatures: *You have worked in the field of inverse scattering. Could you tell us how inverse scattering is used for scientific applications?*

WMB: The increasing demand of imaging and target identification require new powerful and flexible image interpretation techniques. The inverse scattering approaches are used to determine the characteristics of the object (its shape and internal constitution) from the measurement data of radiation scattered from it by applying inverse scattering algorithms. Because the EM field is vector in nature, complete polarization combinations are required to get full understanding of the features.

Signatures: *What are the possible uses of polarimetric data in disaster management, protection of flora and fauna etc.?*

WMB: The polarimetric data obtained from POLinSAR sensors is very useful for understanding environmental hazards such as earthquakes, volcano eruptions, cyclonic severe storm approaches and so on. At low frequencies for the detection of electromagnetic precursor signatures generated by tectonic stress accumulation, fully polarimetric tri-axes magnetic fluxgate sensors aid to get seismology. The infrasonic sensors are required to get the early warning of severe weather vortex motion such as encountered by tornados etc. The polarimetric data is useful in the classification of landforms, surface vegetation cover, and for the detection of irregular growth patterns caused by severe storms or also by plant diseases. The wetland and arid land polarimetric SAR assessment can be helpful in identification of the flora and fauna that can flourish or are placed under severe environmental stress. Environmental stress-change monitoring helps in the estimation of the depletion of the forests and wildlife so for example approximately 2.7% of birds' species are lost every year in Keoladeo bird sanctuary.

Signatures: *Professor Boerner, you have had a long innings in the field of RS. What is your considered assessment of Indian microwave RS program?*

WMB: India during the past ten years is advancing rapidly across all spheres of human and technological activities; and it is also progressing a lot in the field of RS. I personally know many Indians who are exceptionally good in understanding of theories and principles of RS for both the optical and the microwave spectral domains. By exposing good Indian acumen to other countries, Indian RS programs can be benefited especially for microwave radiometric and radar sensor technology. I emphasize on the SAR system which is developed by India in that it is really commendable. Fully polarimetric sensor data sets are very much required by the global community and India is very close to providing such as well. I would rather suggest that "by catching the young minds right from schools and groom them" will be the best thing Indians must learn from Europeans to accomplish their future RS related tasks successfully. We require good knowledge in mathematical modeling, theoretical physics and geophysics, electronics and computer signal/image processing, and applying the principles to diverse fields.

Signatures: *Your current interests include emerging topics such as optical polarimetry. What are the current research trends in this domain and what potential does optical polarimetry hold for the future?*

WMB: Optical polarimetry has great future. Polaroid and especially fully polarimetric digital cameras are mainly used for military applications. It is very useful in detection of targets. Fully polarimetric lidar sensors can be used for detection of meteors, space debris. A fully polarimetric scattering matrix approach has recently been developed for understanding the object also for the optical scattering fields. However, the future use of optical sensors will become ever more limited due to atmospheric to mesospheric pollution created by a steep increase of aerosols, haze, fogginess and cloud cover.

Signatures: *How do you foresee the future of RS using so far unused spectral regions such as Tera Hertz frequencies?*

WMB: Terra hertz frequencies can be used in the field of remote sensing for rapid detection of aerosols. Water vapor in the atmosphere also shows several sharp absorptions in Tera Hertz frequency range. So, in order to identify water vapor resonance and humidity profiling Tera Hertz frequency sensors has great use in field of RS. More participation is needed from all the countries in this regard although India at ISRO-VASSC/SPL at Trivandrum already has attained a remarkable lead position.

Signatures: *We understand that your interests include geo-electromagnetism. Is there any relation or interaction between geo-electromagnetism and the solar radiation on Earth? Are there any RS techniques available to study the aspects of geo-electromagnetism?*

WMB: The level of ionizing radiations that are received from sun is proportional to the solar flux.

The solar perturbances affect the geo electromagnetic environment especially at the Polar Regions. To study the aspects of geo electromagnetism, low frequency measurements are made by measuring the energy of the potentials for the current across the earth. These low frequency measurements are still made at every 10 seconds interval but to get the true picture it has to be done at millisecond interval. Many ground geo-magnetic flux sensor systems in Canada, Japan, Taiwan and in Russia are used for monitoring geo electromagnetism, and it is essential for India to catch up and also build well designed network of these essential sensors for predicting tectonic stress-changes.

Signatures: *We are told that you are a lover of nature and are interested in studying polarimetry in nature. Could you share your thoughts about this particular interest?*

WMB: There are many phenomena in the nature from which one can learn scientific principles of polarization. The eyes of insects / bees as well as fish have certain sensors which use polarization information for navigation. It helps the bee to get the pollens and honey. They move in elliptical fashion in front of their bee-hives. Their slow movement is the indication of nearness of pollen. Birds chirp to get the polarimetric signatures, which help them to unite their family members. The animals are also sensitive to geomagnetic field and they perform natural RS. I would like to praise the Hindu culture and vedas for laying great emphasis on nature, and thus have contributed greatly to the protection of biodiversity on a large scale.

Signatures: *Professor Boerner, We thank you very much for sparing your time for ISRS-AC. Would you like to say anything else for our readers?*

WMB: I expect more participation from India in the field of microwave RS. Various workshops and seminars should be taken up to bridge the gap in this essential field of research. For example, the POLINSAR Workshop series developed by ESA/ESRIN not only for Europe and Canada as well as China, should immediately be extended to India with ISRS and ISRO serving as the Indian Lead-institutions. RS experts dealing not only with optical but much more so with microwave remote sensing should come forward for the environmental protection and become a part or member in the government ministry for environment. We all have to unite for the common cause to carry out advances in field of remote sensing. I wish more technical papers from India in the coming years to be submitted to the GRSS Transactions. In fact I would like to propose very close collaboration and alignment of the well established ISRS across India with the IEEE-GRSS, the world leading society for advancing especially microwave remote sensing required as tool for day and night all weather implementation.

It will be my special desire to advance close collaboration of ISRS with IEEE-GRSS commencing in the near future.

ISRS Updates November-December 2010

ISRS Symposium, 2010

- Annual convention of ISRS & National Symposium on "GIS and Remote Sensing in Infrastructure Development" was organised in Lonavala during December 1-3, 2010.
- There was one pre-symposium tutorial on 'Soft Classification Techniques' organised at Pune during November 29-30, 2010
- During the symposium there were 16 technical sessions, one theme session on "Infrastructure Development" and two special sessions on "India and ISPRS" and "Hyperspectral Remote Sensing".
- The Vikram Sarabhai Memorial Lecture was delivered by Padmashree Pramod Kale.
- The unique feature of this symposium was large participation of students, including those sponsored by ISRS.

ISRS Symposium, 2011

- ISRS Annual Convention and National Symposium, 2011 will be conducted during November 9-11, 2011 at Bhopal on the theme "Empowering Rural India through Space Technology".

ISRS Symposium, 2012

- ISRS Annual Convention and National Symposium, 2012 will be held in Delhi.

Book Published by ISRS

- Indian Society of Remote Sensing has published a book on "Hyperspectral Data, Analysis Techniques and Applications", edited by R. R. Navalgund and S. S. Ray. The 156 page book contains 8 articles by experts from India and abroad, along with a glossary of terms. The price of the book is Rs. 495/- (Hardbound). Interested members may contact Secretary, ISRS for procuring a copy of the book.

Monographs by ISRS

- Indian Society of Remote Sensing plans to publish high quality monographs. The monographs should be ideally within 100 pages, with a lot of colour illustrations, written (preferably) by a single author dealing with current research trends in any aspect of Remote Sensing and GIS: science and applications. The interested members can submit their proposals to the Joint Secretary, ISRS.

Call for Articles

Readers are requested to contribute short articles for publication in the forthcoming issues in their own words, preferably as per the editorial calendar given on page-3, either as a brief survey of state of the art or as articles on specific work carried out by them, or as novel concepts related to the specific theme(s). The deadline for inclusion in the next issue on **"Industry Contributions to Remote Sensing Activities"** is April 20, 2011.

- Editorial Team

Synthetic Aperture Radars Developed in ISRO

Tapan Misra, SAC, Ahmedabad, Email: misratapan@sac.isro.gov.in

1. Introduction: Synthetic Aperture Radars have unique imaging capabilities to exploit various terrain characteristics, and their development has been central to the Microwave Remote Sensing (MRS) Programme of ISRO. Imaging sensors, which witnessed a beginning in airborne application, have, over the period, graduated to spaceborne platforms.

The beginning of MRS programme was made way back in the early part of 1980s, in concurrence with the Optical Remote Sensing programme. Though all weather and day-night operation capability of Microwave Remote Sensors was understood at that time, its fructification needed a longer incubation period precisely because of the requirement of development of an array of complex technologies and algorithms. Development of this programme called for a higher level of investment in terms of both financial and technological implications. As a result, the evolution of MRS programme resulted into development of various sophisticated key technologies required for this programme, and consequently, has delivered SAR systems successfully.

2. Airborne SAR Development: In the evolutionary phase of MRS Programme, development of SAR needed mastering of both sophisticated radar technology and complex SAR processing algorithm. Since spaceborne SAR was highly cost intensive, airborne version of SAR was embarked upon as a cost effective route to mastering the SAR technology and all its nuances. Over the period, both airborne and spaceborne versions of SAR technology development have taken vibrant shape in ISRO towards harnessing their utilization potential.

2.1 X-Band Side Looking Airborne Radar: Development of Side Looking Airborne Radar (SLAR) in X-band (Table-1) was basically used for the development of radar technology and it was in flying condition from 1985-1989. The view of the SLAR system and a typical scene imaged by this system is presented in Fig.-1. SLAR provided imaging over 2-5 km swath with 50 m-100 m resolution. Compared to today's technology, its capability was primitive; but it acted as a test bed to test various new technologies like the radar itself, data recording system and on-board Quick Look Display (QLD) system. Further, the experience gained by experimenting with this system, acted as a foundation for the subsequent development of the complex SAR technology.

Fig.-1: SLAR System Mounted in Dakota and a Sample of Imagery Obtained by SLAR

2.2 Airborne Synthetic Aperture Radar (ASAR): ASAR (Airborne SAR) was the first proud foray of ISRO in SAR development. The aim of this development was not only technology attainment but also the demonstration of application potential. Consequently this system was configured in C-band providing 6 m resolution over 25 km swath. Detailed specifications of the ASAR system is presented in Table-1. Though the breadboard model was tested in 1992, the aircraft was lost in an accident in 1994.

The development was continued in a new aircraft and the ASAR system was used for experimentation since 1997. For the first time, a modest narrow swath (2.5 km) Real Time Processor was demonstrated in this system.

The high point of this project was the development of a sophisticated SAR processor involving motion sensing and compensation. In fact, it had a novel two

track motion compensation processor which added to the robustness of the system. This algorithm was implemented on a parallel processing system consisting of 8 Xeon processors. A sample image generated by ASAR along with photograph of the system can be seen in Fig.-2.

ASAR has been used to demonstrate flood mapping and monitoring operation in 2003-2004 (Fig.-3). ASAR experience provided the impetus for development of an improved version of C-band airborne SAR, DMSAR (SAR for Disaster Management), exclusively for flood monitoring activity. ASAR experience has demonstrated quick reaction to flood related emergency as airborne SAR system is more effective than its spaceborne counterpart. Space SARs, with their fixed orbital configuration, cannot ensure quick reaction to flood situations.

Table-1:Summary Specifications of Airborne Imaging Radars Developed in ISRO

	SLAR	ASAR	DMSAR
Frequency	9.6 GHz (X-Band)	5.3 GHz (C-Band)	5.35 GHz (C-Band)
Polarisation	HH	VV/HH	VV/HH
Platform/ Altitude	Dakota (2-3 km)	Beechcraft (8 km)	Beechcraft (8 km)
Resolution/Swath	50-100 m/ 5 km	6-8 m/ 25 km	<2 m/6 km 3 m/ 25 km 5 m/50 km 10 m/70 km
PRF	850 Hz	425-525 Hz	452 Hz
Peak Power	25 kW	2 kW	8 kW
Antenna Length/ Pattern	2 m/ Cosine Weighted	1.3 m/ $Cosec^2$	1.3 m/ $Cosec^2$

Fig.-2 : ASAR System Mounted in Beechcraft and a Sample of Imagery Obtained by ASAR

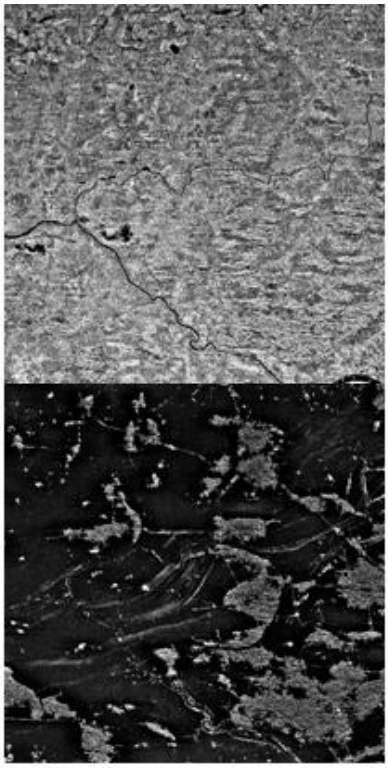

Fig.-3: Preflood and During Flood Image over Maligaon, Assam, Imaged by ASAR in 2004

2.3 DMSAR – Airborne SAR for Disaster Management: DMSAR was developed to aid flood monitoring and assessment of damage to infrastructure, for which four resolution modes were provided (Table-1). DMSAR was test flown for the first time in Nov. 2005. It was calibrated completely and its effectiveness in flood assessment was evaluated in 2006. Several flight campaigns have been carried out since then.

To support its high resolution and wide swath capability, the ASAR processing algorithm was significantly modified. A new algorithm called *Track Steering* algorithm was developed (patented) to process in high resolution modes. The DMSAR processor is now available on three platforms:

(a) A parallel machine with 32 Itanium processors
(b) In house developed Near Real Time Processor (NRTP). This is a portable system which can be carried in the Beechcraft itself and taken to base camp for processing and dissemination of DMSAR data.
(c) *GARUDA* computing grid provided by CDAC. Using this grid, DMSAR data can be processed simultaneously on an array of computing nodes available in academic and research institutions across India.

Fig.-4 shows the photograph of DMSAR in operation and also a sample of high resolution imagery obtained by it. Fig.-5 depicts a typical flood region, mapped by DMSAR, over Dharbhanga, Bihar in 2007. Fig.-6 shows the devastating breach of Koshi river in Nepal in Sept. 2008 as captured by DMSAR. This breach resulted in change of Koshi river track and devastating flood of Bihar plains.

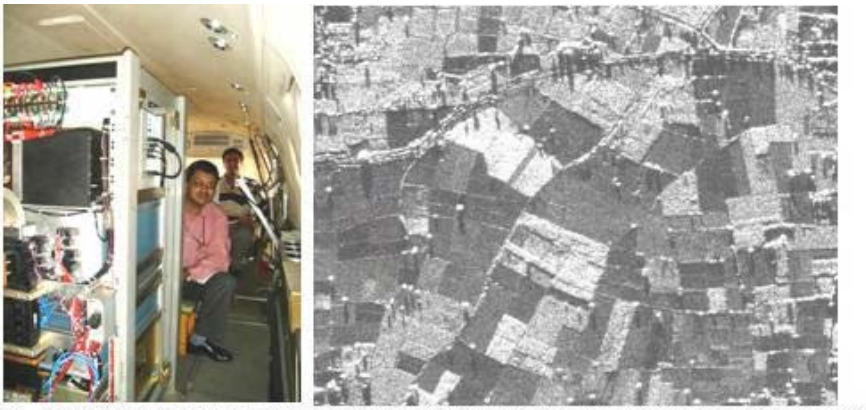

Fig.-4 : DMSAR System Mounted in Beechcraft and a Sample of High Resolution Imagery Obtained by DMSAR

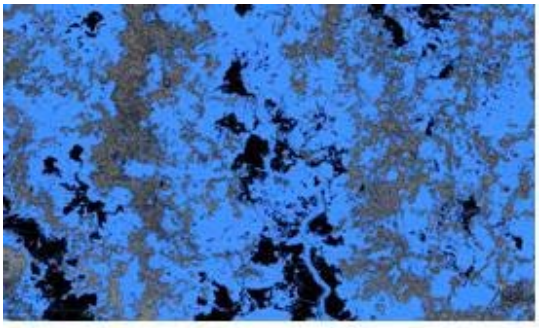

Fig.-5: Extent of Flood from Preflood Image Obtained On 23/06/07 And Flood Image Obtained On 03/08/07 over Dharbhanga, Bihar; Blue Colour: Flooded Region & Black Colour: Perennialy Water Logged Region

Fig.-6 Koshi River Breach Imaged by DMSAR in 2008

3. RISAT – Radar Imaging Satellite, ISRO's First SAR Satellite: Radar Imaging Satellite (RISAT) slated for launch in 2011 will carry C-band multi-mode SAR as the sole payload. RISAT-SAR payload, delivered to ISAC on 29 July, 2010, is a multimode SAR which will operate from a sun synchronous orbit at a nominal altitude of 536 km. The basic imaging modes, which have been identified for this payload, are as follows (Fig-7):

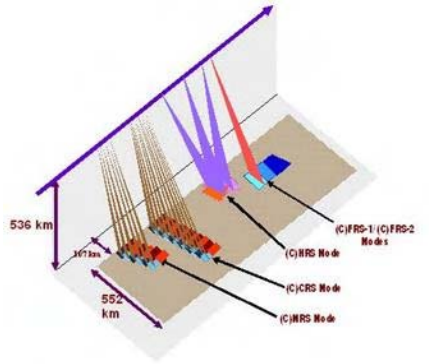

Fig-7 Imaging Modes of RISAT

- Coarse Resolution ScanSAR Mode (CRS): 50 m resolution, 223 km swath, co and/or cross polarisation.
- Medium Resolution ScanSAR Mode (MRS): 25 m resolution, 115 km swath, co and/or cross polarisation.
- Fine Resolution Stripmap Mode-1 (FRS-1): 3 m resolution, 25 km swath, co and/or cross polarisation
- Fine Resolution Stripmap Mode-2 (FRS-2): 9 m resolution, 25 km swath, Quad polarisation.

In CRS and MRS modes, systematic coverage of the globe will be completed in 13 and 26 days respectively. An experimental mode called High Resolution Spotlight Mode (HRS) has been added to provide a sliding spotlight image of 10 km x 10 km with better than 2 m resolution in co and/or cross polarization. Provision is also kept for an experimental capability to increase the azimuth extent up to 100 km in HRS mode.

On experimental basis, a new polarimetry option, called Circular (Hybrid) Polarimetry, is available for all the resolution and swath modes mentioned above. In this polarimetry option, in FRS-2 Mode, the resolution will improve to 3m in place of 9m. This polarimetric operation is a unique scheme, available for the first time in RISAT, and in this option, a circularly polarised signal is transmitted and received signal is captured in two orthogonal polarisations, namely H and V. Parameters of the various imaging modes are provided in Table-2. To indicate Hybrid polarimetry operation, the imaging modes are prefixed with C.

The SAR can image on either side of the track by roll tilting of the spacecraft. However, in one orbit, only one side of the orbit can be imaged.

Table 2: RISAT-1 SAR imaging parameters

Altitude		536 km				
Frequency		5.35 GHz				
Swath Coverage		Selectable within 107 – 659 km off-nadir distance on either side				
Incidence angle coverage	Total (107–659 km)	12.25deg – 55.02deg				
Imaging modes		(C)HRS	(C)FRS-1	(C)FRS-2	(C)MRS	(C)CRS
Swath/Spot (km)		10x10	25	25	115	223
Experimental		100x10				
Polarisation		Single/Dual (Co+Cross), Hybrid	Single/Dual (Co+Cross), Hybrid	Quad Hybrid	Single/Dual (Co+Cross) Hybrid	Single/Dual (Co+Cross), Hybrid
Slant Range Resolution		<2m	3m x 2m	9m x 4m & 3mx4m (Hybrid Polarimetry)	21-23m x 8m	41-55m x 8m
Worstcase minimum Sigma naught		-15.8 dB	-16.8 dB (107 – 659km off-nadir) <-18 dB (310 - 659km off-nadir)			
Azimuth ambiguity		< -21.47 dB				
Range ambiguity		<-23 dB (107-600km off-nadir), <-15.6 dB (for the rest)				

SAR system, on-board RISAT-1, is configured on a dual receiver concept, providing identical resolution and swath in both simultaneous operation in co- and cross-polarisation or Hybrid Polarimetry. The system is configured around a dual polarized active antenna with radiating elements. 6m x 2m antenna is configured in three identical panels of which the central one is fixed and rest two are deployable. Each of the panel consists of 4 tiles of size 1m x 1m each. Signal can be transmitted to either or both polarisations of the linear array. One can set the phase difference between the polarisations in transmit mode. Nominally the phase difference between H and V transmission is kept at 90 degree to aid circular polarisation transmission in Hybrid polarisation mode. During receive, the phase difference between the channels is kept at zero phase difference.

Both of the TR pair receive DC power from a miniaturised EPC called Power Control and Processing Unit (PCPU). Each such TR pair is controlled for synchronous operation by an ASIC based TR control computer (TRC). All the TR module pairs in a tile are managed by a Tile Control computer (TCU). TR modules, along with other Tile Electronics (like TRC, TCU, PCPU, RF power dividers, harness) are mounted on the back side of the antenna.

The complete payload management is done by Payload Controller. Typical parameters of the SAR payload are shown in Table-3.

The RISAT-1 spacecraft has been built around the SAR payload, in order to optimise the spacecraft weight and structure. RISAT satellite in fully deployed configuration is shown in Fig.-8. The prism shape of the satellite allows stowing of the active antenna in three folds around the prism structure. In-orbit mass of the satellite will be around 1850 kg, of which the SAR payload will contribute around 950 kg. The battery sizing is done such a way that it is possible to operate maximum of 10 minutes duration in each orbit. The satellite has a capability of storing up to 240 Gbits of data in on-board solid state recorder (SSR). The on-board data transmitter can transmit with a maximum data rate of 640 Mbits/sec in X-band, on two polarizations (RHC and LHC) on the same X-band carrier.

Table-3: RISAT-SAR Payload Parameters

Frequency	5.350 GHz			
Antenna Size	6m x 2m			
Pulse width	20 μsec/10 μsec (Hybrid Polarimetry)			
Average DC Input Power	3.8 kW max			
	HRS	FRS-1	FRS-2	MRS/CRS
PRF	3500 Hz	3000 Hz	3000 Hz	3000 Hz
Quantisation	2/3 BAQ	2/3/4/5/6 bit BAQ		
MAX. Data Rate	1478 Mbits/sec	1112 Mbits/sec	564 Mbits/sec	284 Mbits/sec

One of the important achievements of RISAT development has been establishment of a novel Near Field antenna measurement facility, installed in the integration laboratory itself. This facility is one of a kind. Sample of antenna patterns measured by this facility for a RISAT tile is shown in Fig.-9.

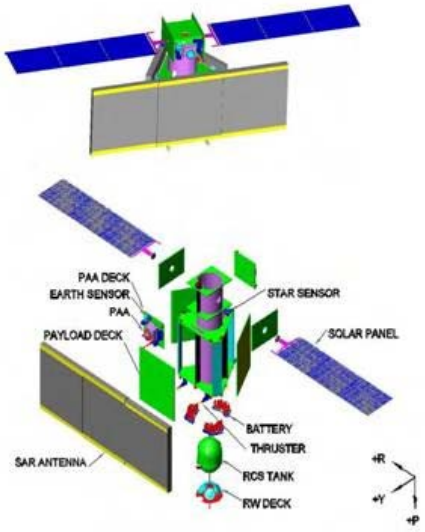

Fig.-8 Integrated and Exploded View of RISAT

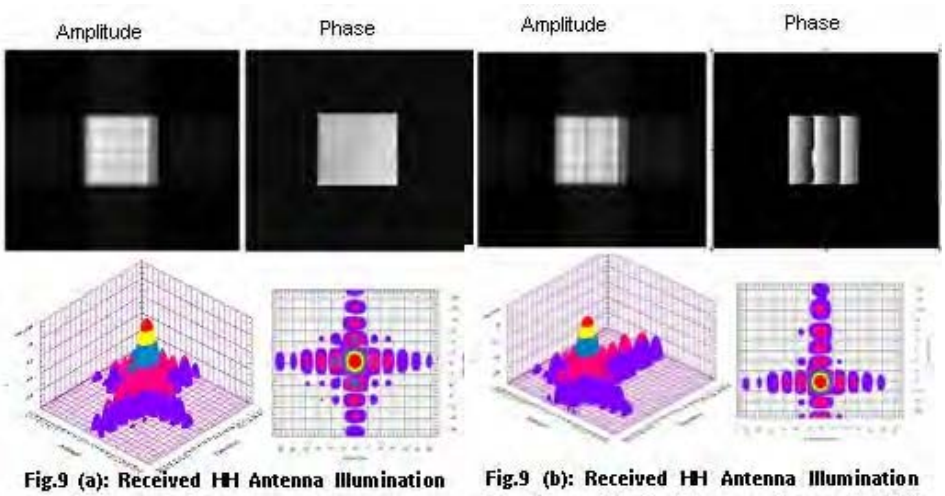

Fig.9 (a): Received HH Antenna Illumination Function and Derived Antenna Pattern for -0.5° Pointing

Fig.9 (b): Received HH Antenna Illumination Function and Derived Antenna Pattern for 9.5° Pointing

Apart from design and development of an active antenna based SAR system, the major achievement of RISAT project has been extensive industrial partnership in developing critical technological elements needed for payload. This involved not only capacity building for production of space qualified hardware in the industry but also extensive qualification of production processes and training. The TR module, along with all the MMICs associated with it, are designed and produced in India itself. Miniaturised pulsed EPC for powering TR module has been a feat of Indian industry. Printed antenna aperture has been designed in ISRO and produced by industry. The ASIC meant for controlling active array antenna elements, has been designed in-house. These achievements are shown in Fig.-10.

The design Verification Model of RISAT has been developed and it was tested fully over a period of one and half years in order to validate reliability of its software and hardware. Thereafter, FM development and integration of panels were carried out. Full-antenna testing has been carried out to successfully characterize the active antenna for all functionalities. RISAT is planned to be launched by 1st quarter of 2011. A glimpse of final FM payload is presented in Fig.-11.

4. L-Band SAR Satellite: L-band SAR is being planned as a successor of RISAT. This SAR will have ScanSAR modes matching with RISAT. It will have stripmap mode of resolution 5 m and swath of 60 m. The interesting addition will be electronically steered spotlight mode providing 2.5 m resolution over 40 km x 40 km spot. Compared to RISAT, it will have additional linear polarimetry mode apart from Hybrid polarimetry.

The satellite is being planned for launch by GSLV. L-band SAR pay load will also carry a demonstration model of Real Time Processor, for the first time, for processing the SAR raw data on the fly. The mechanical configuration of the proposed L-band SAR system is shown in Fig.-12.

5. Chandrayaan-II Dual Frequency SAR: In order to provide continuity of studies for presence of water-ice on lunar surface, Dual-frequency SAR instrument [L-band (1.25GHz) and S-band (2.25GHz)] has been planned as one of the sensors of Chandrayaan-II, scheduled for launch in 2013. It is configured for simultaneous as well as stand-alone operations. This Dual-frequency SAR has circular and full-polarimetric modes of operation. Full-polarimetric mode, an additional feature compared to that with Mini-SAR, is extremely useful to fully exploit the structural details of the lunar surface. The SAR is configured to cater for incidence angle range from 10° to 35° with resolutions from 3m – 80m with a swath of 10km (Fig-13).

Fig.-10 Array of Critical Technology Elements Developed Indigenously For RISAT Project

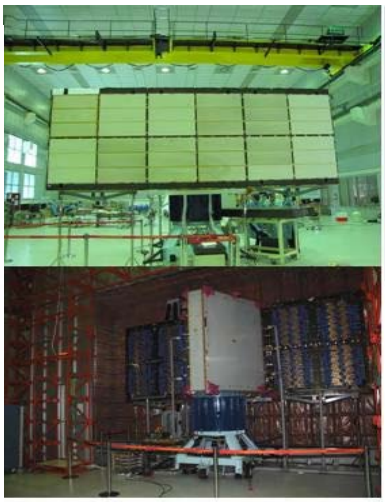

Fig.-11 RISAT Antenna in Deployed Condition Both In Clean Room And In Near Field Test Facility In Clean Room

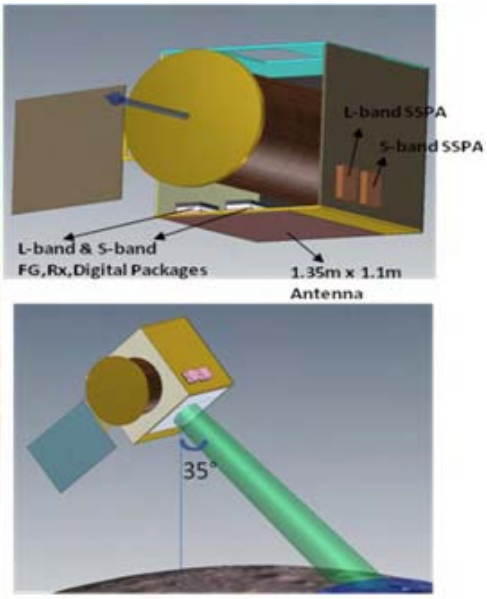

Fig.-13 Schematic of Chandrayaan-II Dual-frequency SAR and its imaging geometry

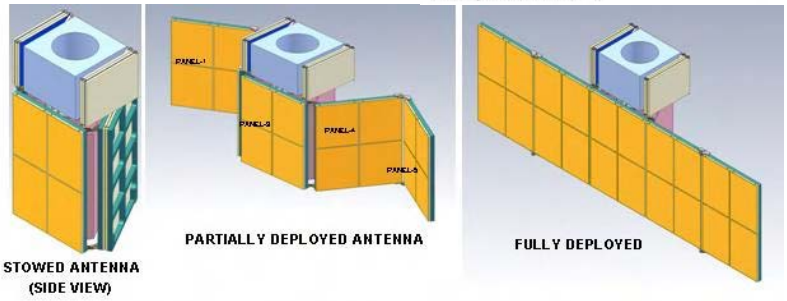

Fig.12: Mechanical configuration of L-band SAR with satellite structure

High degree of miniaturization is being adopted to realize the SAR within stringent mass constraint of 14kg. The L-band and S-band SAR systems share a common aperture of 1.35m x 1.1m planar microstrip antenna. This also doubles-up as a back-up antenna for Rover-communications (TTC) system.

Onboard Signal processor includes Digital Filtering, Range Compression, Azimuth Pre-Summing and Block Adaptive Quantization. These are required to reduce the data rate to manageable limits. Implementation of this processor in limited memory and power constraints is a challenging feature being taken up in this SAR development.

Conclusion: Last two decades have been invested in understanding the nuances of Microwave Remote Sensing technology both in terms of system development and algorithm. It is demonstrated in successful realisation from SLAR to RISAT. Grip over basic technology has been demonstrated in systems mentioned earlier. Knowing the requirement of large number of hardware technology required for achieving SAR systems, industrial partnership has been successfully forged, during the course of RISAT development, for indigenous sourcing of hardware elements. With the launch of RISAT, ISRO will be poised for undertaking many more missions with SAR sensors in future.

Onboard Signal Processing for ISRO's SAR Sensors

Ritesh Kumar Sharma, B Saravana Kumar & Nilesh M Desai, SAC, Ahmedabad, Email: nmdesai@sac.dos.gov.in

1. Introduction: Since mid-1970s, Indian Space Research Organisation's (ISRO) Microwave Remote Sensing Programme (MRSP) has been involved in the design and development of various ground based, airborne and spaceborne microwave sensors like Synthetic Aperture Radar (SAR), Scatterometer, Radiometer and Altimeter. SAR has an unique role to play in mapping and monitoring of large areas affected by natural disasters especially floods, owing to its unique capability to see through clouds as well as all-weather imaging capability. For many applications, the utility of SAR sensor is primarily governed by its capability to quickly generate radar images of the terrain under observation and mapping. This apart, on-board or on-ground real time digital signal processing has always been a major and essential requirement not only for SAR but even for other microwave sensors like Scatterometer, Radiometer and Altimeter, as it results in reduction of instrument data rates and turn-around time for fast delivery products. During 1990s, Space Applications Centre, Ahmedabad had developed and flown a C-band Airborne SAR (ASAR) onboard Beechcraft Superking B-200 aircraft. This ASAR has since been replaced with another C-Band airborne SAR for Disaster Management (DMSAR), with better and multi-mode imaging capabilities. DMSAR is being regularly utilized for estimating the extent of damage over large areas (~50-75 km) and for assessment of the effectiveness of relief measures undertaken during and after disasters like floods. Recently, SAC/ISRO has also completed the design and development of a multi-mode space-borne SAR for Radar Imaging Satellite-1 (RISAT-1) mission. These SAR related developments are being further augmented by follow-on SAR missions like L-Band Polarimetric LEO SAR, X-Band Agile small satellite SAR and L & S-Band Dual Frequency MoonSAR onboard Chandrayaan-2.

One of the major requirements of SAR missions is the generation and availability of SAR information or data products in real or near-real time with very fast turnaround times. Hence, in the last 15 years, reconfigurable Multi-Mode Quick look Real time Processor (QLP) and Near-Real Time hardware SAR Processor (NRTP) based on multi-DSP or FPGA configuration and meeting the requirements for various SAR mapping modes have been evolved and developed. The sections below trace the evolution of onboard and onground SAR processors for airborne and spaceborne SARs.

2. Real Time Signal Processor and Display System for C-band ASAR: During 1990s, an Airborne Synthetic Aperture Radar (ASAR) system, with 6-8 m range resolution and 20-25 km swath coverage, onboard Beechcraft Superking 200 aircraft was developed. Therein, Onboard Quick Look Real-Time SAR signal processing was employed for the first time in 1994-95. This Real Time Signal Processor and Display (RTPD) system was configured around fixed point Digital Signal Processor (DSP) based multi-processor architecture. It generated a true multi-look, selectable limited swath (2.5 km) ASAR image with 6m x 6m resolution or a full-swath (20 km) image with reduced resolution (48m x 48m). Subsequently, this RTPD unit was upgraded using custom designed DSP boards based on floating point DSP. The off-line ASAR processor was based on conventional Range Doppler algorithm along with the motion compensation and mosaicing to obtain the 25 x 25 km radar images. A four CPU Xeon workstation was used to generate offline ASAR images.

3. Quick Look and Near Real Time SAR processing for DMSAR: In 2005-6, ASAR has been replaced with another C-Band airborne SAR for Disaster Management (DMSAR), with imaging capabilities of 2-30 m resolutions, with swath coverage of 6-75 km. DMSAR is operational and is being regularly utilized for estimating the extent of damage over large areas (~50-75 km) and for assessment of the effectiveness of relief measures undertaken during and after disasters like floods. For DMSAR in order to optimize onboard recorder storage suitable data compression technique

along with variable rate formatting are also employed using reconfigurable FPGAs. A Quick Look SAR Processor (QLP) on-board aircraft produces real time full swath images. A similar but separate ground based Near-Real Time high precision full swath Processor (NRTP) has also been developed. QLP/NRTP is a CompactPCI based system consisting of COTS Multiprocessor DSP modules and associated peripheral boards. Two-dimensional SAR processor and motion compensation tasks are performed by DSP boards and the processed image data are displayed on the monitor screen as well as stored on a suitable recording media. A Single Board Computer (SBC) performs the overall control and co-ordination tasks for the various DSP processors and other interfaces.

4. Data Compression and SAR Processing for RISAT-1 SAR: RISAT-1 SAR operates in various operating modes viz. Stripmap, Sliding Spotlight and ScanSAR, depending on the resolution (2m/3m/25m/50m) and swath coverage (10 km/30 km/120 km/240 km) requirements. RISAT-1 SAR data is required to be compressed due to limited onboard storage and limited real time X-Band data transmission link bandwidth (640 Mbps). A dual-channel Single Board ultra-high speed Data Acquisition and Compression Subsystem (DACS) carries out data Compression along with variable rate formatting. BAQ data compression algorithm developed for SAR mission is a lossy data compression technique based on minimizing the mean squared error between the original and reconstructed SAR data.

Quick Look real or near-real time SAR processor is also being developed for all the proposed modes of RISAT -1 SAR operation. This NRTP will generate images with real time quick look as well as 100 minutes near-real time product turn-around times. It will also be initially utilized for a quick pre-launch and post-launch validation of RISAT-1 SAR. This full-fledged hardware SAR processor is based on Commercial-Off-The-Shelf (COTS) multiprocessor DSP boards yielding a sustained processing throughput of 10 GFLOPS. Same hardware is reconfigurable as QLP or NRTP. Figure-1 shows the various onboard and onground signal processors developed for ISRO's ASAR, DMSAR and RISAT-1 SAR missions.

5. SAR Processing Algorithm: The range and azimuth compressions are the major processing tasks involved in onboard SAR processing. In view of the large time and bandwidth involved for both the range and azimuth compression, it is computationally more efficient to implement the correlation process by Fast Convolution.

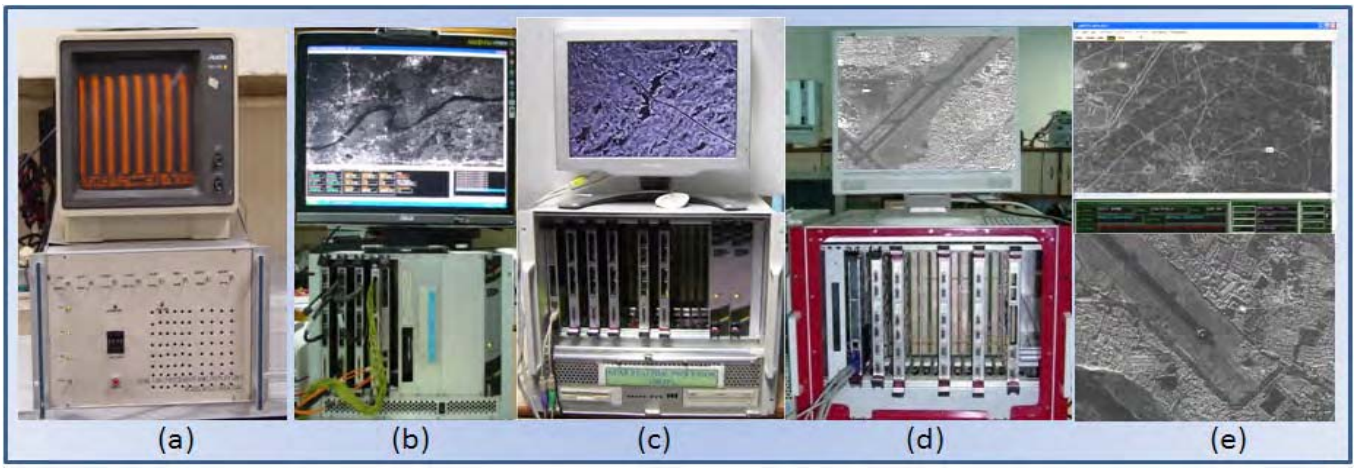

Fig-1: Photographs of (a) ASAR RTPD (b) DMSAR QLP unit (c) & (d) DMSAR NRTP-1 and NRTP-2 unit (e) DMSAR images generated using QLP/NRTP

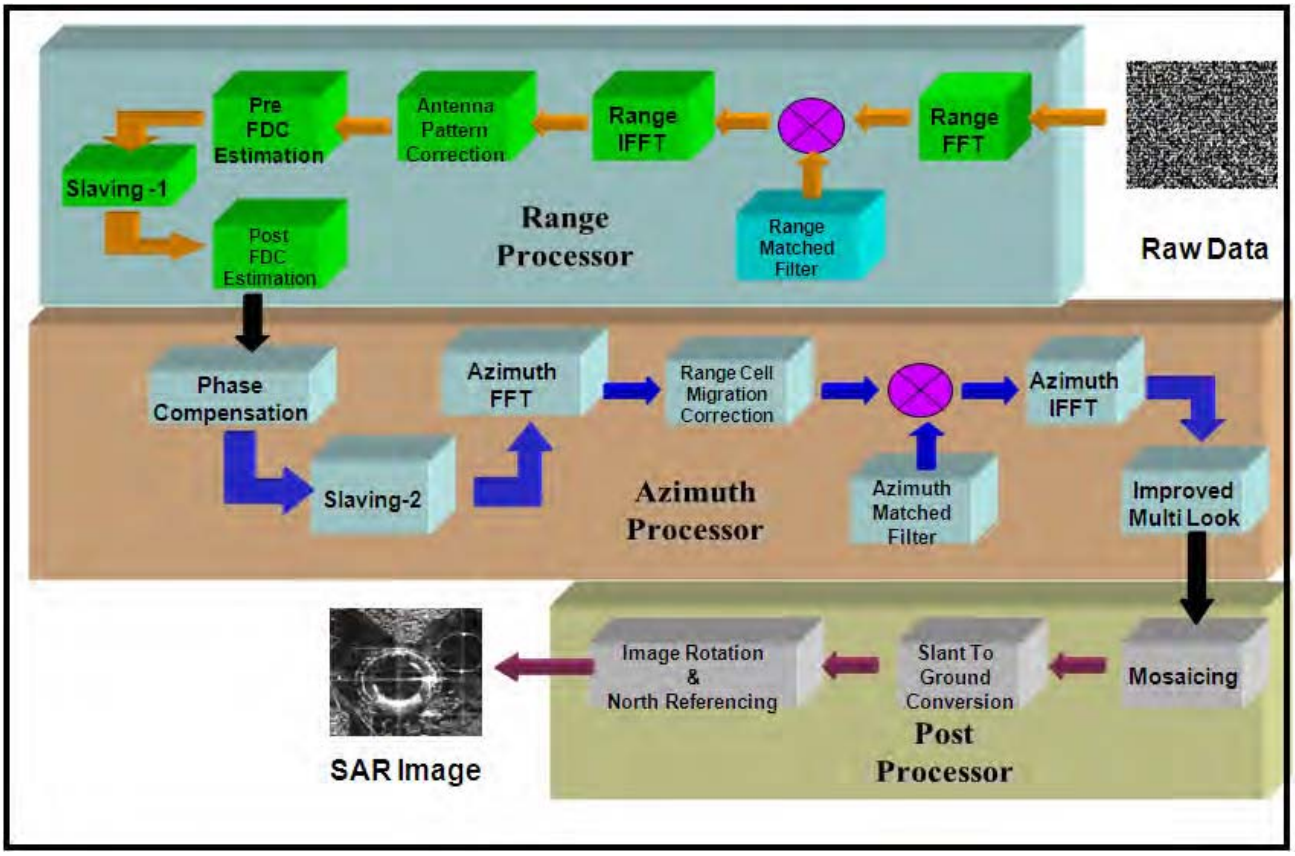

Fig- 2: Onboard SAR Processing Algorithm

The aircraft under goes random turbulences which introduces motion errors in the acquired SAR data. Hence, the processing algorithm has to compensate these motion errors in addition to standard SAR processing tasks. The complete DMSAR processing algorithm is shown in Figure-2.

Range compression of the signal is carried out by taking the FFT of the signal, complex multiplication with the range reference function followed by the Inverse FFT. Due to the variations in the antenna pattern the brightness of the SAR image varying as per the pattern. To achieve the uniform brightness throughout the image, the antenna pattern correction is required. Azimuth compression is also done in the frequency domain in order to use one array multiply to simultaneously compress a whole family of point targets, which have the same slant range of closet approach, but different azimuth locations. The data after range compression is transformed into the frequency domain (azimuth) by taking the FFT in azimuth direction. Azimuth compression algorithm is effective only if the point target trajectory lies parallel to an azimuth line. This can be achieved by performing Range Cell Migration Correction (RCMC) using the interpolation method.

In order to employ block-processing efficiency of FFT based SAR processors, it is necessary that the SAR raw data is sampled at equal spatial distance. But SAR data is sampled at equal time interval. As the along track velocity changes for fixed Pulse Repetition Frequency (PRF) operation, the spatial interval (V/PRF) changes, so it is necessary to slave PRF with along track velocity such that equal spatial interval is maintained. In order to satisfy this uniform sampling requirement for Azimuth FFT, V/PRF slaving of the data is performed, since the same is not done onboard. Additionally motion compensation tasks need to be performed for DMSAR. Motion sensing is performed on the IGIS velocity vectors (available in auxiliary data) to obtain a better estimate of the flight velocities. The phase compensation and window tuning tasks are performed to correct the phase errors that are introduced due to non-straight line flight track. The improved multi-look (IML) algorithm is required to

remove the speckle noise from the final image. Mosaicing involves appropriately positioning of the processed image blocks depending on the antenna pointing position and is calculated from the Doppler centroid. For onboard Quick Look DMSAR processor, only standard SAR processing steps like range and azimuth compression are performed. The ground based NRTP generates high precision SAR images by performing additional motion compensation tasks on the raw DMSAR data.

6. Data Compression and SAR processing for L-Band Polarimetric SAR: RISAT-1 follow-on mission will carry an L-band Polarimetric SAR operating in stripmap and ScanSAR modes and will mainly cater to applications related to agriculture and soil moisture analysis. For L-Band SAR, a single hardware module caters to both data acquisition and Block Adaptive Quantization (BAQ) compression of raw data and onboard transmit chirp requirements. A prototype version of this unit has been developed. A full-fledged onboard SAR processor is also being developed as a technology demonstrator. Each and every FPGA is connected in mesh configuration via a 64 bit high speed bus to faciliate interprocessor communication. Additionally LVDS serailizer and deserializer are provided for off-board I/O. Multiple such boards would be utilized to implement the full-fledged onboard SAR processor. The onboard SAR processor will be packaged on a ruggedized conduction cooled ATR chassis and would weigh about 10 kg and consume 250 watts power.

7. Onboard SAR Processing for Chandrayaan-2 Dual frequency MoonSAR: The ambitious L&S-band dual frequency SAR onboard ISRO's Chandrayaan-2 mission will operate in 200 km lunar orbit at a frequency of 1.25/2.5 GHz in different polarimetric modes with resolution capabilities of 2-20 metres. It would weigh ~17 kg and consume less than 200 Watts of power. Considering the different types of constraints imposed by lunar science satellite missions, wherein there is a high premium on weight, volume and space for sensor and its electronics miniaturization of various onboard subsystems for this SAR has been taken up. A miniaturized design configuration for the different onboard digital subsystems for this L/S-Band SAR while preserving the high resolution and high signal bandwidth has been worked out. The various constituent onboard modules of digital subsystem of SAR viz. digital chirp generator, dual channel data acquisition, range signal processor, data compression unit and payload controller have all been accommodated in a single board solution in this new design configuration. This single board configuration of digital subsystem will weigh about 1 kg and consume 6 watts power.

8. Conclusions: The onboard real time SAR signal processor is a technologically new and challenging element in SAR sensors. This paper gives an overview, design configuration and salient performance details of the different onboard and ground based SAR signal processing systems already built or being developed for ISRO's airborne and satellite missions involving microwave sensors viz. DMSAR, RISAT-1 SAR, L-band Polarimetric LEO SAR and Chandrayaan-2 MoonSAR. It is also envisaged that these developments would be significant first steps in the direction of configuring real time full swath configurable SAR processors for ISRO's future spaceborne SAR missions. This approach will enable direct generation of information products in real time.

Acknowledgements: The authors would like to thank Dr. R.R. Navalgund (Director, SAC), Shri A.S. Kiran Kumar (Assoc. Director, SAC), Shri S.S. Rana and Shri V.R. Gujraty (Ex-DDs, MRSA) and Shri Tapan Misra (DD/MRSA) for their guidance and encouragement to Microwave sensors and SAR Processor related developmental activities. The authors also wish to acknowledge the contributions of all their colleagues in MRSA, Scientist/Engineers and other staff members of SAC/ISRO and other ISRO centres, who are involved in the activities related to Microwave Remote Sensors.

References

[1] "FPGA based Reconfigurable DSPs for ISRO's Spaceborne Microwave Radars", 15th IEEE Intl. Conf. on High Performance Computing-1,HiPC Workshop on high performance

FPGA/reconfigurable computing, 17-20 Dec., 2008, Bangalore.

[2] "RISAT-1 Multi-Mode SAR Processing Using Advanced Computing Elements", IGARSS-2008, 6-11 July, 2008, Boston, MA, USA

[3] "Near Real Time SAR Processors for ISRO's Multimode RISAT-1 and DMSAR", 7th European Conf. on SAR, EUSAR-07, 2-5 June, 2008, Friedrichshafen, Germany.

[4] "Advanced DSP based High Performance Computing for ISRO's Synthetic Aperture Radars", 14th IEEE Conf. on High Performance Computing HiPC-2007, 18-21 Dec.,07, Goa.

[5] "Results from Quick Look & Near Real Time SAR Processors for Disaster Management Appl.", International Radar Symposium, IRSI-2007, 10-13 Dec., 2007, Bangalore.

[6] "Emergency Product Generation for Disaster management using RISAT and DMSAR Quick Look SAR Processors", 5th Asia-Pacific SPIE Intl. Remote Sensing Conf., 13-17 Nov 06, Panaji, Goa.

[7] "COTS Multiprocessor DSP Configuration for Real /Near Real Time SAR Processors", International Radar Symposium, IRSI-2005, 20-22 Dec., 2005, Bangalore.

[8] "Real time processor for airborne SAR for disaster management", International Radar Symposium, IRSI-2003, 3-5 Dec., 2003, Bangalore.

[9] "DSP based Real Time Processor Configurations for Microwave Sensors", 6th Intl. workshop on DSP, 23-25 Sept. 1998, ESTEC/ESA, The Netherlands

[10] "Preliminary Design Review Document for Disaster Management SAR (DMSAR)", SAC/ISRO Internal report, December-2004.

[11] "Preliminary Design Review Doc. for Quick Look/Near Real Time SAR Proc. for RISAT-1", SAC/ISRO Internal report, April- 2006.

[12] "Onboard Signal Processors for ISRO's Microwave Radars", IAC-09-B1.4.12, 60th IAC-2009, 12-16 Oct., 2009 at Daejeon, Republic of Korea.

[13] "Dual Frequency SAR for Chandrayaan-2-Baseline Design Review Document", SAC/MRSA/CHANDRAYAAN-2 SAR/BDR/01/2010, pp-125, September-2010.

Forthcoming RS related Conferences Outside India	
Sydney, Australia Apr 10-15, 2011	34th International Symposium on Remote Sensing of Environment , Visit: http://www.isrse34.org/
Munich, Germany Apr 11-13, 2011	Jurse 2011: IEEE GRSS and ISPRS Joint Urban Remote Sensing Event, Visit: http://www.jurse2011.tum.de
Antalya, Turkey May 03-08, 2011	Gi4DM: GeoInformation for Disaster Management, , Visit: http://www.gi4dm2011.org/
Forthcoming Chapter Activities	
Popular Lectures and Space Science Exhibition **Feb 05-06, 2011**	Popular Lectures on "Chandrayaan-1 mission" by Shri Jignesh Bhatt and "Remote sensing and its applications" by Shri Bhagirath M Mankad are planned to be delivered at Narmadanagar community science centre, Bharuch Science festival. Space science exhibition and video shows are also planned to be organized during the science festival.
PR Pisharoty Memorial Lecture **Feb 10, 2011**	PR Pisharoty Lecture on "Recent advances in optical and radio remote sensing of the Earth's atmosphere" by Prof. A Jayaraman, Director National Atmospheric Research Laboratory, Gadanki and Program Director, Space Science Office, ISRO HQ Program Director, Space Science Office, ISRO HQ, Bangalore.

SAR Signal Processing & Data Products

Santanu Chowdhury, SAC, Ahmedabad, Email: santanu@sac.isro.gov.in

1. Introduction: Synthetic Aperture Radar (SAR) is an active microwave imaging system with the capability to penetrate cloud cover and image during night. The SAR image represents the Radar reflectivity (backscatter) of the target as a function of position. It measures the back scattering coefficient σ_0 as a function of incidence angle, wavelength & polarization - in an amplitude calibrated system & can measure the relative phase between different polarizations (SAR Polarimetry) & two receiving antennas (SAR Interferometry) - in a phase calibrated system. SAR achieves high resolution in the range by the pulse compression technique. Here the peak power is lowered and a long pulse is transmitted to keep the average power at a high level for better signal to noise ratio (SNR). Signal processing of the received signal allows compression from low to high range resolution. The SAR achieves high azimuth resolution by synthesizing a longer antenna from the movement of a physically small antenna by utilizing the forward sensor motion. Spaceborne SAR sensors have been flown in various frequencies. Earlier SAR missions e.g. SeaSat (1978), SIR-A (1981), SIR-B (1984) and recently JERS-1 (1998) and ALOS (2006) have operated in L band. ERS1 (1991), ERS2 (1995), Radarsat-1 (1995), Radarsat-2 (2007) and ENVISAT-1 (2002) have operated in C band. SIR-C/X-SAR (1994) operated in L, C & X bands. TerraSAR & RISAT-2 operate in X band. The soon to be launched ISRO's RISAT will operate in C band.

2. SAR Signal Formation: The SAR sensor transmits a signal and illuminates the target. It receives the backscattered echoes of the signal from the target. The data acquisition system with a point scatter response $(h_a(\tau,t:r))$ measures the complex reflectivity $(\gamma^0(r,t))$ of the terrain and stores the raw data $(d(\tau,t))$ in a 2-D matrix (where r is the slant range coordinate, τ is the fast-time (range) & t the slow time (azimuth).

The point target response of the received SAR signal is as follows:

$$h_a(\tau,t:r)=[wa(t,r)\times\exp\left\{-j\frac{4\cdot\pi}{\lambda}R(t;r)\right\}]\otimes[wr(\tau)\times ch\left(\tau-\frac{2\cdot R(t;r)}{c}\right)] \quad \textbf{.....(1)}$$

(i.e. Point scatter response = Azimuth Signal ⊗ Range Signal)

where, $wr(.)\&\ wa(.)$ is the range & azimuth weighting

$ch(.)$ is the transmitted chirp

$$R(t-t0;r_0)=\sqrt{r^2+V^2(r)\cdot(t-t_0)^2}$$

$V(.)$ is the relative velocity of platform with respect to target

The information of the target is compressed using a correlation operation to generate the complex SAR image $(u(r,t))$. The transmitted range signal (range chirp) has a priori frequency modulation. The received azimuth signal also has a frequency modulation (azimuth chirp) encoded due to the Doppler effect arising from the varying range.

3. SAR Processing Steps: The target information is spread in both the range and the azimuth directions, the envelope of which is shown in Fig. 1(a). SAR image formation or SAR focusing involves the compression of the received signal in the range and azimuth directions.

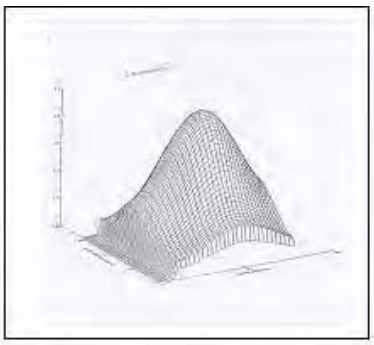

Fig. 1 a : 2D Chirp Signal as a function of range and azimuth

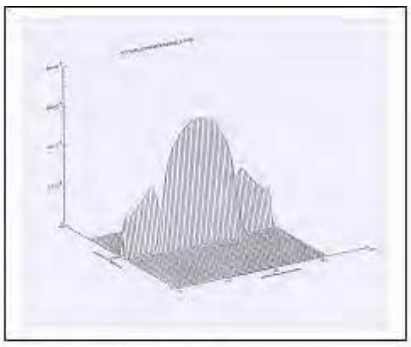

Fig. 1 b : Range Compressed Signal

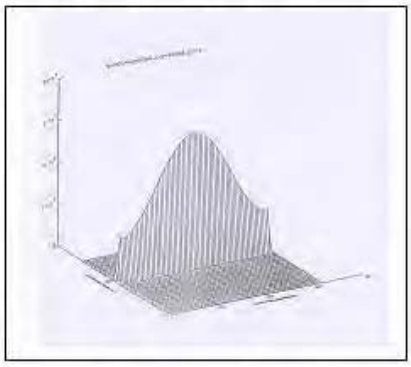

Fig. 1 c : Quadratic Migration Corrected Signal

Fig. 1 d : Azimuth Compressed

The compression of the range and the azimuth signal (matched filtering) is effected by the two correlation operations of the chirps with the appropriate reference functions. The range compression is straightforward and the received range signal is correlated with the complex conjugated time inverted replica of the transmitted pulse. This range compressed signal spans through multiple resolution cells (Fig. 1 b). As a consequence of the given target being viewed at a varying range, the range compressed signal lies in a curved path. This effect is termed as range cell migration or range walk. The curved path (in memory) of the range cell migration is usually corrected (Fig. 1 c) along with azimuth compression (Fig. 1 d). The azimuth reference filter has to be constructed using the Doppler information for carrying out azimuth compression. Multi-look technique to reduce the speckle noise at the cost of azimuth resolution degradation is done to increase the radiometric resolution for σ_0 measurements. Range and azimuth compressed data is detected and geocoded images can be formed using SAR geolocation algorithm. The SAR geolocation algorithm uses precise Range information and Doppler information for the given target and is capable of estimating the coordinates without using inputs from attitude sensors (e.g. star sensor). The various pre-processing steps involved are decoding of Block Adaptive Quantized samples to I & Q complex raw samples, Correction of Power & Phase imbalances and Doppler Centroid estimation. The algorithms which are often used for SAR image formation (Ref. 1) are Range Doppler Algorithm (RDA), Chirp Scaling Algorithm (CSA), ω-k Algorithm (ωkA).

4. SAR Acquisition Modes: SAR data can be acquired in a number of modes such as Stripmap mode, Alternate Polarisation mode, ScanSAR mode or Spotlight mode (Fig 2). In the stripmap mode, the antenna pointing angle is kept constant as the radar platform moves. The beam sweeps along the ground at an approximately uniform rate, and a strip of ground is imaged. The azimuth resolution is governed by the antenna length. The alternate polarization mode is like the stripmap mode except that the transmitter polarization is switched a number of times in the synthetic aperture. In the ScanSAR mode, the antenna beam is switched in

range many times during a synthetic aperture. A much wider swath is covered at the cost of azimuth resolution. Best resolution can be achieved in the Spotlight mode by steering the beam gradually backwards as the sensor passes the scene. Coverage in the along-track direction is a fraction of the along-track traversed distance.

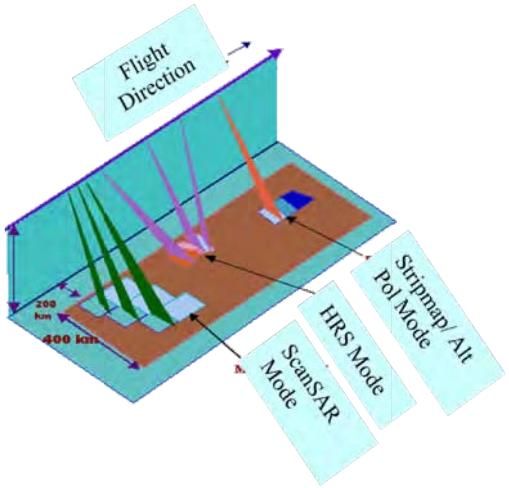

Fig 2 : Various SAR modes

Raw data for ERS-1 & multi-polarized L band DLR E-SAR have been processed using SAC/AIPG software as shown in Fig.3.

Similarly, two adjacent beams of Radarsat-1 ScanSAR data are processed as shown in Fig, 4. RISAT is a C band radar with multiple modes of operation. It has an azimuth resolution of 3 m in Stripmap mode, 9 m in Alternate Polarization mode, 24 m in medium resolution ScanSAR and 50 m in course resolution ScanSAR modes. It has slant range resolution of 2 m for Stripmap mode, 4 m for Alternate polarization mode and 8 m for both the ScanSAR modes. It also has a spotlight mode with azimuth and slant range resolutions of around 1m. Images obtained using SAR image formation algorithms are affected by speckle noise. Speckle is a random multiplicative noise. Fig 5 depicts reduction of speckle using image processing techniques (Ref. 2).

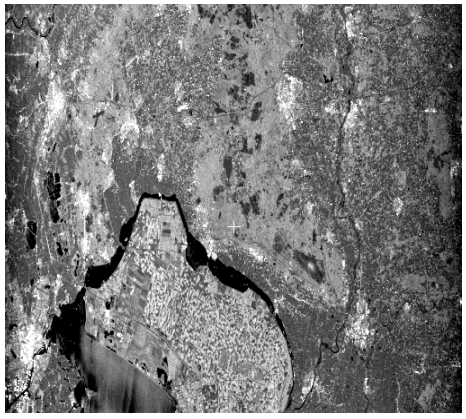

Fig 3(a): C band ERS-1 image

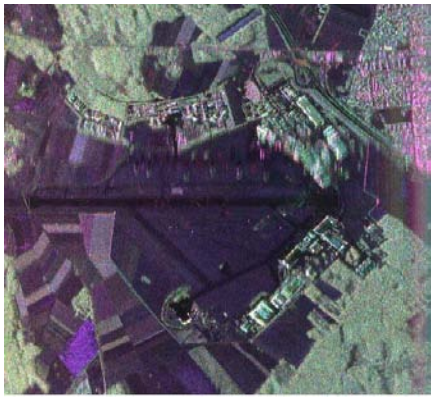

Fig 3(b): L band DLR E-SAR image

Fig 4(a): C band Radarsat-1 S5 beam data

Fig 4(b): C band Radarsat-1 W2 beam data

Fig 5(a): Original SAR Image

Fig 5(b): Speckle Reduced SAR image

5. SAR Data Products: SAR products are available after different levels of processing. Level 0 consists of raw signal product. Level 1 consists of geo-tagged products. Level 2 consists of ellipsoid geocoded products. Precision geocoded products, Terrain geocoded products, In-SAR products, Speckle reduced products, Pol-SAR products, Multi-date registered products, Large area mosaic products etc. are the Value Added Products. SAR raw slant range and geocoded products are provided in CEOS format. Value added products are often provided in GeoTiff format.

References

[1] Digital Processing of Synthetic Aperture Radar Data – Algorithms and Implementation, Ian G Cumming & Frank H Wong, Artech House, Boston, 2005.

[2] Understanding Synthetic Aperture Radar Images, Chris Oliver & Shaun Quegan, Artech House, Boston, 1998.

Call for Articles

Readers are requested to contribute short articles for publication in the forthcoming issues in their own words, preferably as per the editorial calendar given on page-3, either as a brief survey of state of the art or as articles on specific work carried out by them, or as novel concepts related to the specific theme(s). The deadline for inclusion in the next issue on **"Industry Contributions to Remote Sensing Activities"** is April 20, 2011.

- Editorial Team

Signatures, Newsletter of the ISRS–AC, Vol. 22, No.4, Nov-Dec 2010

A Tutorial on the Application Potential of SAR for Characterising Land Targets

Parul Patel, SAC, Ahmedabad-380015, Email: parul@sac.isro.gov.in

1. Introduction: Microwave remote sensing has emerged as an important tool for monitoring earth resources owing to its unique sensitivity to dielectric and physical properties of the target being sensed. These properties when coupled with its all weather capability further enhance the potentials of microwave remote sensing for earth resources management. India is on the verge of having its own SAR sensor onboard indigenously built Radar Imaging Satellite, RISAT, a C band SAR with quad polarisation and circular polarimetry capability. In this article, remote sensing using Synthetic Aperture Radar is described along with its potential land applications. A few illustrations exhibiting the physical process that takes place when microwaves interact with the target under consideration are also included. While discussing how various target properties influences SAR signatures, the impact of frequency, polarisation and incidence angle on SAR backscatter are also highlighted. Application potential of recent advancements in Interferometric SAR (InSAR)/ Polarimetry Interferometry are also discussed.

2. Dependence of SAR Signatures on Land Target Properties: SAR return signal is affected by sensor parameters like the wavelength, polarisation and incidence angle at which the sensor is being operated and target dielectric and geometrical properties in general. Different terrain targets exhibits different impact on radar return signal, for example a built-up land shows high backscatter owing to presence of dihedral and trihedral corner reflector effect, where as calm water returns a very low backscatter due to specular reflection. Vegetated land gives intermediate backscatter depending upon dielectric and geometrical properties of the vegetation along with the soil underneath the vegetation. Bare soils can yield very high to very low backscatter depending upon their dielectric and surface roughness conditions.

In order to understand the sensitivity of SAR to land targets, let us look at the parameters that affect the SAR return signal from an agricultural land. SAR return signal is affected by target dielectric and geometrical properties. In general, SAR backscatter from an agricultural terrain is strongly influenced by the moisture content and surface roughness conditions of the soil, dielectric and geometrical properties of the vegetation prevailing in the agricultural fields at the time of data acquisition.

2.1 Soil Moisture Dependence: As can be observed from (Fig.-1) at microwave frequencies, dielectric constant of dry soil is around 3 and that of water is around 80. Hence dielectric constant for moist soil, which is a mixture of the two, ranges between 3 and 30. As the dielectric of a material increases, the Fresnel reflectivity also increases resulting in an increased backscatter. Thus SAR backscatter is directly related to moisture content of the target under consideration. i.e. A dry field would yield low backscatter, hence would appear in dark tone and a moist field would appear in bright tone due to high backscatter. However, soil texture determines the dielectric property of soil water mixture, hence is one of the target parameter that significantly affects SAR backscatter, which is discussed latter.

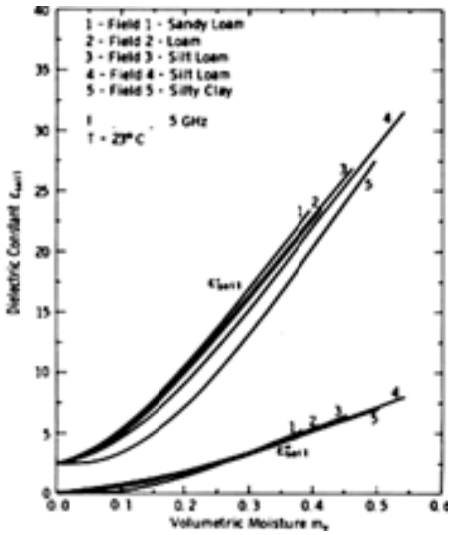

Fig. 1: Variation of Dielectric constant with soil moisture (Ulaby et al., 1986)

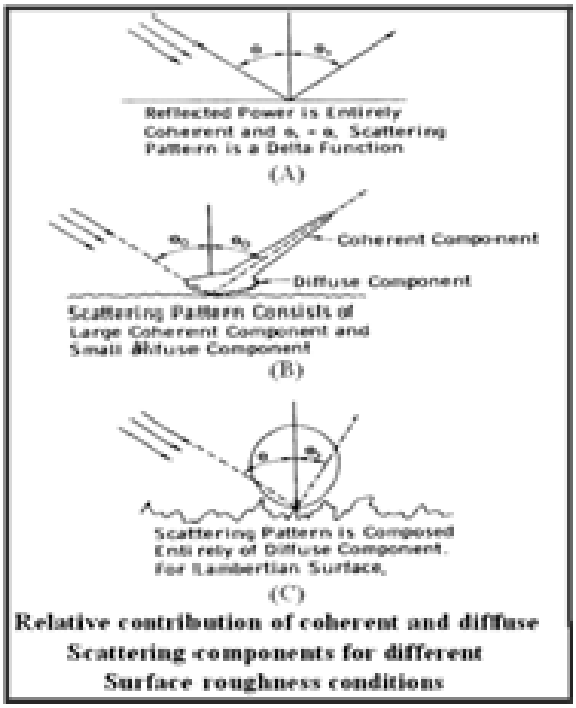

Fig. 2: Scattering from different rough surfaces (Ulaby et al., 1986)

Table-1: Cut-off limits for a smooth surface at 45° for C, L and P bands		
Wavelength (λ) cm	**Inc angle (θ)**	**Smooth criterion (h <)**
5.6	45°	0.25
23.5	45°	1.04
85	45°	3.76

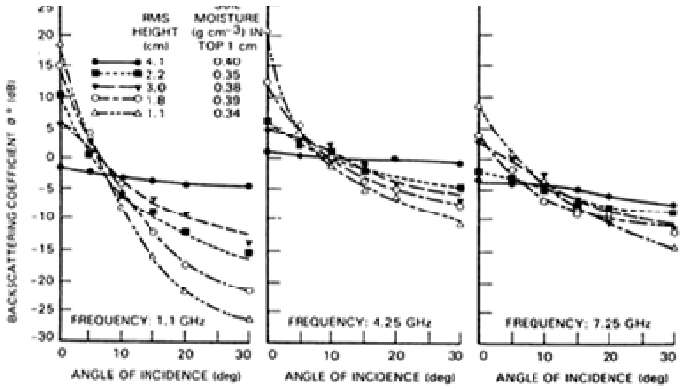

Fig. 3: Effect of incidence angle on surface roughness at 1.1 GHz, 4.25 GHz and 7.25 GHz (Ulaby et al., 1986)

2.2Surface Roughness Dependence: Surface roughness is another important parameter that significantly affects the SAR backscatter from the soil. A smooth field would appear as dark due to a low backscatter, as a smooth surface gives rise to specular reflection whereas a rough field would appear brighter due to higher non-coherent scattering component, resulting in an increased backscatter towards SAR antenna (Fig.-2). Here it is interesting to mention that magnitude of surface roughness itself is a function of frequency and incidence angle at which the surface is being observed. It indicates that the characterization of a soil surface into smooth and rough class changes with the SAR sensor parameters. According to Fraunhofer criterion, a surface will appear smooth if the surface rms height h satisfies the following condition given by,

$$h < \lambda / 32\cos(\theta) \qquad (1)$$

where, h = rms height, λ is wavelength and θ is the incidence angle.

Table-1 gives the cut-off values of rms height values for a surface to be considered as a smooth surface illuminated at 45° incidence angle at C, L and P-bands.

Hence as the wavelength increases the same field starts satisfying the smoothness criterion, i.e. for longer wavelength almost all the agricultural fields appear as smooth. Thus a field that is rough for C band could be medium rough for L band and smooth for P band.

Impact of surface roughness on SAR backscatter can be studied from Fig.-3. As can be observed from Fig.-3, for a rough surface, the SAR backscatter signal strength at low and high incidence angle are compatible with each other whereas for a smooth surface, the SAR backscatter signal strength at a higher incidence angle is much less than that at low angle of incidence, hence, the (σ°low_incidence - σ°high_incidence) is high for smooth fields and low for rough fields as can be observed from Fig.-4.

Angular behaviour of multi-incidence angle SAR data can be exploited to estimate surface roughness. (σ°low_incidence - σ°high_incidence) can be used as an indicator of the surface roughness conditions prevailing in the agricultural fields at the time of satellite pass.

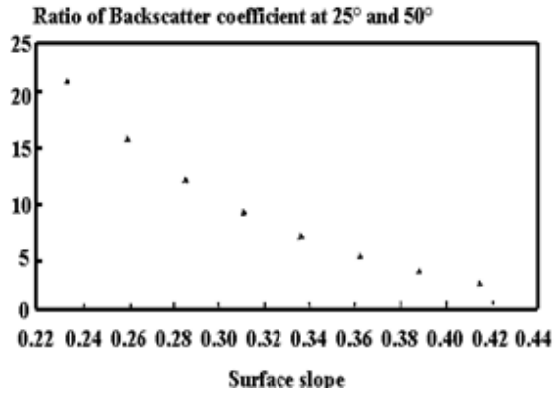

Fig. 4: Sensitivity of multi-incidence angle SAR ratio to surface roughness

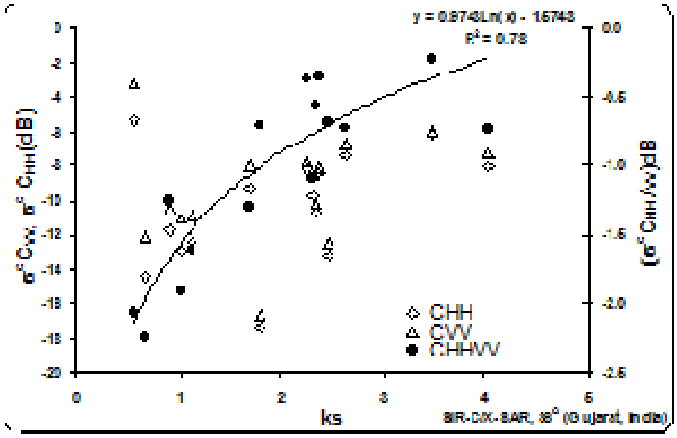

Fig. 5: Sensitivity of multi-polarisation SAR ratio to surface roughness (Srivastava et al., 2006a)

Similarly polarisation behaviour of SAR backscatter can also be exploited to arrive at surface roughness information as can be observed from Fig.-5. It is seen from Fig.-5. that while like-polarisation themselves are not directly related to surface roughness, the like-polarisation ratio can be used to infer about surface roughness.

2.3 Vegetation Cover Dependence: SAR backscatter for a vegetated terrain depends upon the vegetation volume, dielectric and structure of the vegetation constituents along with the dielectric of surface roughness of underlying soil. For given vegetation, the penetration depth depends on frequencies of SAR sensor as depicted schematically in Fig.-6. It also depends on polarisation as well as incidence angle. For example a shallow incidence angle SAR operating at C-band penetrating only in the upper layer of the canopy where as the crop would become almost transparent to P-band. At the same time, at near nadir incidence angle even C band can reach to the soil underneath the crops. Interaction of SAR signal with various constituents of vegetation cover results in multiple scattering of the incoming signal. Higher strength of cross polarised signal as compared to bare smooth soil from a vegetated terrain is in general attributed to the depolarisation accounting due to multiple scattering within vegetation.

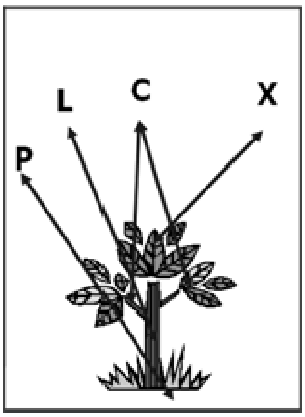

Fig. 6: Interaction of multi-frequency SAR with different constituents of vegetation cover

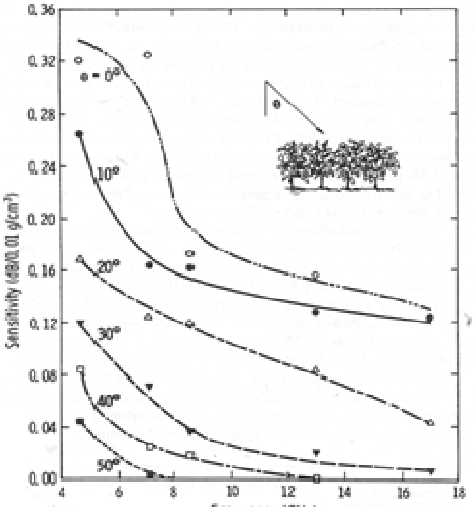

Fig. 7: Effect of frequency and incidence angle on penetration of SAR through vegetation. (Ulaby et al., 1986)

Fig.-7 gives sensitivity of SAR backscatter at different frequency to soil moisture conditions underneath a crop cover at different angle of incidence. At low incidence angle, radar backscatter can penetrate through crop cover where as at higher angle of incidence, the path length of the SAR signal within vegetation volume is higher resulting in lower sensitivity to moisture conditions underneath the crop cover.

2.4 Penetration Depth: The penetration depth of SAR is dependent on wavelength hence, in order to understand SAR backscatter from soil, it is also important to know the depth of soil profile from which the SAR is sensing the soil moisture. The depth of penetration for a given target is governed by wavelength of incident microwaves signal and the dielectric of the target as given below.

$$\delta \cong \frac{\lambda * \sqrt{\varepsilon''}}{2\pi * \varepsilon'} \qquad (2)$$

where, ε' and ε'' are real and imaginary part of the dielectric constant.

It can be seen that for a given target, longer wavelengths have higher penetration depth as compared to shorter wavelengths. At the same time, it is the moisture content of different layers of soil profile depth that determines the SAR backscatter at different wavelength.

3. Application Potentials of SAR for Different Land Applications: Having understood the dependence of SAR backscatter on land targets' properties we shall look at how this dependence is exploited for different land applications.

3.1 Soil Moisture Studies: In order to understand the sensitivity of SAR to crops and soil moisture, let us look at the parameters that affect the SAR return signal from an agricultural land. SAR return signal is affected by the sensor parameters viz. wavelength, polarisation and incidence angle at which the sensor is being operated and target dielectric and geometrical properties in general. Soil texture determines the dielectric property of soil water mixture, hence is one of the target parameter that significantly affects SAR backscatter.

Surface roughness is another important parameter that significantly affects the SAR backscatter from soil. A field that is smooth would appear dark due to low backscatter, as smooth surface gives rise to specular reflection whereas a rough field would appear brighter due to higher non coherent scattering component, resulting in an increased backscatter towards SAR antenna. Here it is interesting to mention that magnitude of surface roughness itself is a function of frequency and incidence angle at which the surface is being observed.

SAR backscatter for a vegetated terrain depends upon the vegetation volume, dielectric and structure of the vegetation constituents along with the dielectric of surface roughness of underlying soil. For given vegetation, the penetration depth of different frequencies depends on the frequency, polarisation as well as incidence angle. For example a shallow incidence angle SAR operating at C-band penetrating only in the upper layer of the canopy where as the crop would become almost transparent to P-band. At the same time, at near nadir incidence angle even C band can reach to the soil underneath the crops. The soil depth with which the incident microwaves interact also varies from one wavelength to the other. The penetration depth of SAR signal is dependent on wavelength. For a given target, longer wavelengths have higher penetration depth as compared to shorter wavelengths.

3.1.1 Incorporating Soil Texture Effect: Wet soil is a heterogeneous mixture of soil, water and air pockets. In general, the water in wet soil can be further divided into bound water and free water.

The percentage of free water and bound water present in a soil medium, which depends on the surface area of soil particles present in the soil medium, determines the dielectric constant of a soil medium. As the surface area of soil particles in a soil medium depends upon the particle size and the relative proportions of various-sized particles in a given soil hence, the dielectric constant of wet soil varies with soil texture. The amount of soil moisture at wilting point (15 bar pressure) is very tightly held with soil particles. Thus, there is a strong synergy between bound water and water at 15 bar pressure as both represents the amount of water which is very tightly held with soil particles. Since the amount of water free to interact with the incident microwaves gives significant contribution to the SAR backscatter, is close to the amount of water available to plants per unit volume of soil. A soil moisture measure defined in terms of water that is above the wilting point (SM_AWP) as given by Equation (3) is found to be very useful.

SM_AWP=(Observed soil moisture from sampling location – Soil Moisture at 15 bar pressure for the same location) (3)

In an experiment over smooth bare fields alone it was observed that by representing soil moisture in terms of SM_AWP, R^2, the correlation coefficient, increased considerably from 0.88 to 0.96 as compared to the case where soil moisture is represented as gravimetric soil moisture. At the same time, it was observed that the rms error for SM_AWP was the lowest at 0.62, as compared to that of 2.23 obtained for model developed using gravimetric soil moisture over an independent dataset. Thus, SM_AWP effectively incorporates the effect of soil texture in soil moisture estimation using microwave remote sensing by representing the soil moisture in terms of the water available to plants in that soil medium.

3.1.2 Incorporating Surface Roughness Effect: Surface roughness significantly affects SAR backscatter response of a target. Hence, for fallow fields, monitoring and mapping of soil moisture with higher accuracy calls for incorporating the effect of surface roughness in the soil moisture retrieval model. For a rough surface, the SAR backscatter signal strength at low and high incidence angle are compatible with each other whereas for a smooth surface, the SAR backscatter signal strength at a higher incidence angle is much less than that at low angle of incidence, hence, the $(\sigma^\circ_{low\_incidence}-\sigma^\circ_{high\_incidence})$ is high for smooth fields and low for rough fields. Angular behaviour of multi-incidence angle SAR data can be exploited to incorporate the effect of surface roughness in the soil moisture retrieval model. The effect of surface roughness in the soil moisture estimation can be incorporated by using $(\sigma^\circ_{low\_incidence}-\sigma^\circ_{high\_incidence})$ as a surface roughness indicator as given by equation-4.

$$SM\_AWP = A + B*(\sigma^\circ_{low\_incidence}) + C*(\sigma^\circ_{low\_incidence}-\sigma^\circ_{high\_incidence}) \quad (4)$$

Although the model given by equation-4 is able to incorporate the effect of surface roughness in the soil moisture retrieval model, the time difference between the acquisition of lower and higher incidence angle SAR data restricts the use of this model if there is large difference in between the acquisition of lower and higher incidence angle SAR passes. Availability of simultaneously acquired dual polarized (HH/VV) Envisat-1 ASAR data has provided the opportunity to exploit the sensitivity of like polarization ratio (HH/VV) towards surface roughness conditions. One can use the like polarization ratio to incorporate the effect of surface roughness in the soil moisture retrieval model, given by equation- 5.

$$SM\_AWP = A + B*(\sigma^\circ_{VV}) + C*(\sigma^\circ_{HH}-\sigma^\circ_{VV}) \quad (5)$$

3.1.3 Incorporating Vegetation Effect: When SAR views a crop-covered field at higher incidence angle it undergoes an increased path length through the vegetation volume, resulting in higher interaction with crop canopy. It is observed that for crop covered fields, the return signal at higher incidence angle, $\sigma^{\circ}_{high\_incidence}$, is an effective crop canopy descriptor as it represents the overall effect of crop cover, i.e. the combined effect of crop type, crop structure, crop volume, canopy moisture etc. in the soil moisture retrieval model. Fig.-8 shows SAR images at low and high angle of incidence and their response to soil moisture underneath vegetation. An empirical model for soil moisture retrieval for crop covered soil can be developed by including an additional term of $\sigma^{\circ}_{high\_incidence}$ in the soil moisture retrieval model as a crop canopy descriptor. Thus for the crop covered area the soil moisture retrieval model is as given by equation-6.

$$SM\_WAP = A + B*(\sigma^{\circ}_{low\ incidence}) + C*(\sigma^{\circ}_{high\_incidence}) \quad (6)$$

With the availability of simultaneously acquired like (VV) and cross (VH) polarized Envisat-1 ASAR data, one can overcome the limitation of non availability of simultaneous acquisition of multi-incidence angle SAR data. From crop covered fields, depolarisation takes place due to multiple reflections within vegetation volume. As the amount of depolarisation is much higher for larger vegetation volume and larger amount of dielectric discontinuities within the vegetation volume, it is obvious that amount of depolarisation can be used as an indicator of the overall vegetation cover. Hence, the effect of crop cover can be incorporated in the soil moisture retrieval model by including an extra term of cross-polarized SAR backscatter (σ°_{VH}) in the soil moisture retrieval model. This model can be written in the form of equation-7.

$$SM\_WAP = A + B*(\sigma^{\circ}_{VV}) + C*(\sigma^{\circ}_{VH}) \quad (7)$$

Srivastava et.al 2009a have combined all the three approach to arrive at large area soil moisture estimation using multi-incidence angle SAR.

3.1.4 Deeper Layer Soil Moisture: Wavelength is one of the most important sensor parameter that affects soil moisture estimation, as it is the wavelength that determines the depth from where the signal is coming back. As longer wavelengths have higher penetration depth within the soil medium, longer wavelengths sense soil moisture from deeper layers as compared with shorter wavelengths that mostly interacts with soil surface or very small soil column (0-10 cm) near soil surface.

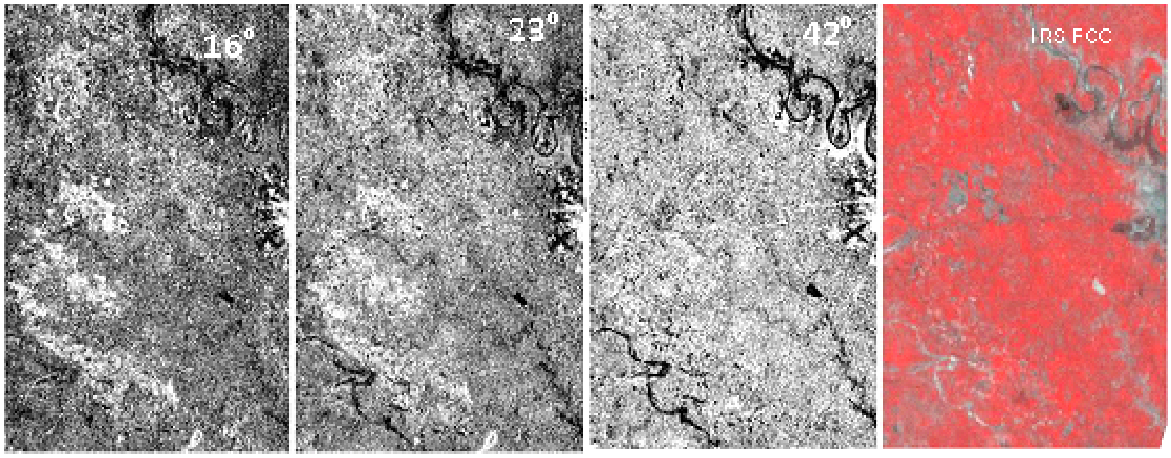

Fig. 8: Effect of incidence angle on penetration of SAR through vegetation. (Patel et al., 2001)

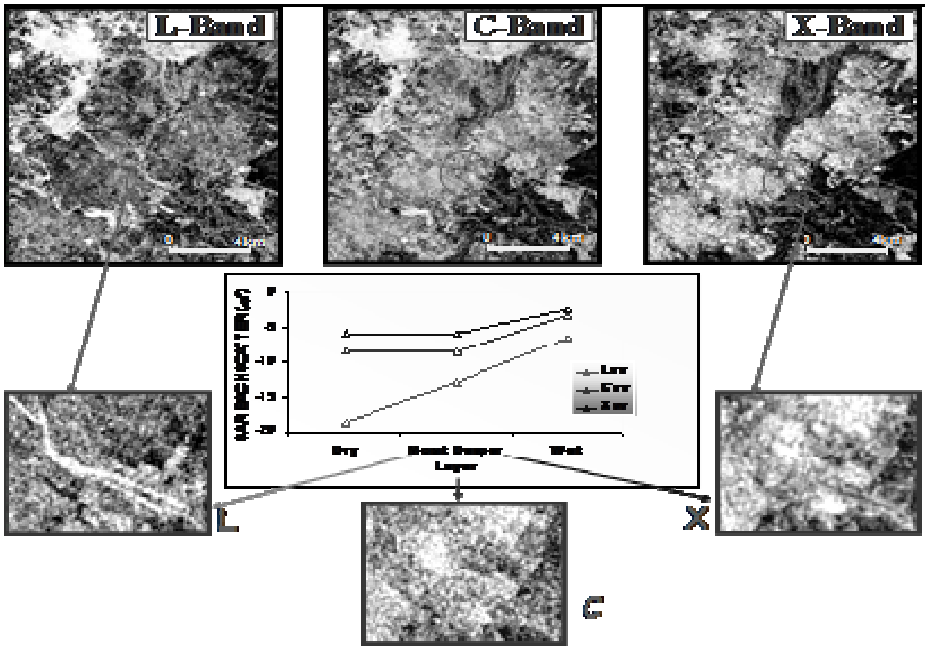

Fig. 9: Multi-frequency SIR-C response to deeper layer soil moisture (Srivastava et al., 2006a)

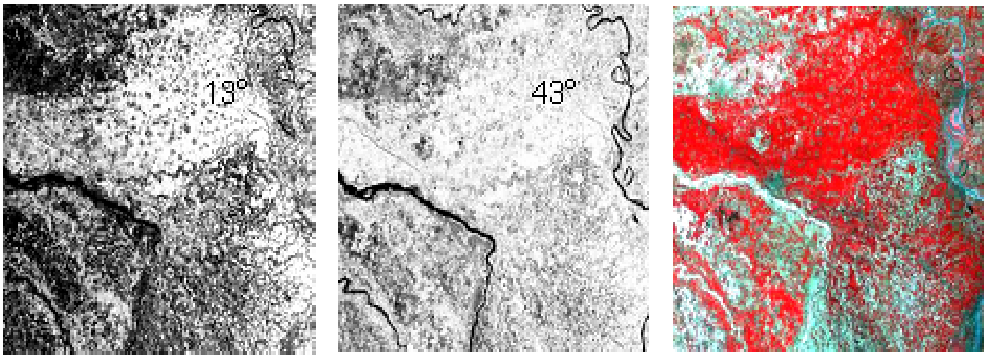

Fig. 10: Radarsat-1 and IRS L-III sub images, Parts of Burdwan district, West Bengal, Patel et al., 2002)

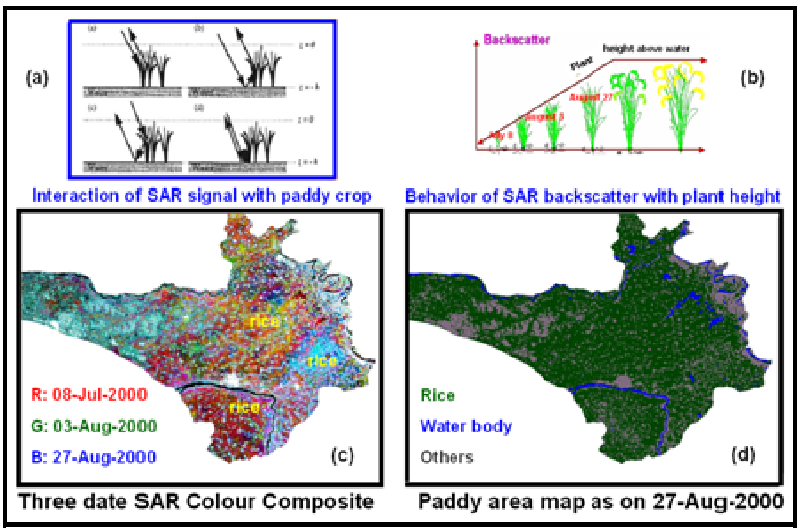

Fig. 11: Monitoring of paddy using Radarsat-1 SAR data

However, due to non-availability of longer wavelengths in most of the operational satellites (e.g. ERS-2, Radarsat-1, Envisat-1, proposed Radarsat-2, proposed RISAT etc.) the potential of SAR is limited only up to surface soil moisture estimation. Potential of longer wavelengths to estimate deeper layer soil moisture was clearly brought out as seen in the Fig.-9 showing SIR-C/X-SAR data over Bhavnagar, Gujarat that operated in the L, C and X bands. In Fig.-9, it is clearly seen that L-band is able to sense deeper layer soil moisture. subimages shown in Fig.-9 exhibit that C-band and X-band are not able to sense deeper layer soil moisture due to their low penetrability within soil medium.

3.2 Crop Studies:

3.2.1 Multi-Incidence Angle SAR Crop Signatures: For vegetated terrain, the incidence angle, the angle between the direction of the incident radiation and nadir, affects the SAR return signal significantly. For a given wavelength a higher interaction of the incident radiation with the vegetation takes place when applied at shallow angle of incidence angle due to an increase in the path length within the vegetation volume. Similarly, due to reduced path length within the vegetation volume SAR backscatter at low angle of incidence in less affected by the vegetation volume and is able to pick up the underneath cover. A pair of low and high incidence angle Radarsat-1 SAR images shown in Fig.-10 demonstrates this phenomenon. The crop during data acquisition was mostly Boro rice, grown during January to March. It can be seen that the cropped area (seen in red tone in IRS-L-III FCC) shows two distinct tones at 13^{o} incidence angle SAR image owing to higher penetration, where as the 43° incidence angle shows uniform backscatter for the cropped area due to increased path length in the crops. Thus angular SAR response can be exploited to enhance the sensitivity of SAR to soil moisture as well as crops by selecting low angle for soil moisture and high incidence angle for crop studies.

3.2.2 Temporal SAR Crop Signatures: Temporal SAR signatures can be exploited to study SAR response to crop growth. In particular, it is exploited to study rice, which belongs to the grass family with a 120 day growth cycle and is grown in flooded fields with 10-50 cm of standing water for most of its growth period. The method of growing rice in water filled puddle fields provides a unique temporal signature to identify rice using temporal SAR data.

During the early growing stage, rice fields are flooded. The soil surface is almost completely covered by water. This gives a very low backscatter return due to specular reflection in the forward direction. As the crop grows, the plants emerge above the water surface and the backscatter increases steadily due to volume scattering from the canopy (Fig.-11). Due to the masking of the underneath soil with a constant background of water, the radar backscattering is sensitive only to the plant's total biomass, its moisture content and the plant's geometry. It has been observed that there exists a high correlation between radar backscattering and plant height (above water surface) as shown in Fig.-11(b). Fig.-11(c) shows the false colour composite generated using temporal Radarsat-1 SAR backscatter images acquired over parts of Bardhman district of West Bengal. It can be observed in the Fig.-11(b) that up to around 90 days after transplantation, the SAR backscatter increases with crop height. This unique signature has been used to arrive at a decision rule based model to classify rice crop (Figure-11d). Thus the characteristic temporal backscatter of wetland rice as it grows over water filled field was found useful to delineate the rice crop grown area. In fact, rice crop parameter retrieval models have also been

developed using this temporal SAR response to rice crop growth. For example Choudhury and Chakraborty, 2002, have arrived at transplantation date using characteristic response of temporal SAR to rice crop growth.

3.3 Forest Plantation: The SAR backscatter from a forested land is affected by the volume, structure, dielectric and the soil cover underneath the forest vegetation. Srivastava et al. 2009b have studied Multi-frequency and multi-polarized SAR response to thin vegetation and scattered trees.

3.3.1 C and L Band Multi-Polarisation SAR Forest Signatures: Impact of frequency can be observed on SAR response to plant density as shown in Fig.-12. Fig.-12 shows scatter plot of SAR backscatter vs. plant density of Prosopis juliflora over parts of Bhavnagar district taken during the space flight SIR-C/X-SAR mission at nominal incidence angle of 36^{o}. It can be observed that in comparison to C band, L band is more sensitive to plant density in general and within polarisation cross polarised is better as compared to like polarisation for mapping plant density. Within like polarisation HH polarisation is found to be better as compared to VV polarisation. The sensitivity differences in like polarisation backscatter is attributed to the plant structure of Prosopis Juliflora which is more of a shrub type.

3.3.2 C, L, P Band Multi-Polarisation SAR and P band PolInsar Forest Signatures: The distribution of various constituents of the forest vegetation significantly affects SAR backscatter. In general, for a forested land, C-band interacts with leaves and twigs, L-band can interacts up to branches and even up to trunk depending upon the vegetation volume where as P-band can interact up to the trunk as well as the soil underneath the vegetation. Patel and Navalgund 2008 and Patel et al. 2009 have used polarimetric target vector decomposition technique to delineate forested areas from non forested areas and to characterise different category within Keoladeo National Park. Fig.-13 shows the multi frequency, multi-polarised SAR backscatter from three categories of tree plantation. As can be observed from Fig.-13, SAR backscatter from Prosopis, Jamun as well as Kadam did not show much variation amongst themselves at C-band. Since C-band interacted mostly with the top layer of the canopy where as L-band which could penetrate deeper in the vegetation volume, showed an increase in backscatter from Prosopis to Kadam to Jamun in the order of increasing vegetation volume. However of tree structure on PolInSAR Coherence was studied.

Vegetation is a typical natural volume scatterer. Incident wave penetrates volume scatterer and it interacts with these scatterers as a whole. Volume scatterers are characterised by a finite vertical distribution of scatterers with varying phase centre in the vertical direction centre in the vertical direction (i.e. z direction) depending upon the polarization state. As a direct consequence, they are affected by geometrical decorrelation in form of volume decorrelation. The variation in the interferometric coherence with varying polarisation can be seen over the forested areas in Fig.-13. Fig.-13 shows the variation of P band Backscatter along with the P-band PolInSAR coherence at different polarisation for different forest vegetation. One can notice the striking difference in the backscattering and coherence variation patterns. For the case of Prosopis juliflora, Jamun and Kadam the SAR backscatter at P band is mostly uniform whereas the PolInSAR Coherence values are showing very high variance amongst these categories. The variation in coherence is attributed to difference in the phase centre of different polarisation arising due to oriented volume component for a given forest vegetation structure. The little difference in the cross polarised coherence for almost all the vegetation categories indicates that most of the cross polarised signatures are resultant of random volume component of the forest vegetation.

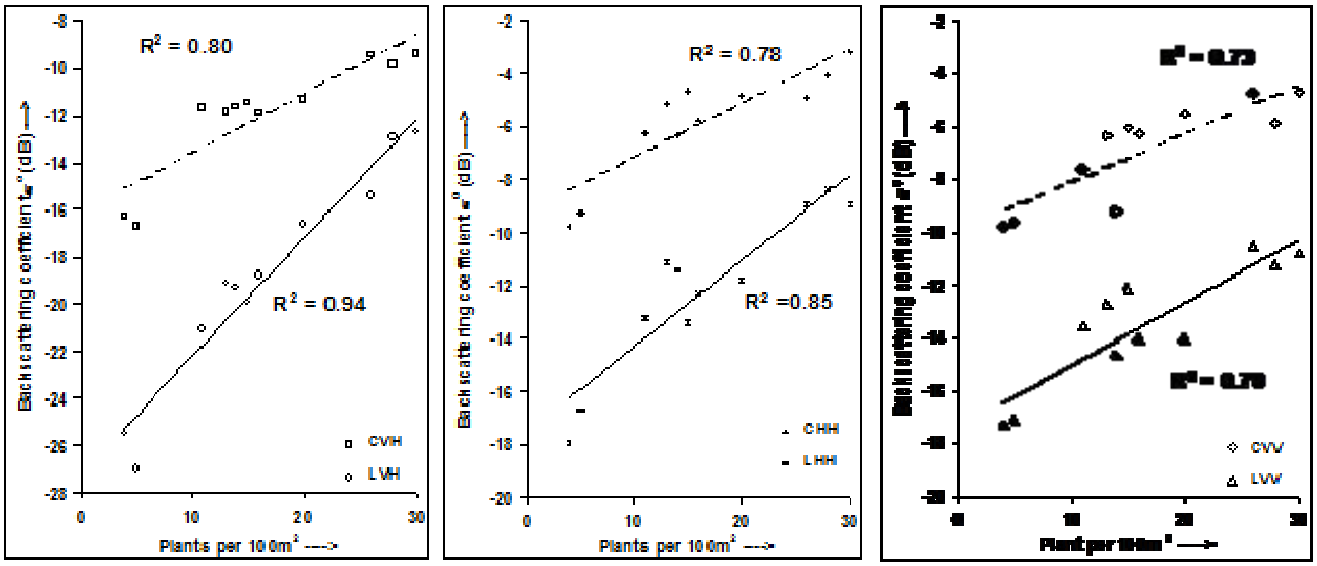

Fig. 12: Variation of multi-polarised SAR backscattering coefficient at C band and L band with varying plant density (Patel et al., 2006a)

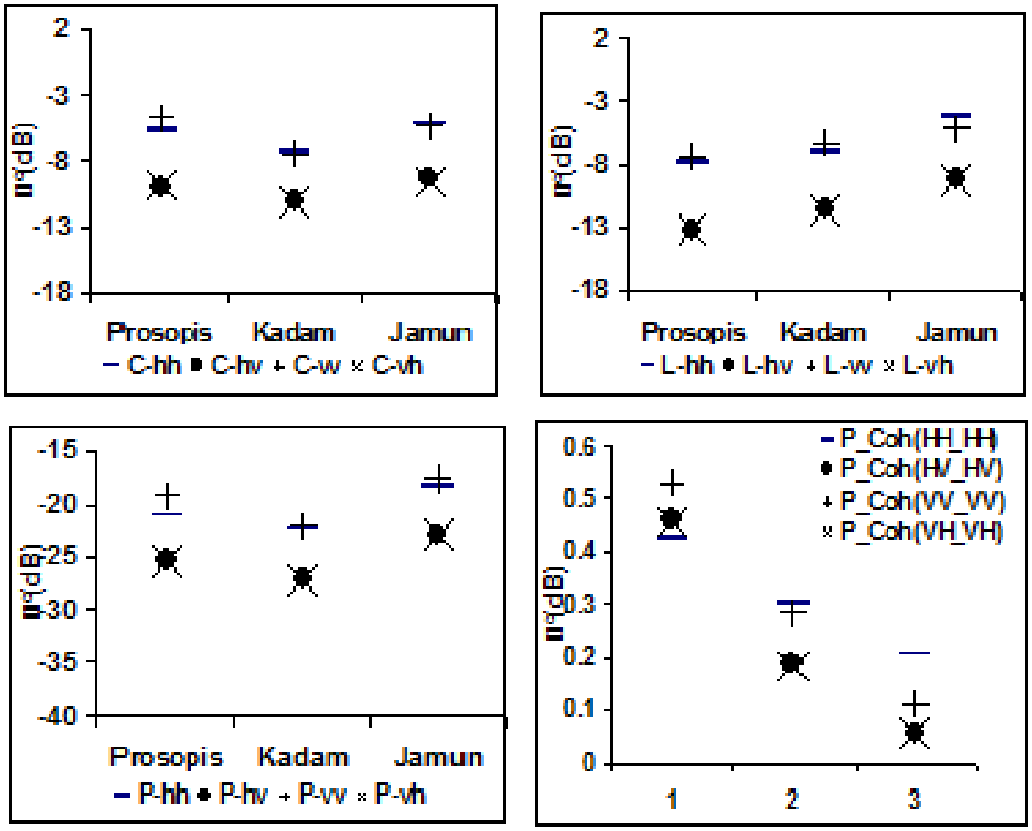

Fig. 13: Multi-frequency and multi-polarization SAR signature along with PolInSAR coherence values for three forest plantations.

3.4 Flood Damage Assessment: Imaging radars exhibit enhanced returns from flooded areas having varying degrees of vegetation canopy closure, which obscure flood boundary in visible and near infrared images. Fig.-14 shows signal enhancement occurring primarily in flooded terrain under a closed canopy. Signal enhancement occurs for long wavelength when flooded forest vegetation is being viewed, similar enhancement for shorter wavelength is observed while imaging flooded grass, marsh and cropped fields. It has been observed that C-band and X-band cannot penetrate the canopy of forest vegetation where as L band is able to penetrate the canopy and reflects off the smooth water surface and the vertical trunks of the trees and returns a strong reflected backscatter. However for L-band, grasses are almost transparent and underneath water reflect the energy in the opposite direction. Thus water underneath grasses acts as open water for L band where as for C band and X band water underneath grasses and cropped fields enhances backscatter.

Use of Radarsat-1 SAR data has been demonstrated for mapping flash flood affected rice fields over parts of West Bengal, India. Fig.-15 shows the C-band Radarsat-1 images acquired before and after the flood event and corresponding flash flood affected rice areas which were delineated with the help of four date temporal SAR data. Rice areas were delineated using three date Radarsat-1 ScanSAR data acquired during early paddy crop growth stages. Radarsat data acquired post flood event during grain filling stage was used for flood damage assessment. Analysis of backscatter characteristic of known sites showed distinct separation of submerged fields from normal fields due to very low backscatter. This was mainly due to the sensitivity of SAR data to water. Partially submerged fields showed 3 to 4 dB decrease in backscattering coefficient as compared to that from the areas not affected by the flood event. A decision rule algorithm was developed based on these signatures of post flood Radarsat-1 SAR data and applied on the rice mask to delineate submerged, partially submerged and normal category of rice fields. This provides useful information to assess the damage caused due to flood. Maximum damage was assigned to the submerged fields since lodging of crop had occurred in these areas and they were under water for more than 5 days, as date of satellite pass was after 4 days of the flood event. This study shows that SAR data can be effectively used not only to monitor flood events but also to assess the crop damage in case of wet land rice.

3.5 Water & Man Made Features Studies: Potential of Radar data for the delineation of surface water extent, when coupled with its all weather capability and ability to acquire data during day / night makes Radar a unique choice for the mapping of surface water extent particularly during floods. In general, water is a smooth surface that gives a low SAR backscatter as most of the incident radiation is reflected in the direction away from the receiving antenna in case of most of the SAR system which are monostatic. In contrast to this, settlement areas appear in bright tone owing to corner reflector image. Fig.-16 shows the SAR backscatter from water and a village at C, L and P bands at all the four polarisations.

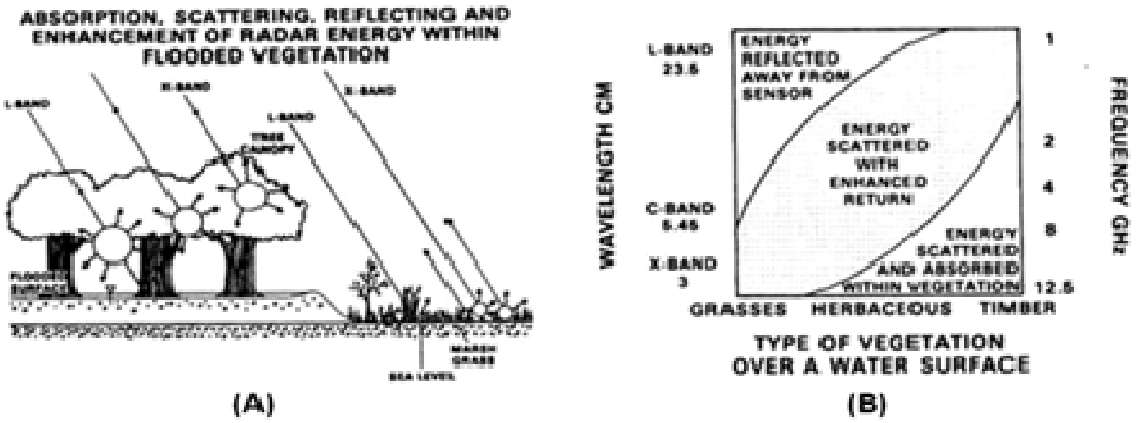

Fig. 14: (A) Effect of flood on X and L band Radar; (B) Relative Radar return response for different wavelengths and vegetation

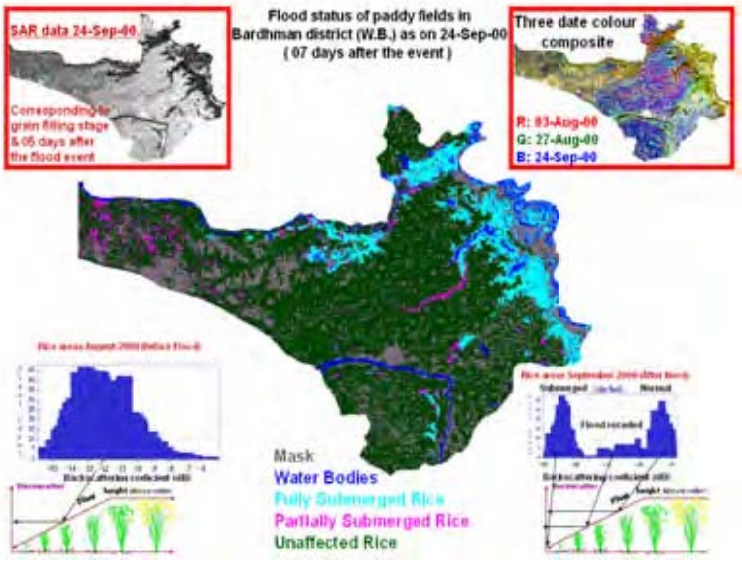

Fig. 15: Assessment of damage in paddy crop caused due to flood using RADARSAT-1 ScanSAR data, (Patel et al., 2004)

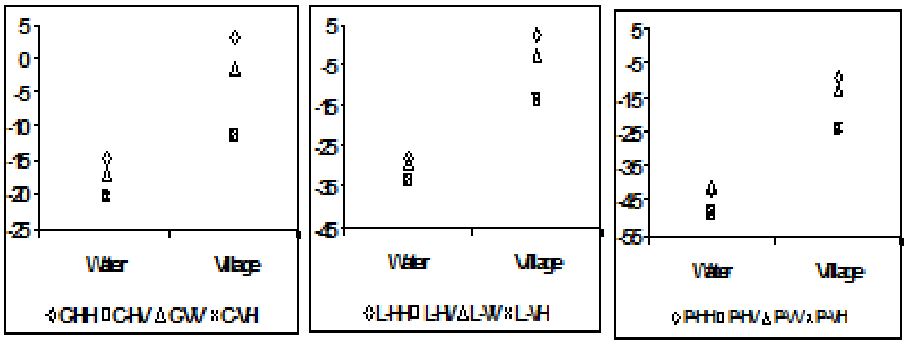

Fig. 16: SAR backscatter from water and village at C, L and P bands for all the four polarizations.

It can be observed that the water is giving very low backscatter for all the frequency and polarisation. Fig.-16 shows that for built up land, while SAR backscatter from HH and VV polarisation is on higher side, SAR backscatter at HV as well as VH polarisation is relatively low for all the frequency. This is due to the fact that built up land is not highly suited for depolarisation of the incident wave hence cross polarised SAR backscatter is observed to be relatively low.

3.5.1 Detection of Human Settlement Using Higher Incidence Angle Radarsat-1 SAR Data: RADAR backscatter is largely determined by the physical properties of surface objects such as surface roughness, orientation and dielectric behaviour. In contrast to this, on an optical FCC, signature of habitation, fallow land and gullied land are mixed with each other and therefore in case of digital classification of human settlements there is lot of commission /omission error from fallow fields and wasteland categories like gullied / ravine land. On a SAR imagery, habitation structure mostly exhibits corner reflector effect resulting in a very high backscattering coefficient for habitation as compared to that of agricultural land (both crop covered fields and fallow fields) and gullied land with very low backscattering coefficients. Moreover, in case of high incidence angle SAR data it is likely that the incidence angle falls within ± 10° of the bore-sight, giving rise to very strong backscatter (+2dB to +6dB). Potential of higher incidence angle SAR data in detection of human settlement can be appreciated with the help of Fig.-17. Fig.-17 clearly indicates that for the detection of human settlement, higher incidence angle SAR data is far superior to standard false colour composites generated with the help of optical data.

As human settlements (both cities and villages), which are clearly seen as bright scattered spots on SAR data are mixing with fallow land and gullied land. On this data set a study was taken up to explore potential of SAR data for digital detection of human settlements. Study indicated that human settlement could be digitally classified with classification accuracy as high as 98.23% using SAR data alone. However due to mixing of few categories of wasteland with fallow land, overall classification accuracy as low as 75.59% is achieved when SAR data alone is used. It was observed that synergic use of SAR and optical data acquired in the month of February proved to be the best showing highest overall classification accuracy of 89.33% with classification accuracy of human settlement to be 93.10%.

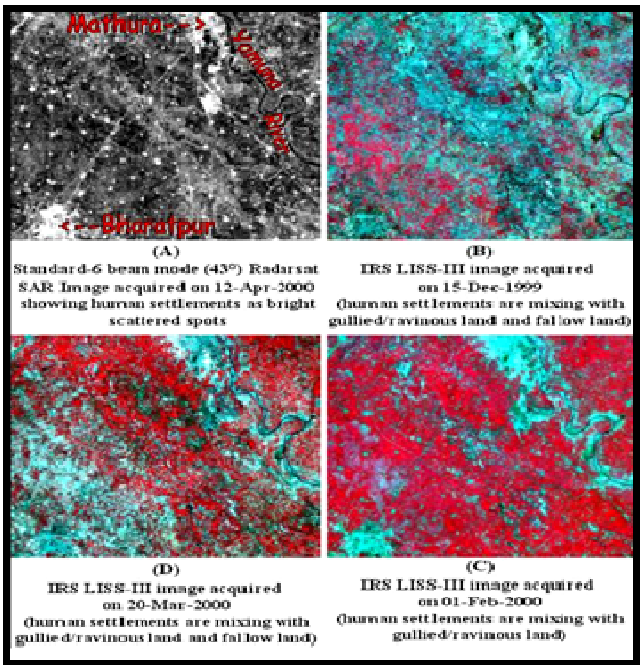

Fig. 17: Multi-date optical and higher incidence angle SAR image over parts of Agra, Mathura and Bharatpur districts. Human settlements are clearly seen on SAR image as bright scattered spots whereas they are mixing with fallow land and wasteland categories on all the three optical images (Srivastava, et al.2006c).

3.5.2 Delineation of Surface Water Using InSAR Coherence: Although calm water generally yields low return, if the water surface is perturbed by the surface wind, the SAR return varies from medium

bright to very bright. The dramatic effect of wind on sensitivity of SAR backscatter towards surface water is clearly visible in Fig.-18. The potentials of Interferometric coherence can be exploited to delineate surface water bodies even in windy conditions. The parameter that is used for this purpose is interferometric coherence, which relies on the random dislocation of scatterers between two SAR passes rather than actual surface roughness conditions or actual SAR backscatter.

Since no water surface can remain steady between any given passes, random dislocation of scatterers is considerably high in case of water bodies as compared to land features, hence water bodies exhibits low InSAR coherence. This leads to accurate identification and mapping of surface water bodies and surface water extent as seen in Fig.-19. Fig.-19A & Fig.-19B, show the intensity images of interferometric pair (14-Apr-1996 and 15-Apr-1996). The corresponding coherence image generated with the help of phase information of these image pairs is shown in Fig.-19C. Coherence image clearly delineate the water from its surroundings. This provides an excellent example indicating that the InSAR technique is a very promising tool for mapping surface water extent in particular, for flood mapping which normally occurs with associated cloudy and rough weather conditions. More recently SAR polarimetry is being used for characterising land targets using target vector decomposition which classifies the target vector based upon its interaction with incoming SAR signal.

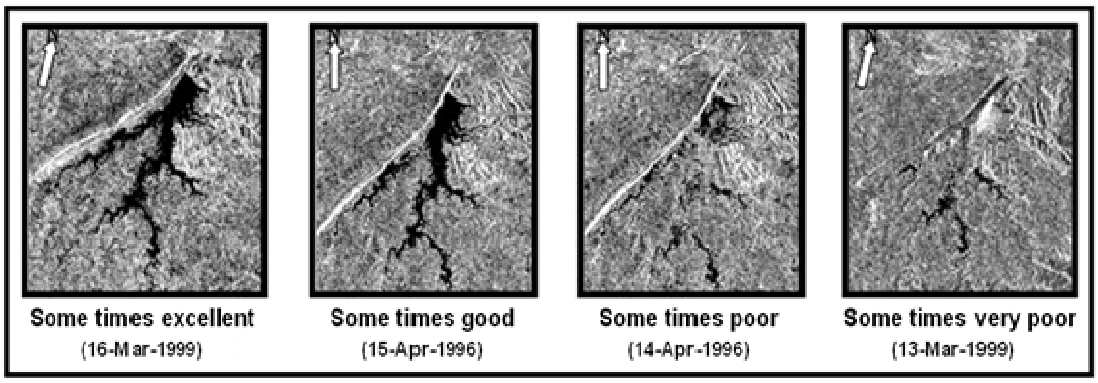

Fig. 18: Surface water extent as seen on SAR imagery

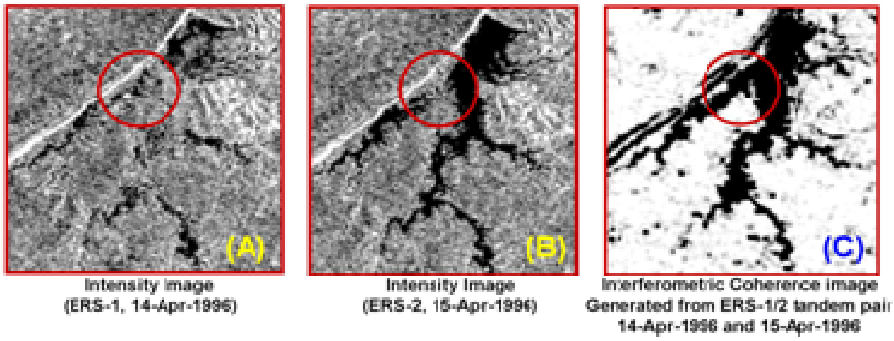

Fig. 19: Delineation of surface water under windy conditions using InSAR coherence (Srivastava et al. 2006b).

Acknowledgements: Author would like to express her gratitude to Dr. Ranganath R Navalgund, Director, Space Applications Centre, for his keen interest and encouragement during course of many studies which are included in this article. Author is also thankful to Dr. J S Parihar, Deputy Director, EPSA, Dr. Ajai, Group Director, MPSG, Dr. Manab Chakraborty, Group Director, ATDG, Dr. A K Shukla, Head, CVD, and Dr. Shiv Mohan, Head ATDD, for their support and encouragement.

References:

[1] Chakraborty, M. and Panigrahy. S., 2000, A processing and software system for rice crop inventory using multi-date RADARSAT ScanSAR data. *ISPRS Journal of Photogrammetry & Remote Sensing*, 55, 119-128.

[2] Choudhury, I. and Chakraborty, M., 2002, "An Empirical Approach to Retrieve the Transplantation Date of Rice Crop Using Radarsat SAR Data", *IAPRS & SIS, Vol.34*, Part 7, ISSN 1682-1777, "Resource And Environmental Monitoring", December 3-6, Hyderabad, India, 2002.

[3] C. Barbier, 2006, "Synthetic Aperture Radar - Another Look at Earth and Planetary Surfaces", *European Research Consortium for Informatics and Mathematics (ERCIM)-News*", 65, 12-13.

[4] C. H. Papas,1988, Theory of Electromagnetic Wave Propagation, Dover

[5] F. F. Sabins, 2007, Remote Sensing Principles and Applications, Waveland press, Inc.

[6] F. M. Henderson and J. Lewis, 1998, Principles & applications of Imaging Radar: Manual of Remote Sensing, Vol. 2. John Wiley & Sons, Inc., 461-465

[7] F. T. Ulaby, R. K. Moore, and A. K. Fung, 1986, Microwave Remote Sensing, Active and Passive, Volume 1, Artech House, Norwood, London.

[8] F. T. Ulaby, R. K. Moore, and A. K. Fung, 1986, Microwave Remote Sensing, Active and Passive, Volume 2, Artech House, Norwood, London..

[9] F. T. Ulaby, R. K. Moore, and A. K. Fung, 1986, Microwave Remote Sensing, Active and Passive, Volume 3, Artech House, Norwood, London..

[10] H. S. Srivastava, P. Patel, Y. Sharma and R. R. Navalgund, 2009a, Large-area soil moisture estimation using multi-incidence-angle RADARSAT-1 SAR data. *IEEE Trans. Geosci. Remote Sensing*, **47**, 2528–2535

[11] H. S. Srivastava, P. Patel, Y. Sharma and R. R. Navalgund, 2009b, "Multi-frequency and multi-polarized SAR response to thin vegetation and scattered trees" *Current Science, 97(3),* 425-429.

[12] H. S. Srivastava, P. Patel, Y. Sharma, and R. R. Navalgund, 2007,"Detection and Density Mapping of Forested Areas using SAR Interferometric Technique, *International Journal of Geoinformatics, 03(2*), 1-10.

[13] H. S. Srivastava, 2007, "Interaction of multi-frequency and multi-polarized DLR ESAR data with various targets: A case study with C, L and P Bands acquired at all the four linear (VV, HH, VH & HV) polarizations", presented at *JEP-MW conference*,15-16 May 2007, Ahmedabad, India, sponsored by Space Applications Centre (ISRO).

[14] H. S. Srivastava, P. Patel and R. R. Navalgund, 2006a, "How far SAR has fulfilled its expectation for soil moisture retrieval?" *Proc. SPIE* Vol**.** 6410, 641001

[15] H. S. Srivastava, P. Patel, and R. R. Navalgund, 2006b, "Application potentials of Synthetic Aperture Radar Interferometry (InSAR) for land cover mapping and crop height estimation", *Current Science, 91(6),* 783-788.

[16] H. S. Srivastava, P. Patel, Y. Sharma and R. R. Navalgund, 2006c, "Comparative Evaluation of Potential of Optical and SAR Data for the Detection of Human Settlements Using Digital Classification", *International Journal of Geoinformatics, 02*(03), 21-28

[17] H. S. Srivastava, P. Patel, M. L. Manchanda and S. Adiga, 2003, Use of Multiincidence angle RADARSAT-1 SAR data to incorporate the effect of surface roughness in soil moisture estimation, *IEEE Trans. Geosci. Remote Sensing, 41(07*), 1638-1640

[18] K. J. Ranson, S. Saatchi and G. Sun, 1995, Boreal forest ecosystem characterization with SIR-C/X-SAR, *IEEE Transaction on Geoscience and Remote Sensing, 33,* 867-876.

[19] M. C. Dobson, C. Craig, F. T. Ulaby, T. Le Toan, A. Beaudoin, E. S. Kasischke and N. Christensen, 1992, Dependence of Radar Backscatter on Coniferous Forest Biomass, *IEEE Transaction on Geoscience and Remote Sensing, 30(2)*, 412-415.

[20] M. C. Dobson, F. T. Ulaby, L. E. Pierce, T. L. Sharik, K. M. Bergen, J. Kellndorfer, J. R. Kendra, E.

Li, Y. C. Lin, A. Nashashibi, K. Sarabandi and P. Siqueira, 1995, Estimation of forest biophysical characteristics in northern Michigan with SIR-C/X-SAR, *IEEE Transaction on Geoscience and Remote Sensing, 33*, 877-895.

[21] M. I. Skolnik, 2008, Radar Handbook, McGraw-Hill.

[22] Panigrahy, S., Chakraborty, M., Manjunath, K.R., Kundu, N., Parihar, J.S., 2000, Evaluation of RADARSAT ScanSAR Synthetic Aperture Radar data for rice crop inventory and monitoring, *Journal of the Indian Society of Remote Sensing*, 28, 59-65

[23] P. A. Harrell, E. S. Kasischke, L. L. Bourgeau-Chavez, E. M. Haney and N. L. Christensen, 1997, Evaluation of approaches to estimating above ground biomass in southern pine forests using SIR-C data, *Remote Sensing of Environment*. 59, 223-233.

[24] P. Patel, H S Srivastava and Ranganath R. Navalgund, 2009, "Use of SAR polarimetry to characterise wetland targets of Keoladeo National Park", *Current Science, 97(4),* 529-537.

[25] P. Patel and R R. Navalgund, 2008, "Target vector decomposition for Hybrid polarimetry", Proceedings of ISRS-2008 National Symposium on '*Advances in Remote Sensing Technology and Applications with Special Emphasis on Microwave Remote Sensing*', Ahmedabad, Dec 18-20, 2008.

[26] P. Patel, 2007, Polarimetric SAR classification using physical based scattering mechanism: comparative evaluation of L and P bands, *Conference of Joint Experiment Project Towards Microwave Remote Sensing Data Utilisation (JEP-MW), Conference Papers*, 15-16 May 2007, SAC, Ahmedabad, pp. 2:42-2:57.

[27] P. Patel, H. S. Srivastava, S. Panigrahy and J. S. Parihar, 2006a, Comparative evaluation of the sensitivity of multi-polarized multifrequency SAR backscatter to plant density, *International Journal of Remote Sensing, 27(2),* 293-305.

[28] P. Patel, H S Srivastava and Ranganath R. Navalgund, 2006b, "Estimating Wheat Yield At Grain Filling Stage: An Approach For Estimating Number Of Grains Using Cross-Polarised ENVISAT-1 ASAR Data", *Proc. SPIE* Vol. 6410, 641001, SPIE Digital Library (http://spiedl.aip.org) Vol.6410, Paper Number: 641009, pp. 01-12

[29] P. Patel and Sushma Panigrahy, 2004, "Methodology to estimate flood damage to rice production using temporal synthetic Aperture Radar data." *International Symposium on Natural Hazards- INTROMET-2004*, 24th to 27th February 2004.

[30] P. Patel , H S Srivastava , Sushma Panigrahy and Manab Chakraborty, 2003, "Effect of Crop Cover and Surface Roughness on sensitivity of SAR backscatter to soil moisture" Presented at the 1st *International conference on Microwaves, antenna, Propagation and Remote Sensing- ICMARS-2003* organized by International Center for Radio Science at Jodhpur during 17th to 19th December, 2003.

[31] P. Patel, S Panigrahy and M Chakraborty, 2002, Performance of RADARSAT Extended Low Beam SAR data for Soil moisture Retrieval, *Asian Journal of Geoinformatics, Vol. 2*, No. 3, March 2002, pp. 85-91.

[32] P. Patel and Sushma Panigrahy 2002, Monitoring soil moisture condition of rice fields using steep and shallow incidence angle Radarsat synthetic aperture radar data – a case study from India., , *Proceedings of ISPRS technical commission VII symposium on Resource and Environmental Monitoring* held at Hyderabad December 3-6,2002

[33] P. Patel, Mohan, S., Sharma, S., Sutrodhar, A. K., Khawas, B. K. and Das, D. K., 2001, Evaluation of multi-incidence angle RADARSAT SAR data for soil moisture estimation, Physical Methods of Soil characterization, Narosa Publishing House, New Delhi, 2001, pp.133-140.

[34] Orsamby, J. P., Blanchard, J. P. and Blanchard, A. J., (1985), Detection of lowland flooding using active microwave systems, *Photogrammetric Engineering and Remote Sensing*, Vol. 51, No. 3, pp. 317-328.

[35] R. M. Green, 1998, Relationships between polarimetric SAR backscatter and forest canopy and sub-canopy biophysical properties, *International Journal of Remote Sensing*. 19, 2395-2412.

[36] T. Le Toan, A. Beaudoin, J. Riom and D. Guyon, 1992, Relating Forest Biomass to SAR Data, *IEEE Transaction on Geoscience and Remote Sensing*, 30(2), 403-411.

[37] U. Wegmuller and C. L. Werner, 1995, SAR interferometric signatures of forests *IEEE Trans. Geoscience. Remote Sensing, 33,* 1153–1161

Signatures, Newsletter of the ISRS–AC, Vol. 22, No.4, Nov-Dec 2010

Microwave Remote Sensing Applications for Terrestrial and Lunar Surface

Shiv Mohan, SAC, Ahmedabad, Email: shivmohan@sac.isro.gov.in

Remote Sensing of the earth's surface at visible and infrared wavelengths has provided useful scientific data for various earth resources applications. However, under cloud cover conditions, operational capabilities of visible and IR sensors are limited. In contrast, clouds are more transparent at microwave frequencies. Hence microwave sensors play an important role in data collection which is independent of weather and sunlight conditions. Besides, sensitivity of microwaves for moisture is of importance in providing information about soil moisture, canopy moisture and snow wetness. In addition, cloud penetration capability of microwaves help in providing timely and reliable data for studies related to vegetation monitoring, flood area assessment and surface water mapping. The characteristics of radar images that have been especially useful for geological studies are – sensitivity to surface roughness geometry and surface slope. This capability of radar images help in detecting subtle variation in surface topography, which in turn can be related to geological features. Capability of radar frequencies to penetrate surfaces is of tremendous value in acquiring subsurface geological information. In recent years, role of microwave remote sensing for planetary remote sensing has revealed new observations of lunar surface, which is also discussed here.

A number of applications demonstrated using radar sensors for various land and water resources studies are being discussed here. Recent studies on SAR interferometry have also shown encouraging results. SAR applications to soil moisture and crop monitoring has been a subject of study for more than two decades. Major concern was to identify the important crops for early acreage estimation. The microwave data has been used extensively for agricultural applications because of need of data for crop discrimination and acreage estimation. In general, radar backscatter from a crop consists of contribution from soil backscattering, vegetation volume backscattering and backscattering from soil vegetation double bounce interaction. The contribution of each component would be variable depending upon the growth of the crop. Thus, radar backscatter would be temporally varying and the component of each scattering would be governed by the dielectric and roughness of soil and vegetation. For a single band data, one would be using temporal signatures of the crop for accurately discriminating the crop. Due to non availability of Polarimetric data, multi-date data was used for crop acreage estimation. The potential of single date multi-polarised data is found to be superior in advancing the date of crop acreage forecasting. Multi-date data analysis for crop discrimination (Fig. 1) is compared with polarimetric SAR observations (Fig. 2), showing ability of polarimetric SAR for crop discrimination. Major crops of the study are Rabi crops namely wheat, gram and mustard. Overall classification accuracy was better than 90% using multi-temporal or polarimetric SAR data. Thus, polarimetry would help in early assessment of crop acreage. Similar observations are noted for other crops.

The assessment of soil moisture had been another area of research since long. The knowledge of soil moisture is important for the development of global hydrological cycle. The moisture content of soil varies with relative dielectric constant of soil and hence its microwave scattering coefficients. Efforts are being made by developing a suitable model for minimizing the effect of roughness and vegetation. Alternatively, relative moisture was also found to be suitable for many applications. Fig 3 shows relative moisture for the areas covering parts of Karnataka. A similar method was used for assessing the drought conditions in areas covering parts of Orissa.

Investigations of vegetation structure are important in the understanding the potential role of microwave

sensors for deriving estimates of forest biomass and vegetation structure. In deciduous forests, the leaves were believed to be most important scatters of X-band waves; however, L-band wave with HH polarization penetrated through leaves and were scattered back from the branches of trees. Plant height, density, geometry, and the presence or absence of standing water at the surface influence the SAR response, but incidence angle and polarization can also have a significant effect. Multi-polarization SAR data may be used to estimates forest properties such as total tree biomass, basal area and tree height. Radar surveys for mapping of forested areas and determining the extent to which forest density, type, species could be identified on SAR image has also been reported. A typical model relating radar backscatter with biomass is shown in Fig 4, whereas biomass index at two frequencies is shown in Fig. 5.

Flood is a natural hydrological hazard which occurs frequently. Timely information about the flood is important for the decision makers. Flood plain and flood inundation mapping, surface water mapping including estuary and wet land survey, have received considerable attention. Floods occur in India almost every year and cause considerable damage to crops, human life, property etc. One of the important information required is the nature and extent of the damage caused by floods in the flood prone areas. Thus, flood mapping during the flooding and flood plain mapping after the flood recedes is essential. The applicability of microwaves in these areas is unique because of the sensitivity of microwave radiation to surface geometry, slope and its capability to penetrate through clouds, which are prevalent during the flooding period.

In microwave region, a snow layer causes both attenuation and scattering of signal. The dielectric properties of snow at a given frequency are generally dependent on the relative proportion of liquid and solid water present in the snow by volume, density and crystal structure. Radar echo from snow covered terrain consists of contribution resulting from the backscattering by the snow-air interface, scattering from underlying soil or ice and volume scattering from snow layer. Sub-surface imaging is another area of interest. In case of desert terrain, radar signals penetrate the surface and subsurface images of targets result. Fig 6 shows a typical signature of limestone buried in sand cover. Signal decomposition techniques using polarimetric SAR has been a topic of concern for various researches. Fig 7 shows comparative performance of full and hybrid polarimetric data indicating advantages of full polarimetry over hybrid techniques. Classification methods using polarimetric parameters like entropy and scattering angle is shown in Fig. 8. The evolution of interferometric SAR has given rise to a new way of generating high resolution DEM and land cover maps. Fig 9 shows a typical comparison of optical data with interferometric method for land use study indicating the success of such methods.

Ocean wind speed and direction is another suitable application of SAR data. The roughness created by the winds can be picked up by the SAR sensors causing a suitable relation between wind speed and direction. Wave front study is another important application. Wave front appears when two water masses meet, that is ocean water and river water, turbid water and less turbid water, and water with different temperatures. Bathymetry relates to the expression of bottom topography on sea surface during calm conditions, mostly suitable for coastal areas studies. Oil release from ship during accident or cleaning tanks during transit influences the marine environment. The detection of oil spill becomes feasible due to dampening of short wave and creates large patches of low reflectivity. Oil spills/Slick look alike may include natural thin film, threshold wind speed areas, wind sheltering by land mass, rain fall, current shear zones, internal waves and upwelling.

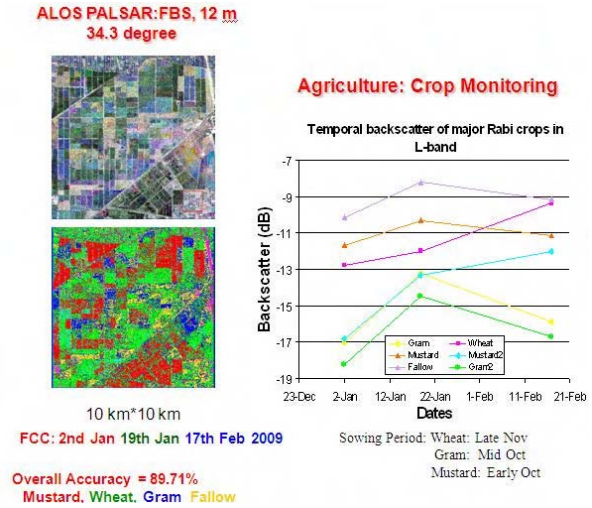

Fig-1

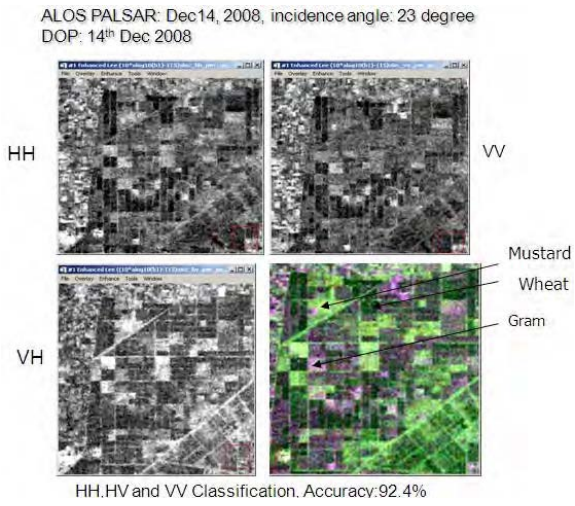

Fig-2

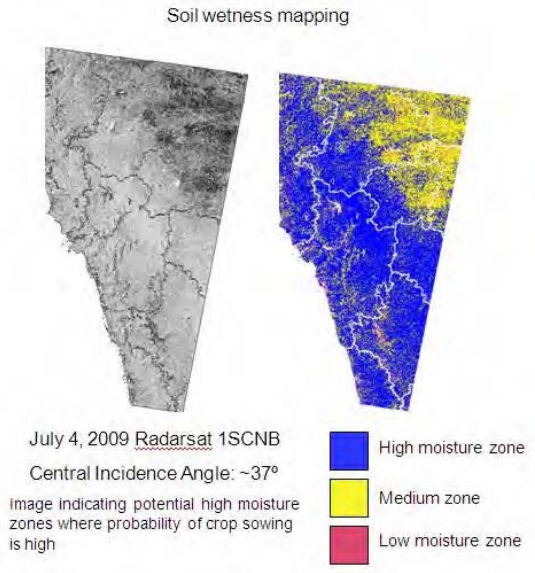

Fig-3

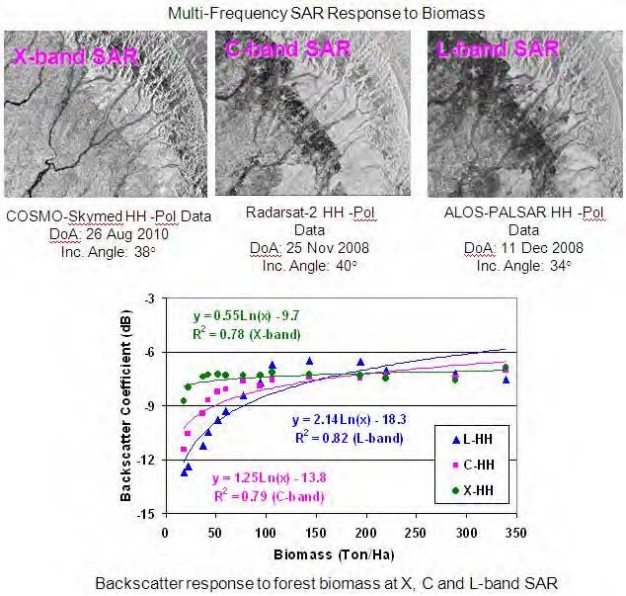

Fig-4

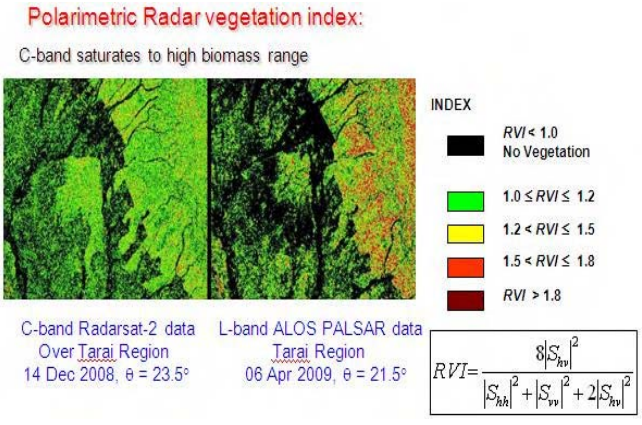

Fig-5

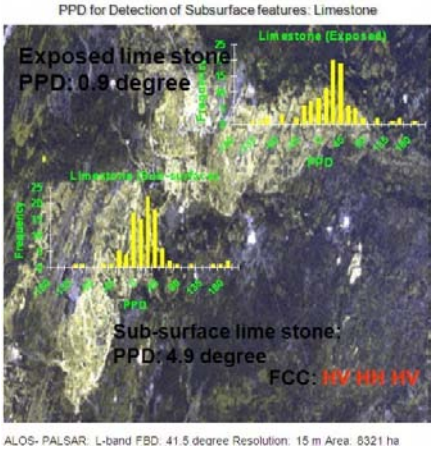

Fig-6

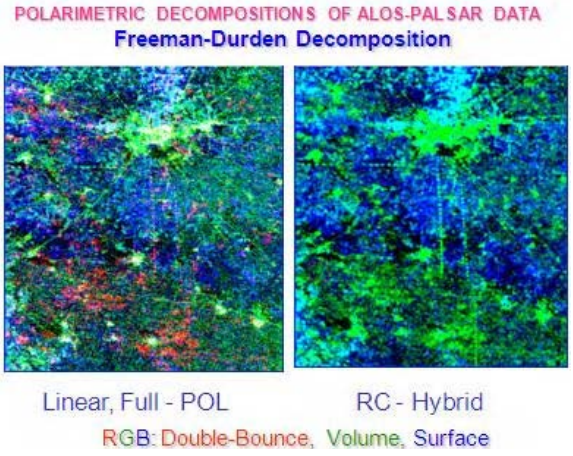

Fig-7

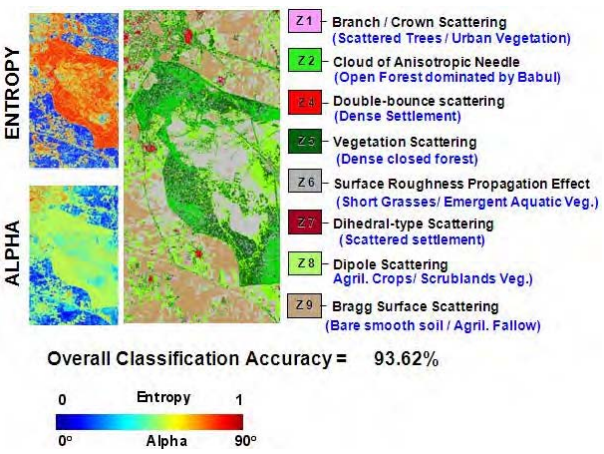

Fig-8

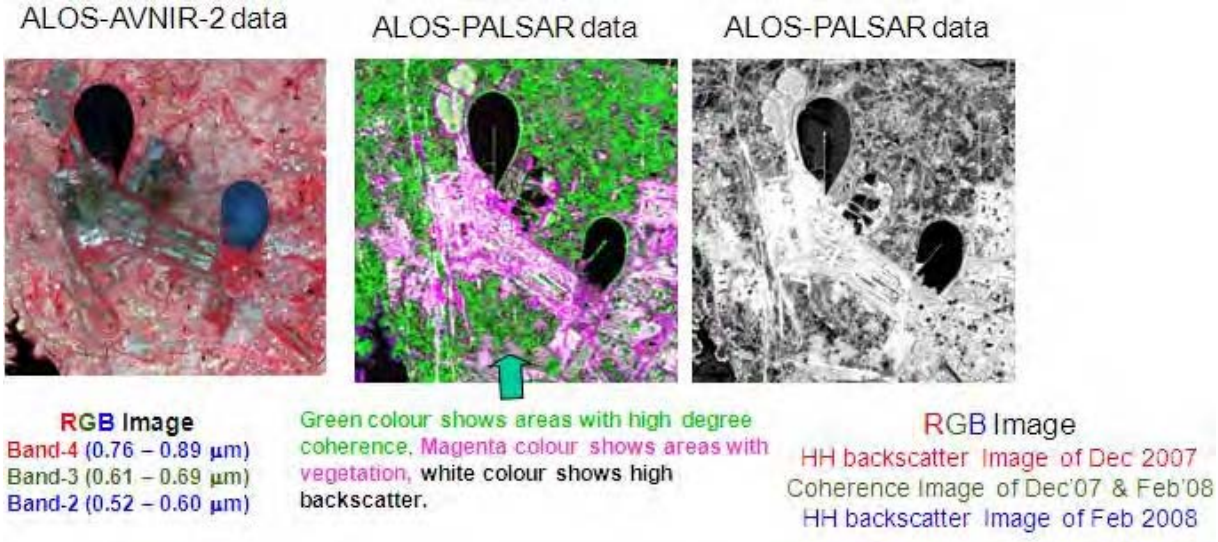

Fig-9

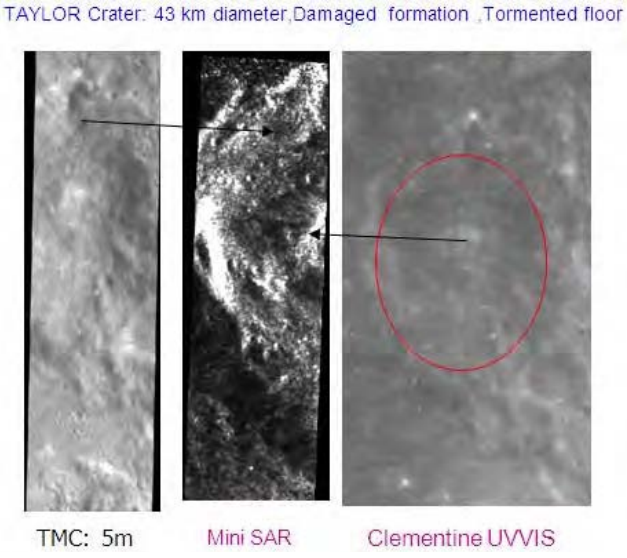

Fig-10

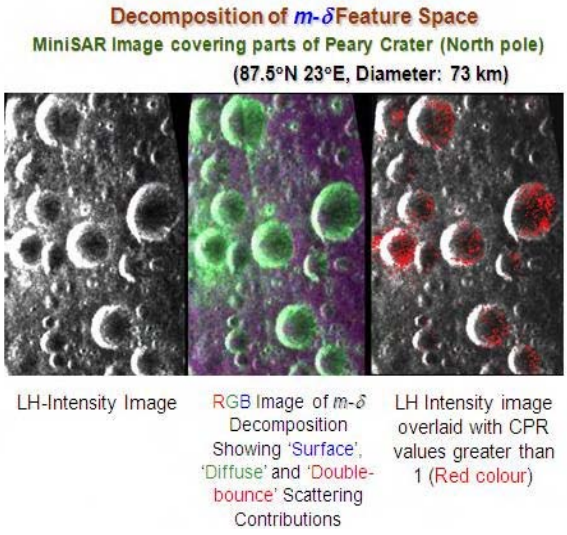

Fig-11

Planetary exploration has become important because of the region that microwave can penetrate through planetary atmosphere as well as surface of the planets. Lunar surface is a rocky surface full of craters with no trace of life. The microwave remote sensing of lunar surface provides answer to some of the questions related to water ice, knowledge on material's physical and electrical properties. Due to penetration of signal in the regolith, new insight to structural details could be provided. Fig 10 shows a comparison of optical and mini SAR data. The damages due to formation of crater are hidden below the lunar regolith, which is clearly depicted in SAR image.

Typical planetary surfaces reverse the polarization during the reflection. The ratio of received power from same sense (Right circular) to the opposite sense (Left Circular), or vice-versa. This is called radar circular polarization ratio (CPR). Most of the Lunar surface has a low CPR, which is considered to be the normal signal return. Some targets with high CPR are characteristic of rough surface or planetary ice. Generally, fresh craters are more rough than old craters, thus fresh craters are identified with the help of CPR. Some surfaces like ice embedded in regolith or below the regolith also tend to have high CPR, which is reflected in polar region. Due to permanently under sun shadow, these areas are very cold and water ice is stable (essentially) indefinitely. It is hypothesized that volatile material including water ice could be trapped in such low temperature regions. Mini SAR has estimated a number of such locations on the lunar polar region. A typical mini SAR image showing areas of water ice is depicted in Fig. 11. However, a confirmation on such observation by excluding roughness still needs to be seen. Mini SAR in Chandrayaan-2 with two frequencies SAR would provide many of confirmed observations on water ice.

Naturally Remote Sensing

- Many nocturnal animals have evolved extraordinary rotational ability in the neck. Owls can rotate their neck through 270° and this aid in their vision.
- Most of the birds have their eyes mounted laterally on their heads, which aids them to view 340 degrees except in back of their heads. Falcon has a great sight. It can see a 10 cm object from a distance of 1.5 km.
- Ants can detect the small movements through 5 cm of earth and can see polarized light.
- Cat has a hearing range between 100 and 60,000 Hz. Its olfactory membrane is about 14 sq. cm. as compared to the human's olfactory membrane which is about 4 sq. cm.
- Chameleon eyes can move independently and can see in two different directions at the same time.
- Scorpion can detect air moving at only 0.072 km/hr with special hairs on its pincers and can have as many as 12 eyes.

Compiled by: Amit Shukla

Signatures, Newsletter of the ISRS–AC, Vol. 22, No.4, Nov-Dec 2010

Rice Crop Monitoring in India Using SAR Data: Current Status & Future Prospects Using RISAT Data

M. Chakraborty, S. Panigrahy, C. Patnaik and J. S. Parihar, SAC, Ahmedabad, Email: sushma@sac.isro.gov.in

1. Introduction: Crop area monitoring using remote sensing data is one the major satellite remote sensing application programme in India being done operationally under the aegis of the project Crop Acreage and Production Estimation (CAPE) of Dept. of Agriculture & Cooperation, Ministry of Agriculture, Govt. of India implemented since 1987. Microwave remote sensing has a crucial role in crop monitoring in India as the major crop season known as *kharif* coincides with the monsoon period, thus limiting the availability of optical remote sensing data. Scope of operational use of microwave data for crop monitoring started with the launch of ERS and RADARSAT satellites that provided C band Synthetic Aperture Radar data. Initial investigations showed that rice crop registered a typical and unique temporal radar backscatter, which can be used to identify the rice fields with high accuracy. Interaction of SAR with rice is unique due the specific cultural practice followed by way of flooding the fields called puddling. A constantly flooded field (with constant water depth) acts as a uniform background which allows unambiguous inversion of the observed backscatter to the plant growth. Under this ideal condition, monotonic rise of SAR backscatter from rice fields (from transplantation to peak vegetative stage) observed forms the basis of rice field identification. Even under the non-ideal condition of fluctuating water levels, the growth pattern is unique to identify rice fields from other classes like water, urban, forest etc. (Fig.1 Typical temporal backscatter of lowland rice crop in C band HH polarization SAR data and other classes.)

Based on these observations, the national rice crop monitoring was planned and executed in India since 1999 using Radarsat C band HH SAR data. Area estimates are made well in advance of the crop harvest. Kharif or rainy season rice, which is the main crop in India, is monitored for thirteen states accounting for more than 90 per cent of kharif production.

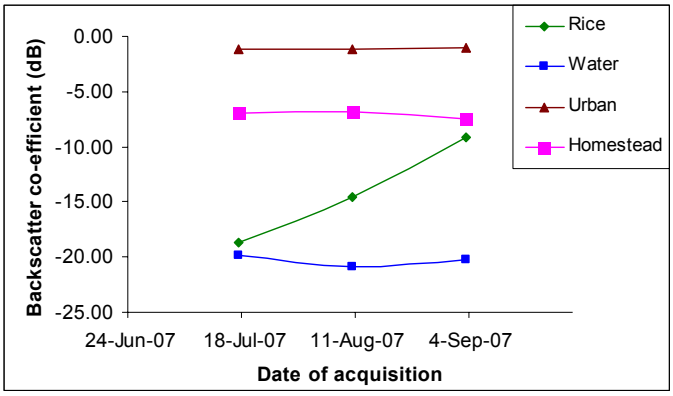

Fig. 1

Since, the area covered is very large, optimisation has been done in terms of choice of data and acquisition dates. Radarsat ScanSAR Narrow beam B data is used. ScanSAR is unique to the Radarsat system. ScanSAR data was selected because of its large swath (300 km) and the Narrow beam B position because of its incidence angle range (31-46 degrees), that is better suited for crop studies. These states get covered by around 34 ScanSAR scenes. Multi-date data were used as dataset to derive information on rice area. First-date data was acquired coinciding with the puddling to transplanting stage. Subsequent two data are acquired with a 24-day repeat cycle. The rice crop calendar is taken into consideration to decide the period of data acquisition. Rice planting in India coincides with onset of monsoon. There is a latitudinal and longitudinal variation in rice planting in India. Similarly, there exists variation within a state due to various cultural practices and socio-economic conditions. Thus, it is rather easy for selecting optimum data set for areas that follow a fixed period of planting like in irrigated systems of Punjab, Haryana, but requires fine tuning for rainfed systems, based on monsoon performance.

2. Current status

2.1 Crop area and condition: A Multiple Scattering Radiative Transfer (RT) model has been calibrated and validated using a large number of samples of *in situ* data of rice crop signature covering a wide spectrum of growing environment and crop variety (Fig.2). Based on this model, decision rules have been developed to classify the temporal SAR data. An early estimate of crop prospects using two-date data acquired within 30-35 days of planting is obtained.

The estimates are updated using third and fourth date data. This procedure also enables to detect flood and moisture stress during the crop cycle. Thus, during the super cyclone of Orissa in 1999, it was feasible to identify the storm surge affected areas with high accuracy and quantify the production loss taking into account the age of the crop and duration of submergence.

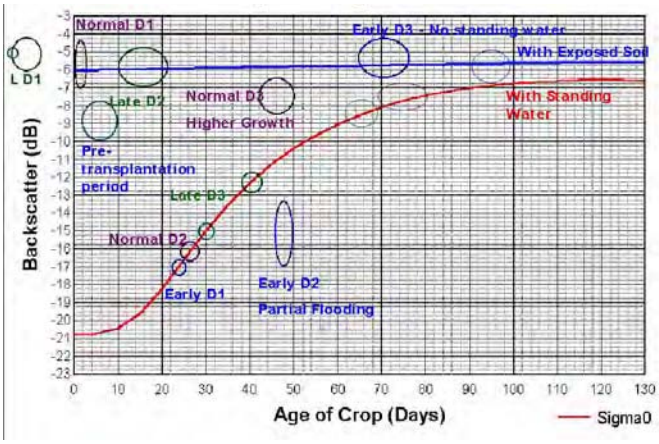

Fig. 2: Multiple Scattering RT model calibrated for Indian rice crop for C band HH polarization data

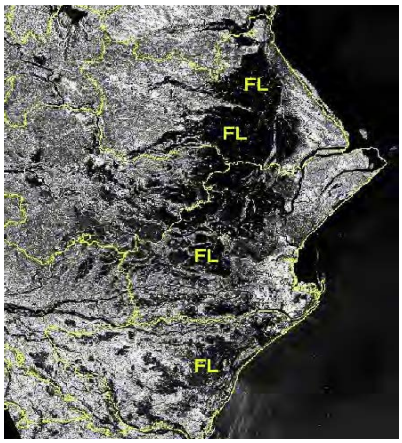

Fig. 3: Radarsat SAR data of Nov. 2, 1999 showing flooded rice fields and other land cover (dark areas marked FL) due to storm surge after Super cyclone (occurred during October 29, 1999).

2.2 Crop Calendar: The procedure enables to compute the progress of planting and obtain the crop calendar spectrum in each state.

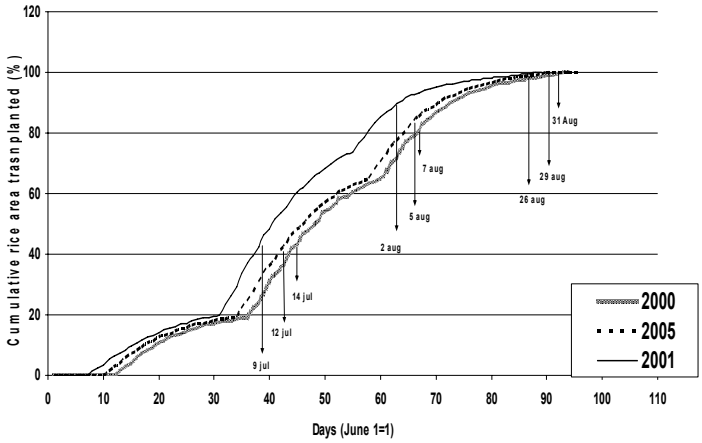

Fig.4: Transplanting period of kharif rice derived using 3 date SAR data for West Bengal; a) Cumulative transplanting curve during 2000, 2001 and 2005

3. Future Prospects with RISAT data: With the launch of RISAT, C band SAR data will be available in dual and quad polarization modes. Some of the additional achievements envisaged using polarimetric data for rice crop are modeling biophysical parameters for crop yield and improving area estimates (timeliness and accuracy).

3.1 Crop yield: Currently a statistical model has been developed for rice biomass estimation using HH polarization data. A Least-square fitting of the backscatter curves with observed biomass (wet) data has been used to generate the calibration curve, which is used for predicting fresh peak biomass. This is used to estimate grain yield using tabulated dry/fresh biomass, harvest index and grain/chaff ratios. Results have shown that though the C band HH polarisation backscatter has a good correlation with rice crop height, the relation with biomass is of limited accuracy. The multi polarised data can enable to develop generic models for biomass estimation with acceptable accuracy.

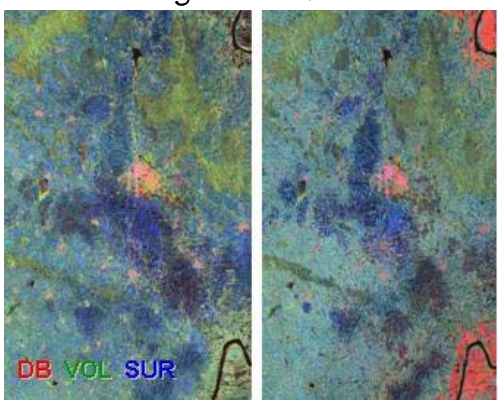

Fig.5: Freeman-Durden decomposed image of polarimetric SAR data 24 days apart. The Red area near the river is rice area that has come up and detected early.

Currently, at least two date data is required to identify the rice fields and estimate the area using single polarization data. Investigations have shown that single date polarimetric data has the potential to identify rice fields with better accuracy.

Figure 5 illustrates this. This will enable advancing the area estimates and also providing multiple estimates. However, for an operational procedure, the current limitation is the volume of data to be analysed as the polarimetric SAR data is still on a small area basis.

Historically Remote Sensing

- Before the discovery of the telescope, the only observing device that people could use was the human eye aided by the variety of sighting devices. The Chinese used armillary spheres, the Neolithic farmers made Stonehenge to point to midsummer sunrise.
- In 1927, Roger Bacon used the principle of the camera obscura to create optical illusions with sunlight.
- Firstly in 1862, the Balloons were used to map a forest. The aerial observations and possible photography, for military purposes were also acquired from balloons in the Civil War during that time.
- In 1879, Eastman discovered the formula for making a successful gelatin emulsion covered dry-plate and built a machine for coating dry plates with the emulsion. These developments led to the invention of rolled paper film. The resulting prints were sharp, clear and free from paper grain distortion.
- In 1906, George R. Lawrence took oblique aerial pictures of San Francisco after the earthquake and fires by using many large kites to lift a huge camera. In 1901 he had also shot aerial photographs from a cage attached to a balloon.
- By the first world war, cameras mounted on airplanes provided aerial views of fairly large surface areas that proved invaluable in military reconnaissance.
- In 1936, Captain Albert W. Stevens had taken the first photograph of the actual curvature of the earth from a free balloon at an altitude of 72,000 feet.
- In 1956-1958, W.M. Stinton discovered absorption features in his spectra of Mars that appeared to be consistent with chlorophyll. This was an interesting application of vegetation remote sensing. However, these observations were later explained as resulting from an absorption band due to deuterated water.

Compiled by: Amit Shukla

Signatures, Newsletter of the ISRS–AC, Vol. 22, No.4, Nov-Dec 2010

Conjunctive use of RADARSAT and ENVISAT Data for Biophysical Parameter Retrieval Research:

A Case Study in Bardhaman district, West Bengal

Indrani Choudhury[1] & M.Chakraborty[2], [1]Visiting Faculty, MG Science College, Ahmedabad; [2]SAC, Ahmedabad

1. Introduction: Rice is the staple food for majority of Asian population representing 35% of their daily caloric intake [10] and accounts for 11 % of global crop land area [13]. Hence, timely monitoring of rice agriculture is very important for agricultural and environmental sustainability, food & water security and assessing green house gas emissions. Sensitivity of Synthetic Aperture Radar (SAR) to crop geometry and flooded condition of rice field, in addition to its all-weather, day-and-night imaging capabilities increase its potential for rice cop monitoring in monsoon Asia [7]. Since the launch of the ERS-1/2, RADRSAT and ENVISAT, a number of studies has demonstrated the potential of C-band SAR data for rice crop research [1; 8; 12]. They reported results on various aspects including experimental SAR data analysis as a function of crop biophysical parameters and temporal change, interpretation of the observations by theoretical modeling, rice growth models for crop yield prediction etc. In different growing stages, rice crop has different conditions (height, structure, moisture content etc.) and these factors affect the SAR return signal, which can be strongly correlated to crop biophysical parameters [11;12] and can form as an input for crop yield and condition assessment models [2]. Temporal change in SAR backscatter from transplanting to maturity stage has proved to be effective for rice crop growth monitoring and condition assessment. Successful crop growth stage identification using satellite data relies on image acquisitions during key crop growth stages. Unique potential of SAR for rice crop research is a well established fact but has limitation due to temporal resolution. Therefore, in the present study, the conjunctive use of RADRSAT and ENVISAT data was explored for rice crop biophysical parameters retrieval research, which will provide complementary information for crop growth models and condition assessment with high temporal resolution and therefore, can improve the estimation of crop growth variables with higher accuracy.

2. Study Area and Data Used: A study area that extends from 22°52′45″ to 23°29′35″ N and 87°34′33″ to 88°16′34″ E was selected in the Bardhaman District, West Bengal. The topography has a gentle slope. The rice fields have bunds whose height varies from 5-50 cm. Kharif rice is the single dominant crop covering around 90% of the total agricultural area [5]. Lal Swarna, a common semi-dwarf variety with life span of 120 days is grown in the district. The crop is having a wide transplanting calendar from June end to August. Transplanting of 20-day old seedlings is the common practice. Three-date RADARSAT SCNB mode, C-band (5.3 GHz, HH polarization and 31-46° incidence angle) data were acquired during July-August with 24-days repetivity. The first date data was acquired on July 12, 2005, coinciding with puddling/transplanting stage. The other two dates (August 5 and August 29, 2005) covered up to vegetative stage of the crop. Multi-parametric ENVISAT data of APP mode (HV/HH) were acquired during September 13 (IS4, incidence angle 31-36°), September 29 and November 7 (IS5, incidence angle 35.8-39.4°), 2005 covering peak vegetative to maturity stage of the crop.

3. Methodology

3.1 Collection of Ground Truth (GT) data: GPS receiver was used to locate the GT sites in 18

villages. Within each village, contiguous rice fields each of size > 0.5 ha were selected for intensive collection of GT data synchronous with the SAR passes. All together 119 data points were collected from a sample plot of 50 m ×50 m throughout growing stage of the crop. GT sites included the information of soil and crop parameters *viz.* soil condition, land category, water depth, field bund height, rice variety, growth stages, general vigour, date of sowing, expected date of harvest, wet biomass, plant height, crop age, other leaf parameters etc. Synchronous GT was collected for each SAR pass and was repeated for all the sites and for all the passes.

3.2 Pre-processing of RADARSAT data: The processing of three-date RADARSAT data was carried out using "SARCROPS" developed around EASI/PACE image processing software [3]. The steps include: i) Data download: Transferring image and header data to hard disk from CDROM; ii) Speckle suppression: Enhanced Lee filter with 5×5 window size was used; & iii) Data calibration: The digital numbers (DN) were first converted to backscatter co-efficient (σ^0) in decibel (dB). The σ0 thus computed was then linearly scaled back to 8-bit (0-255) and written in the same image channel. In this process, the range of backscatter values stored was –26 to -0.5 dB, which contains all information required for agriculture and land cover classes. The dB thus recoded can be read out from 8-bit coded DN. Three-date ENVISAT data were processed using BEST (Basic Envisat and ERS SAR Tool) Software. The steps include: (i) Header analysis: To extract header information data from the file; ii) Full Resolution Extraction: To extract the 16 bit unsigned image from the ESA file; ii) Image filtering: Enhanced Lee filter of 5*5 window size was used; iii) Conversion from amplitude to power; iv) Generation of backscatter image [3]; v) Image flipping: dB image is horizontally flipped (east-west reversal of the data for descending mode) to generate a calibrated dB image. Multi-channel ENVISAT APP (HV/HH) datasets were generated and were imported to .pix format to carry out further analysis. Datasets were truncated to 8 bit. First date of RADARSAT data was geo-referenced using Ground Control Points (GCP) from header and a few additional GCPs from field observations were made using GPS. The other two dates of RADARSAT and the three dates ENVISAT images were co-registered with the first date RADAR data using 35 number of GCP points with second degree polynomial order. In all the cases, RMSE was less than sub pixel level. Processed multi-temporal RADARSAT and ENVISAT data showing all the land covers are depicted in Figure 1.

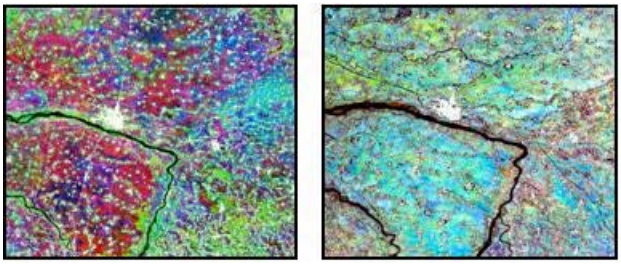

Figure 1: Multi-date calibrated geo-referenced FCC image of RADARSAT and ENVISAT (Cyan = Early Sown Rice; Blue = Normal Sown Rice; Red= Late Sown Rice; White= Urban; Black= Water; Homestead is shown as different shade of gray, green and brown).

3.3. Correlation Analysis: Correlation analysis of crop growth parameters and σ° was carried out using multiple regression techniques using Eq 1:

$\sigma° = ax^2+bx+c$---------- (1)

where x= crop growth parameters *viz.* plant height; crop biomass; crop age; a, b, c are polynomial fit coefficients. 'c' represents the backscatter from water filled field (puddle i.e. 0th height) and can provide a threshold to discriminate the just-transplanted field from puddle field and the linear term gives the sensitivity of SAR to the exposed crop growth parameters, co-efficient 'b' represents the initial response of backscatter increase to crop growth parameters (dB/cm). GT data collected in each

growing stage of the crop corresponding to SAR passes were used for analysis.

3.4. Mapping of Crop Biophysical Parameters: Inversion of empirical modelling i.e. inverting the relationship of σ° versus rice growth parameters were used to generate different spatial maps of crop growth parameters *viz*. rice crop height map, crop age map, biomass map. Inversion of crop growth parameters was carried out using first available date of SAR data acquired immediately after transplantation, which increases the accuracy of inversion. This inverted model is valid only for rice area, whereas in case of non-rice areas due to high backscatter value, model was not found functional. Therefore, the non-rice areas were merged into single classes and coded as zero. Mapping of crop biophysical parameters was generated for each of the date of SAR acquisition, separately for RADARSAT and ENVISAT to retrieve the crop growth parameters from planting to maturity stage of the crop. To determine the beginning of the crop growth stage, the acquisition date at which the backscatter of a rice pixel is the lowest was selected.

4. Results and Discussion: The temporal change in SAR backscatter from puddling/transplanting to maturity stage of the crop was found to be strongly correlated to key growth parameters i.e. crop age, plant height and biomass. The results are found to be similar with the previous studies [5; 11; 12].

4.1 Temporal Backscatter vs. Crop Biophysical Parameters: The empirical model reveals that at the time of transplantation, σ° was found to be –18 dB corresponding to crop age of 20 days. The crop attained its maturity at 100 days with σ° around –6.2 dB (Figure 2a) followed by slight decrease in σ° that is corresponding to the plant drying before harvest [14]. An increase of 11.8 dB was observed from transplanting to maturity stage. The model predicted that at the 0^{th} height, σ° from the puddle field with water surface is around –24 dB as represented by co-efficient 'c' and an increase of 0.33 dB/crop age (in days) as represented by co-efficient 'b'. The fitted curve in Figure 2b, shows an increasing trend in σ° as the crop growth progresses till first head emergence (initiation of panicle emergence [9]) i.e. around 90^{th} day from date of transplantation. Before transplanting i.e. at 0^{th} height, the σ° from the puddle field was found to be around -20 dB (co-efficient 'c') followed by transplanting of crop (-18.4 dB) with height increases at 0.26 dB/cm as represented (co-efficient 'b') and reached to –7.5dB (90^{th} day) with plant height of 90 cm (maximum height as estimated from the model). This is followed by a plateau till plant attained height of 100 cm. An increase of around 11 dB was observed from transplanting to panicle emergence. The model predicts (Figure 2c) that at the initial growth stages i.e. just after transplantation, the σ° was found to be –17.65 dB and it increased till it reached saturation at –5.9 dB when biomass was 5kg/m^2. An increase of 11.5 dB was observed from transplanting to maturity stage.

4.2 Retrieval of Biophysical Map: The crop biophysical maps are depicted in Figures 3a, 3b and 3c. Segmentation was observed, which could able to identify the rice fields at different levels of biophysical parameters from transplantation to maturity stage of the crop. The non-rice areas were presented as white colour.

Validation of the biophysical map generated from the inversion of the empirical models was carried using 1:1 line as depicted in Figure 4. In case of crop age (Figure 4a), the RMSE was found to be 2.80 days, in case of plant height map (Figure 4b), the RMSE was found to be 3.43 cm, in case of biomass map (Figure 4c), the RMSE was found to be 0. 61 kg/m^2.

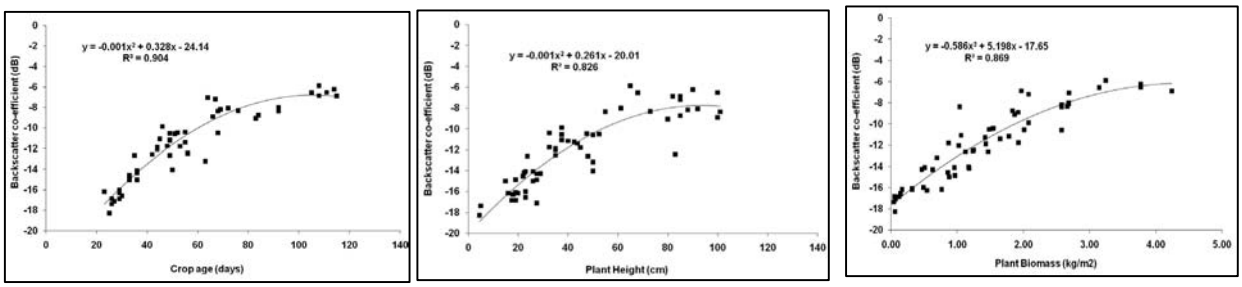

Fig 2: Temporal crop backscatter profile vs. biophysical parameter (2a. Crop age; 2b.Plant height; 2c. Fresh biomass)

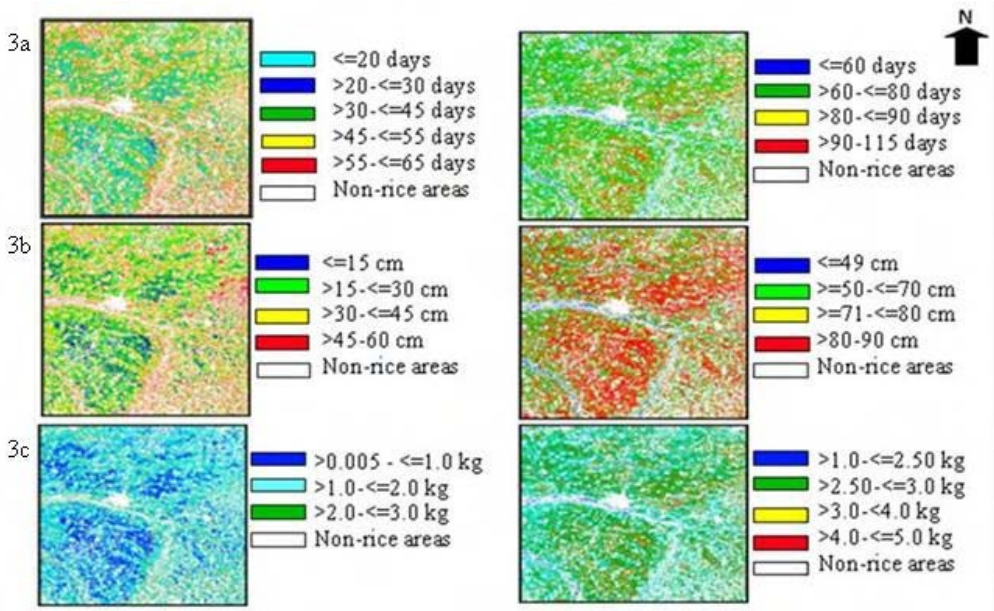

Fig 3: Mapping of crop biophysical parameters (3a. Crop age; 3b. Plant height; 3c. Fresh biomass)

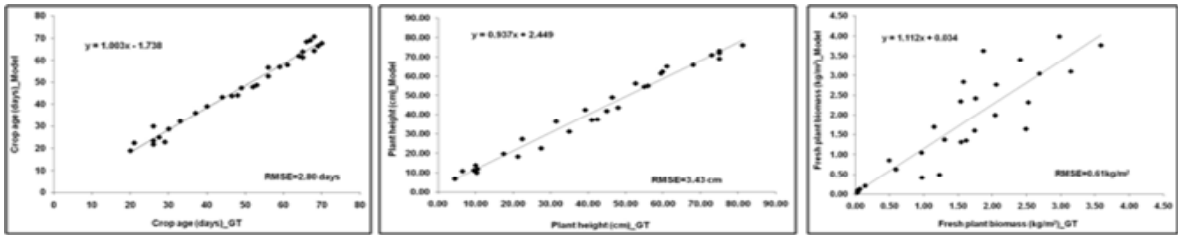

Fig 4: Validation of crop biophysical map (4a. Crop age; 4b. Plant height; 4c.Fresh biomass)

5. Conclusion: This study assesses the synergy of RADARSAT and ENVISAT data for rice crop biophysical parameter retrieval study. A second order multiple regression approach has shown promising results for deriving crop growth parameters from multi-sensor SAR data. These crop growth parameters can be an important input to rice crop yield model and condition assessment. Also, an

inversion of the RADARSAT and ENVISAT images acquired from initial crop growth stage to maturity stage into a map of rice growth parameter enabled to segregate the rice fields at different stages of crop age, plant height and biomass. Validation of the biophysical map shows encouraging result with RMSE 2.80 days, 3.43cm and 0.0.61 kg/m^2 for crop age, plant height and biomass, respectively. It is important to note that the data acquired during initial crop growth period and extending to the maturity stage results in achieving high accuracy for estimation of bio-physical parameter. Results illustrate that the calibrated data from multiple radar sensors can be used in combination. This increases the possibility of acquiring higher temporal coverage for rice growth monitoring and crop biophysical parameters retrieval study.

References

[1] Aschbacher,J.,Pongsrihadulchai,A.,Karnchanasutha-m,S., Rodprom, C., Paudyal, D.R. and Le Toan, T. (1995).Assessment of ERS-1 data for rice crop mapping and monitoring. *Proc. IGARSS,* Florence, Italy, July 1995, pp. 2183-2185.

[2] Brisco, B. and Brown, R.J. (1998). Agricultural applications with radar. *Principles and Applications of Imaging Radars (3rd Edn.)*. Manual of Remote Sensing, **Vol. 2**. John Wiley and Sons, Inc., New York, pp. 381-406.

[3] Chakraborty, M. and Panigrahy, S. (2000). A processing and software system for rice crop inventory using multi-date RADARSAT ScanSAR data. *ISPRS J. Photogramm. Remote Sen.* **55**(2), 119-128.

[4] Chakraborty, M., Panigrahy, S. and Sharma, S.A. (1997). Discrimination of rice crop grown under different cultural practices using temporal ERS-1 Synthetic aperture radar data. *ISPRS J. Photogramm and Remote Sen.* **52**, pp. 183-191.

[5] Chakraborty, M., Manjunath, K.R., Panigrahy,S., Kundu, N. and Parihar, J.S. (2005). Rice crop parameter retrieval using multi-temporal, multi-incidence angle Radarsat SAR data. *ISPRS J. Photogramm. Remote Sen.* **59,** pp**.** 310-322.

[6] Choudhury, I. and Chakraborty, M. (2002). An empirical approach to retrieve the transplantation date of rice crop using RADARSAT SAR data. *Proc. ISPRS,* Hyderabad, India, 2002.

[7] Choudhury, I. and Chakraborty, M. (2006). SAR signature investigation of rice crop using RADARSAT data. *Int. J. Remote Sens.* **27** (3-4), pp. 519-534.

[8] Choudhury, I., Chakraborty, M., and Parihar, J.S. (2007). "Estimation of rice growth parameter and crop phenology with conjunctive use of RADARSAT and ENVISAT", *International Symposium on " ENVISAT Symposium 2007", April 23-27, 2007, Montreux, Switzerland*.

[9] De Datta, S.K. (1981). Principles and practices of rice production. John Wiley & Sons, pp. 221-228.

[10] FAO. (2004). Statistical database of the Food and Agricultural Organization of the United Nations.

[11] Inoue,Y., Kurosu,T., Maeno, H., Uratsuka, S., Kozu,T., Dabrowska Zielinska, K. and Qi,J. (2002). Season-long daily measurements of multi-frequency (Ka, Ku, X, C, and L) and full-polarization backscatter signatures over paddy rice field and their relationship with biological variables. *Remote Sens. Env.***81**, pp. 194– 204.

[12] Le Toan, T., Ribbes, F., Wang, F.L., Floury, N., Ding, K.H., Kong, J.A. and Fujita, M. (1997). Rice crop mapping and monitoring using ERS-1 data based on experiment and modeling results. *IEEE Trans. Geosci. Remote Sens.* **35**(1), pp. 41-56.

[13] Maclean, J.L., Dawe, D.C., Hardy, B. and Hettel, G.P. (2002). *Rice almanac: Source book for the most important economic activity on earth* (3rd Edn.) CABI Publishing.

Signatures, Newsletter of the ISRS–AC, Vol. 22, No.4, Nov-Dec 2010

Microwave Remote Sensing of Nalsarovar

- A Notified Wetland, Gujarat

TVR Murthy & Sushma Panigrahy, SAC, Ahmedabad, Email: murthytvr@sac.isro.gov.in

1. Introduction: Imaging radars provide information that is fundamentally different from sensors that operate in the visible and infrared portions of the electromagnetic spectrum. Although the interpretation of radar imagery is not as fully developed as that of optical data, radar imagery has many advantages over more traditional optical sensors (Smith, 1997).

For example, they can collect data regardless of solar illumination and cloud cover. Not being restricted by clouds is especially important when collecting data during rainy season, when wetlands are often easier to discriminate. The following account gives the microwave remote sensing as applied to local level wetland studies using medium to fine spatial resolution sensors. Radar sensors have potential to penetrate the vegetative canopies to detect the character of the ground layer, soil moisture and flooding beneath the canopy (Kasischke and Bourgeau-Chavez, 1997; Kasischke *et al*., 1997a; Kasischke *et al*., 1997b). Sensitivity of radar to water, due to its high dielectric constant, is extremely valuable to the remote sensing of wetlands. It is not only sensitive to soil moisture but can also differentiate between moist soil and standing water (Kasischke and Bourgeau-Chavez, 1997).

The presence of standing water interacts with the radar signal differently depending on the dominant vegetation type. When exposed to open water without vegetation, specular reflection occurs and a dark is observed (Dwivedi *et al*., 1999). The radar signal is often dampened in wetlands dominated by herbaceous vegetation when a layer of water is present (Kasischke *et al*., 1997a). Conversely, the radar signal is increased in forested wetlands when standing water is present due to double-bounce effect (Dwivedi *et al*., 1999). The double-bounce effect is more pronounce in forested wetlands using L-band (24 cm) data but can also be seen when using C-band (5.6 cm) data (Ustin *et al*., 1991). This high sensitivity to standing water and soil moisture makes radar an efficient tool for determining hydro pattern (Kasischke *et al*., 1997a; Rao *et al*., 1999).

Many of the first studies applying radar to wetlands and other ecosystems used Seasat imagery (Pope *et al*., 1997; Ramsey *et al*., 1998). SAR technology allows the increased spatial resolution that is necessary in regional wetland mapping. Studies conducted with Shuttle Imaging radar (SIR-C) and Japanese earth Resources Satellite (JERS)-1 L-HH band imagery confirmed this finding (Hess *et al*., 1990; Hess *et al*., 1995). C-HH imagery like that acquired by RADARSAT has a limited ability to map flooding beneath forest canopies. C-VV radar imagery, such as European Remote Sensing Satellite (ERS), can be used to map flooding beneath the vegetation canopies but only during leaf-off seasons (Kasischke and Bourgeau-Chavez, 1997). Slatton shows that polarimetric SAR has potential for mapping the major sub-environments associated with coastal herbaceous wetlands http://www.csr.utexas/projects/rs/bol1.html). Discrimination of different types of marshes, swamp thickets and swamp forests is also possible with radar imagery due to varying stem height and density (Pop et *al*., 1994). The combination of L-band JERS-1 and C-band RADARSAT also has the potential to increase wetland-mapping accuracy since these two bands are sensitive to varying structural details due to their different wavelengths.

Radar not only has the potential to detect different types of wetlands; it can also be used to study the condition and function of these valuable areas. Recent advances in radar remote sensing data processing have made the estimation of biomass and other forest parameters possible on a landscape scale (Le Toan, 1992; Kellndorfer, 1998; Kasischke, 1997b). The ratio of cross-polarised (HV or VH)

backscattering coefficients of L- to C-bands was well correlated with biomass (Kasischke, 1997b). Total biomass can be accurately estimated using AIRSAR P-, L- and C-bands and airborne synthetic aperture sensor (Mougin, 1999). C-HH radar can be used to infer inundation patterns in low biomass sites (Kasischke and Bourgeau-Chavez, 1997; Kasischke, 1997a; Hess *et al*., 1995). The use of multi-temporal radar data combined via an intensity, hue and saturation (HIS) transformation has also been found to improve the wetland mapping (Kushwaha *et al*., 2000). The opportunity to explore the potential of radar data will improve as many SAR satellites are currently or will soon be launched. These extra satellites will not only increase the amount of data available for analysis, they will also increase collection frequency and the variety of polarisations and frequencies available (Ramsey, 1997).

2. Study Area: The study area is located between 22°35′00″ – 23°00′00″N and 71°50′00″ 72°10′00″E in the semi-arid lands of Ahmedabad and Surendranagar districts of Gujarat state. Nalsarovar is a shallow wetland dominated by submerged and herbaceous emergent. It is one of the 21 wetlands notified by the ministry of environment and forests, Govt. of India. Nalsarovar falls on the arch that connects the Gulf of Kuchch and the Gulf of Cambay, which separates the Saurashtra from Gujarat mainland. Its biodiversity is explained by the presence of 94 species of phytoplankton, 86 species of zooplankton, 41 species of terrestrial plants, 30 species of aquatic macrophytes, 20 species of fishes, 11 species of herpetofauna, 46 species of terrestrial birds, 260 species of waterfowl and 13 species of mammals. It is a proposed Ramsar site of wetland of international importance.

Calibrated multi-frequency, multi-polarisation airborne SAR as well as SAR data of ENVISAT satellite closely spaced in time with optical data of IRS-P6 LISS-III and (Table 1) was used with a systematically planned field data collection.

3. Methodology: Seven component classes namely: open water, dense emergent vegetation, medium/open emergent vegetation, floating vegetation, tree cover and herbaceous vegetation on islands, surrounding agriculture areas and habitation/settlement were identified in field and were used as signatures for assessing their separability and accuracy of classification. Satellite data was used for mapping and quantitative estimation of biomass of emergent vegetation.

4. Salient Results:

4.1 Separability Analysis: Various components of wetland and its environs were studied for their separability on the SAR data using suitable common sites for signature analysis across P, L, C and X with all the polarisations. In the first step, transformed divergence (TD) is computed to assess the separability as given in Swain & Davis 1978.

The values above 1900 denote well separability followed by 1700 to 1900 as separable and <1700 as poorly separable. Based on the separability analysis (TD) it is inferred that separability values in C-band is mostly 2000 and >1700 for many classes except two open/clear water & water floating vegetation and settlement & fallow land.

4.2 Brightness Value Overlapping Index (BVOI): Computation of BVOI allows to arrive at the band subset that denotes maximum separability between classes and also aids in ordering of bands with decreasing separability. In this method, the range of pixel values within a class is compared, with histogram for all classes with in the bands used for classification. Accumulated percentage of all pixel values having pixel values ranging from minimum to maximum for each class is determined as given by Ma and Olson, 1989. Accordingly, the brightness value overlapping index (BVOI) suggests that C-HH (0.461) has best separability followed by C-VV (0.501), C-VH (0.866), X-HH (0.866), C-HV (0.873), X-VV (0.962), L-HH (1.051), L-VV,HV, P-HV (1.127), P-HH (1.140), P-VV (1.255), P-VH (1.267) and L-VH (1.320).

4.3. Accuracy Assessment: Accuracy of classification was estimated using KAPPA. Accordingly, C-band

shows a kappa coefficient of 0.84 followed by X-band (0.79), L-band (0.64) and P-band (0.45). It can be concluded that C-band with HH, HV, VV and VH are best suitable for delineation of subsystems of wetland (open water, emergent vegetation) and other cover types present in the vicinity of wetland (herbaceous vegetation, agricultural land, fallow land, settlement/ habitation).

4.4. Mapping Structural Components: The structural components of wetland amenable to remote sensing include the extent of wetland, open water (aquatic component), vegetation (submerged and emergent). The combination of HH/HV data (ENVISAT) enabled the delineation and mapping of wetland extent, open water and emergent vegetation (Fig. 1). The submerged vegetation could not be detected because of specular reflection. While signal is increased due to the double-bounce effect when standing water is present under the emergent vegetation. Two sets of microwave data were available corresponding to the optical data. The area statistics of the sub-systems is given in the table 2 for Nov. 05 and Dec. 05.

4.5. Biomass Estimation: *Typha angustata* and *Phragmites karka* dominate the emergent vegetation of Nalsarovar. Statistical analysis has been carried out to find the relationship between the measured biomass of the emergent vegetation and the corresponding backscatter from the satellite data. The following models were selected to represent the best statistical relationship between biomass measurements obtained from reference surface and the mean values of the corresponding microwave data.

$Y_{WBMM} = aX1 + bX2$ & $Y_{DBMM} = cX1 + dX2$

where, Y_{WBMM} = Wet Biomass measured in gm & Y_{DBMM} = Dry Biomass measured in gm, X1 = ENVISAT: HH, X2 = ENVISAT: HV, a = $7387.7e^{0.1015}$ and b = $72754e^{0.2382}$ c = $1835.1e^{0.080}$ and d = $21871e^{0.0936}$

The model equation aided in preparing a biomass map for the Nalsarovar as given in the figure 2. A robust model can be derived in the availability of SAR data encompassing all the seasons in a year.

5. Conclusions: The present study leads to the following conclusions**:**

1. Water spread assessment is higher in case of optical data compared to microwave data.
2. Only emergent vegetation of the total aquatic vegetation is possible from microwave data. It is not possible to delineate the submerged vegetation.
3. With certain enhancements of the optical data, it is possible to distinguish the vegetation within and outside the wetland, and also to delineate the submerged vegetation within the open water.
4. Physical water quality parameters like turbidity, transparency, total dissolved solids and total suspended sediments have shown significant relationship optical data and could be quantitatively estimated. While it is not possible through microwave data.
5. Biomass estimation is possible through both optical and microwave data. However, the estimation is higher in microwave compared to optical data.

Optical data can make a significant contribution to wetland studies, especially for cloud-free areas (periods). Methods that use a combination of different bands (frequencies) and polarisations is optimal but synergistic approaches that use imagery from multiple radar instruments as well as optical data will provide desired results.

Table 1: Data used in the study

1. Multi-frequency and multi-polarisation airborne data				
2. Satellite Data				
S.No.	**Satellite**	**Sensor**	**Bands**	**Date**
1	Resourcesat-1	LISS-III	G,R,NIR,SWIR	12 Nov. 2005
2	ENVISAT	ASAR-IS: 5, Descending	HH/HV	20 Nov. 2005
3	Resourcesat-1	LISS-III	G,R,NIR,SWIR	30 Dec. 2005
4	ENVISAT	ASAR-IS: 5, Descending	HH/HV	25 Dec. 2005

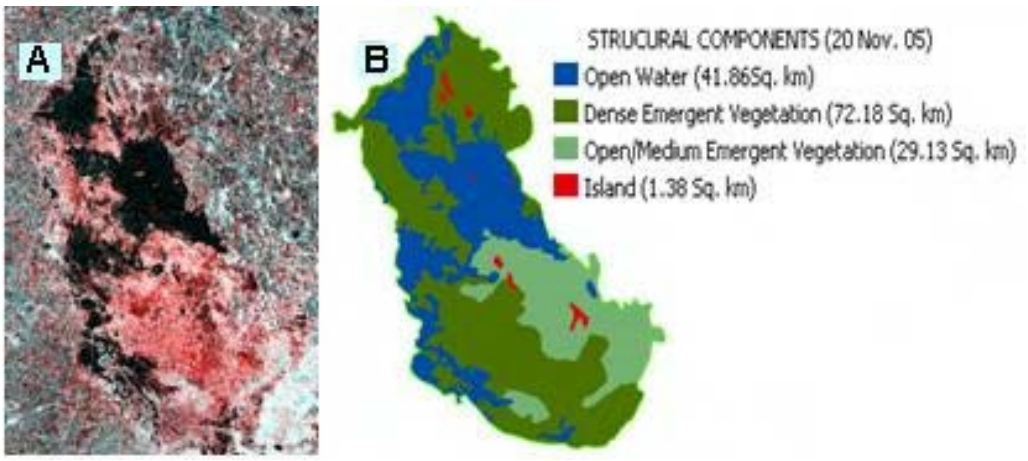

Figure 1: Nalsarovar Lake as seen on (A) ENVISAT (HH/HV) data of 20/11/05 and (B) map of structural components

Table 2: Area under various wetland subsystems derived from microwave data (ENVISAT: HH/HV)

S.No.	Wetland class	Area (km²)	
		20/11/05	25/12/05
1	Open Water	41.86	40.09
2	Dense emergent Vegetation	72.18	71.00
3	Open/medium emergent vegetation	29.13	28.58
3	Islands	1.38	2.06
	Total	144.55	141.73

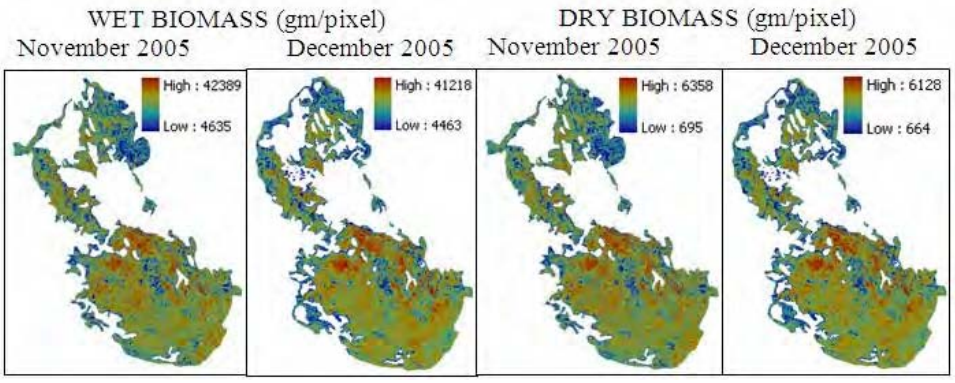

Fig 2: Biomass maps based on the SAR data in conjunction with field measurements

Acknowledgements: Authors are extremely grateful to Dr. Rangnath R. Navalgund, Director, Space Applications Centre, Ahmedabad for the execution of the study. Thanks are due to Dr. J. S. Parihar, Dy. Director, EPSA and Mission Director, EOAM for his support in the study. We are highly thankful to Dr. Manab Chakraborthy, Project Director, JEP-MW and Group Director, ATDG for his constant encouragement in the study. Thanks are due to Dr. Shiv Mohan, Head, ATTD for fruitful discussions. Several colleagues who have rendered help during study. Last but not the least the Forest Department, Gujarat for providing the support during the field data collection.

References

[1] B.R.M. Rao, R.S. Dwivedi, S.P.S. Kushwaha, A.N. Bhattacharya, J.B. Anand and S. Dasgupta, 1999, "Monitoring the spatial extent of coastal wetlands using ERS-1 SAR data", *Int. J. Remote Sensing*, **20(13)**, 2509-2517.

[2] E. Kasischke, L. Bourgeau-Chavez, K. Smith, E. Romanowicz and C. Richardson, 1997a, "Monitoring hydropatterns in south florida ecosystems using ERS SAR data", Proc. 3rd Symposium on space at the service of our environment, Florence, Italy, 71-76.

[3] E. Kasischke, J. Melack and M. Dobson, 1997b, "The use of imaging radars for ecological applications - a review", *Rem. Sen. of Environment*, **59 (2)**, 141-156.

[4] E. Kasischke, L. Bourgeau-Chavez, 1997, "Monitoring south Florida wetlands using ERS-1 SAR imagery", *PE&RS*, **63 (3)**, 281-291.

[5] E. Mougin, 1999, "Multi-frequency and multi-polarisation radar backscattering from mangrove forest", *IEEE Trans. Geoscience and Remote Sensing*, **37(1)**, 94-102.

[6] E. Ramsey and S. Laine, 1997, "Comparison of Landsat Thematic Mapper and high resolution photographs to identify change in complex coastal wetlands", *J. of Coastal Research*, **13(2)**, 281-292.

[7] E. Ramsey, 1998, Chapter7: Identifying wetlands zonation and inundation extent by using satellite remote sensing and ground-based measurement", USGS, Biological Resources Division, Biological Science Report USGS/BRD/BSR-1998-0002.

[8] J. Kellndorfer, L. Pierce, M. Dobson and F. Ulaby, 1998, "Toward consistent regional-to-global vegetation characterisation using orbital SAR systems", *IEEE Trans. Geoscience and Remote Sensing*, **36(5)**, 1396-1411.

[9] K. C. Slatton, M.M. Crawford, J.C. Gibeaut and R. Gutierrez, "Wetland vegetation using polarimetric SAR", http://www.csr.utexas/ projects/rs/bol1.html (last accessed on 19/04/2005)

[10] K. Pope, E. Rejmankova, J. Paris and R. Woodruff, 1997, "Detecting seasonal flooding cycles in marshes of Yucatan peninsula with SIR-C polarimetric radar imagery", *Rem. Sen. of Environment*, **59**, 157-166.

[11] K. Pope, J. Rey-Benayas and J. Paris, 1994, "Radar remote sensing of forest and wetland ecosystems in the Central American tropics", *Rem. Sen. of Environment*, 48(2), 205-219.

[12] L. Hess, J. Melack and D. Simonett, 1990, "Radar detection of flooding beneath the forest canopy: a review", *Int. J. Remote Sensing*, 11 (7), 1313-1325.

[13] L. Hess, J. Melack, S. Filoso and Y. Wang, 1995, "Delineation of inundated area and vegetation along the Amazon floodplain with the SIR-C synthetic aperture radar", *IEEE Trans. Geoscience and Remote Sensing*, 33(4), 896-904.

[14] L. Smith, 1997, "Satellite remote sensing of river inundation area, stage, and discharge: a review", *Hydrological Processes*, 11, 127-1439.

[15] R. S. Dwivedi, B.R.M. Rao and S. Bhattacharya, 1999, "Mapping wetland of Sunderban delta and its environs using ERS-1 SAR data", *Int. J. Remote Sensing*, 20(11), 2235-2247.

[16] Philip H. Swain and Shirley M. Davis, 1978, (Eds) "Remote Sensing: The Quantitative Approach ", McGraw-Hill, New York, P. 396. ISBN 0-07-062576-X.

[17] S. Kushwaha, R.S. Dwivedi and B.R.M. Rao, 2000, "Evaluation of various digital image processing techniques for detection of coastal wetlands using ERS-1 SAR data", *Int. J. Remote Sensing*, 21(3), 565-579.

[18] S. Ustin, 1991, "Opportunities for using the EOS imaging spectrometers and synthetic aperture radar in ecological models", *Ecology*, 72, 1934-1945.

[19] T. Le Toan, A. Beadoin, J. Riom and D. Guyon, 1992, "Relating forest biomass to SAR data", *IEEE Trans. Geoscience and Remote Sensing*, 24(3), 403-411.

Signatures, Newsletter of the ISRS–AC, Vol. 22, No.4, Nov-Dec 2010

Interpretation of ALOS – PALSAR Wide Beam Data over a Part of Kachchh for Lithological Discrimination and Study of Tectonic Processes

T. J. Majumdar[1], F. Bhattacharyya[1] and K. M. Sreejith[2]

[1]Institute of Seismological Research, Gandhinagar – 382 009, [2]SAC, Ahmedabad – 15, Email: tjmajumdar@rediffmail.com

1. Introduction: Radar is an active system which illuminates the surface with a beam of microwave radiation. Radar is most sensitive to surface roughness and soil moisture differences (variation in the complex dielectric constant which is a measure of the electrical properties of surface materials). Radar can penetrate the surface micro-layer in the soil covered areas[1]. Lineaments are extremely well manifested on SAR images, and on several occasions structural features; for example, fractures, folds, faults etc. have been detected, as well as extended in SAR imageries. Also, look angle and direction have a major impact on the response and manifestation of surficial features in SAR imageries. Earlier results have shown that RADARSAT-1 C-band (wavelength ~ 5.6 cm) horizontally polarized images have been found useful for geomorphology, geological structures and rock units mapping[2-6]. The SAR image is more effective than optical imagery for studying features such as surface roughness and topography. This is due to variation in radar backscatter as a function of wavelength, incident angle and polarization. Useful information on terrain morphology and surface relief (related to geological structure) is provided by ERS SAR imagery, due to effect of radar backscatter sensitivity to slope angle and to shadow effects caused by topographic relief[6].

Geological mapping is generally carried out on the basis of field observations by taking traverses along some routes (trails, and river courses). Often traverses have to be limited due to rugged terrain conditions and are time consuming. Aerial photographs have been utilized in such conditions. However, photographs are often distorted laterally and overall view of an area is not properly produced. Satellite image such as LANDSAT, SPOT, JERS, IRS provide excellent image characteristics with synoptic view of large areas. In the present study, ALOS (Advanced Land Observing Satellite - Japan) L-band (1.27 GHz, wavelength ~ 23 cm) WB (Wide Beam) microwave (SAR) image (Fig. 1) has been used for geological interpretation over a part of Bhuj, Kachchh. The scope of the study is to delineate various aspects of the landscape of the area emphasizing on the geology and structural set-up. The study covers an area of approx. 20,000 sq km covering parts of northern and southern Gujarat. The image was interpreted by various GIS and image processing software using a transparent overlay for delineating possible lithological boundaries and tectonic features of regional and local significance.

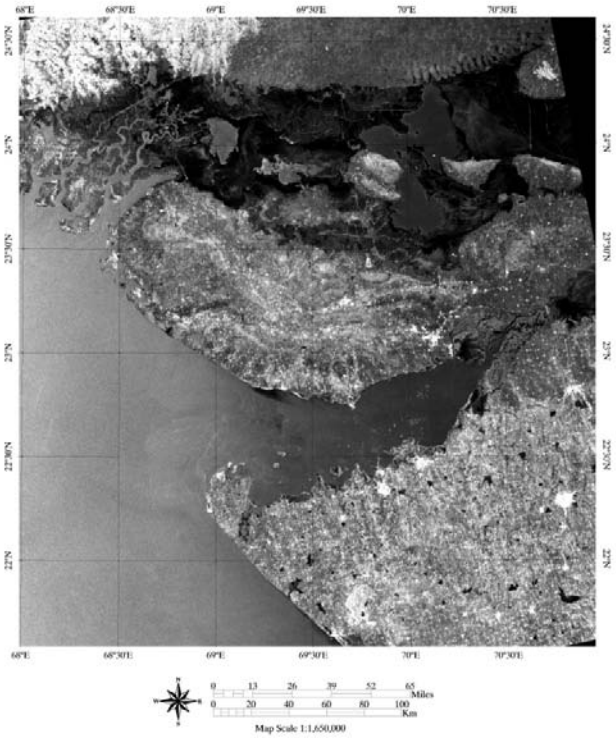

Fig. 1: ALOS-WB Raw Image covering the area of interest

The information obtained from the satellite data, aerial photos and previous maps were transferred into a scanned geo-referenced base map. Based on these data a geological map (scale 1: 2,000,000) has been prepared. Image characteristics of southern part of the study area, mainly covered with the Deccan Traps, are found to have less tonal difference than the areas extending to the northern region. The contact/boundary between different lithologic units of Quaternary, Tertiary and Mesozoic times could be established from the image. Similarly, laterite occurrences recorded along some sections could be mapped from the image. Some of the lineaments observed in the image were found to be linked with major faults. The ALOS-WB image has been found to be an effective tool in identifying lithological contacts and tectonic structures some of which could be verified in the field as well. Most of the rock units are covered by vegetation and alluvial developed on them. Major drainage patterns could as well be recognized from the image.

2. Geology and tectonics of Gujarat: The state of Gujarat comprises an area of approximately 2,00,000 sq km and is enclosed within the North Latitudes 20°10' to 24°50' and East Longitudes 68°40' to 74°40'. Geologically, Gujarat provides a wide spectrum of rock types of different ages[7]. Physiographically, the Gujarat state is divided into three well-defined areas viz., Mainland Gujarat, Saurashtra Peninsula and Kachchh Region (Fig. 2)[7,8]. The region of Kachchh falls in an arid zone, which is the southwestern continuation of the arid belt of northwestern India that includes the Thar Desert in Rajasthan[9]. The first order topography and a long history of devastating earthquakes indicate continuous rejuvenation of the area, which has kept pace with the erosional processes[10]. The landscape of Kachchh is unique in the sense that it has evolved essentially as a result of several phases of tectonic movements since the late Jurassic[11,12]. The tectonic fabric of Kachchh is dominated by E-W trend, which is reflected in the geomorphic set up as well[12,13]. Geologically, Quaternary/Tertiary sediments, Deccan volcanic rocks and Jurassic sandstones resting on Archean basement mainly characterize the Kachchh region[14]. Rifting of Gondwanaland in the early Jurassic or late Triassic involved reactivation of Precambrian structures in the eastern as well as western parts of India and formation of several rift basins like Kachchh, Cambay and Narmada[12]. The rift zone is bounded by a north- dipping Nagar Parker fault in the north and a south-dipping Kathiawar fault in the south. Other major faults in the region are the E-W trending Allah Bund fault, Island Belt fault, Kachchh Mainland fault, Katrol Hill fault, South Wagad fault and Gedi fault. Attempts are made by several workers to interpret the satellite imageries in terms of geology, tectonics, geomorphology, geodynamics and several other aspects[15-19].

3. Details of ALOS data: Advanced Land Observing Satellite (ALOS alias "Daichi") was launched by Japan Aerospace Exploration Agency (JAXA) on 24 January 2006. ALOS is a Japanese solution to high-resolution Earth observation. It is equipped with three mission instruments: Panchromatic Remote sensing Instrument for Stereo Mapping (PRISM), Advanced Visible and Near Infrared Radiometer type-2 (AVNIR - 2), and Phased Array type L-band Synthetic Aperture Radar (PALSAR)[20]. Since ALOS/PALSAR is based on phased-array L-Band antenna technology, the sensor can be operated in various imaging modes referred to as fine-beam single-polarimetric (FBS), dual-polarimetric (FBD), fully polarimetric (PLR), and wide-beam ScanSAR (WB). The latter mode allows for single-polarimetric image acquisitions at a swath width of ~350 km at 100 m resolution[21].

4. Objectives of the study: The study was planned for the following objectives:

- To compare/verify the results of image interpretation with the results of previous works for preparation/upgradation of a

geological/lithological map over the area of interest,

- Recognition of image characteristics of various lithological units in the ALOS-WB scene, and
- Delineation of tectonically weak zones.

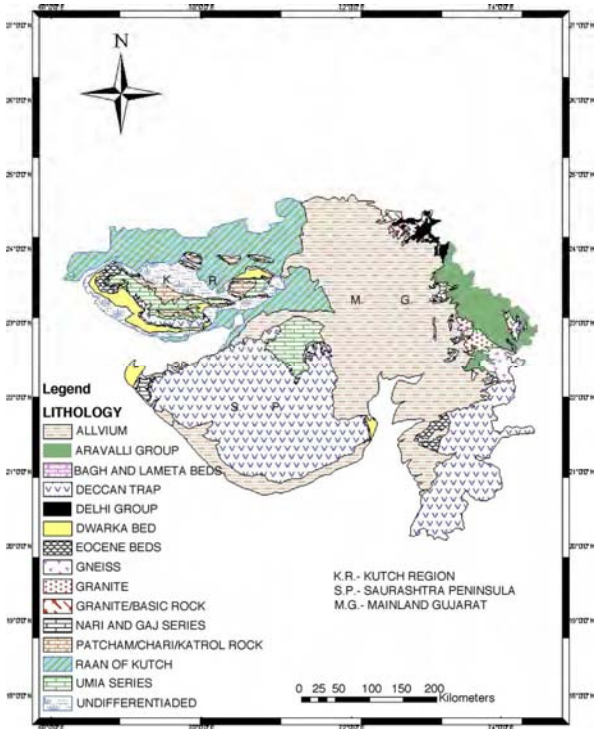

Fig. 2. Generalized geological/lithological map of Gujarat (after Merh 1995)[7]

5. Results and discussion: Figure 3 is the geological/lithological interpretation map of the image. The image has limited spectral resolution. However, rocks of different ages can be very well demarcated from each other in the image. The extreme northern part of the study area is covered by Quaternary rocks, which are marked by very dark patches. There is little color contrast between different rock outcrops, which are monotonous shades of grey. Patcham, Khadir and Bela islands are easily discernable from the image (Figs. 1 and 3). These islands are bounded by the Rann sediments, which are seen as light and dark patches in the image. Island Belt fault is marked by difference of reflectance in the image whereby they separate Mesozoic (Jurassic) and Tertiary rocks. Middle part of the image consists of intertwined network of patches of rocks of different ages.

In the Western part of Kachchh, the Deccan Traps are seen as bright spectral signatures. The Deccan Traps are also seen in southern part of the region with the similar reflectance.

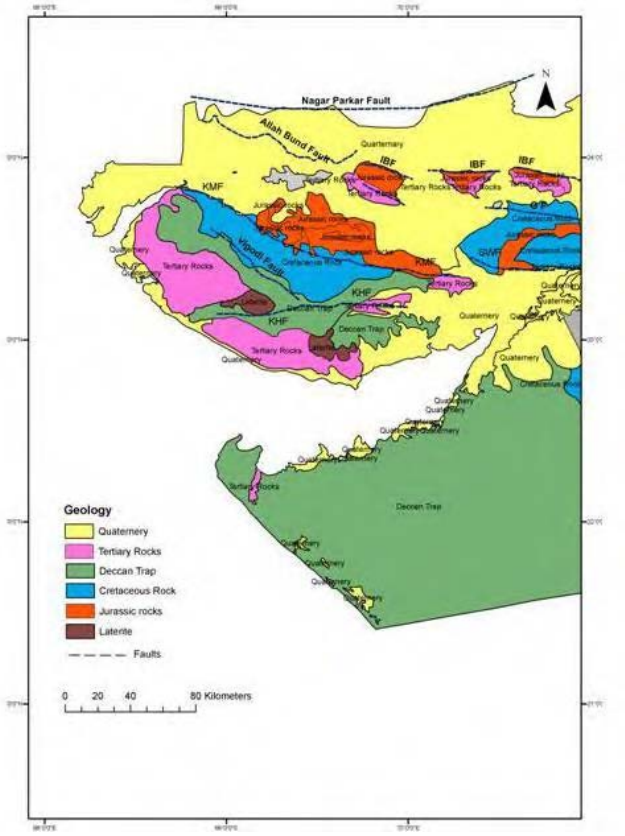

Fig. 3: Interpreted geological/lithological map over the area of interest using ALOS-WB image

Some lineaments are marked in the image (Fig. 4) and are found to be exactly similar to the general trend of major faults of the area. Faults are recognized by the offset formation contacts. Strike faults trend parallel with regional strike and eliminate or repeat beds. All the major faults are striking east-west which is in conformity with the study of earlier workers[12,22,23]. The major structural features are very clearly discernable in the image and could be distinguished by difference in spectral signatures of different lithologies. Kachchh Mainland Fault, Katrol Hill fault, Vigodi fault, South Wagad fault, Gedi fault, Allah

Bund fault and Nagar Parker fault could be easily recognized. The southern part of the study area is marked by the Deccan Traps and patches of Quaternary rocks. Some unidentified features are also found in the image which needs further study and extensive field investigation.

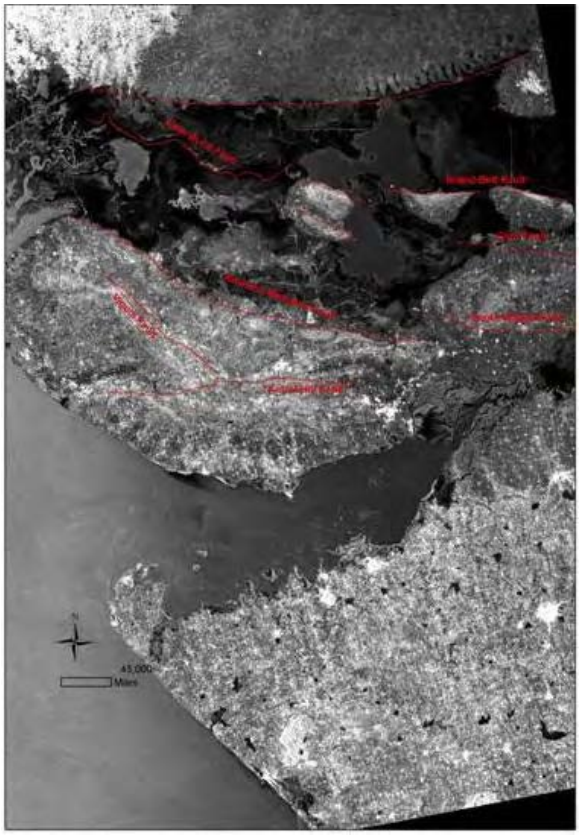

Fig. 4: Major lineaments as detected from ALOS-WB image

6. Conclusions: ALOS WB SAR data seem to possess high potential for geological/lithological interpretation, particularly over an arid zone e.g. Kachchh and major lineament/faults as well as geological classes could be mapped. The classification map, when compared with existing (ground truth based) maps over the region, shows a good amount of matching for the major geological/lithological classes. In addition, a number of new classes could as well be defined. However, more rigorous ground truth studies need to be done before making further meaningful conclusions.

Acknowledgements: The authors wish to thank Dr. B. K. Rastogi, DG, ISR, Dr. R. R. Navalgund, Director, SAC for their keen interest in this study.

References

[1] Prost, G. L., 2001, *Remote Sensing for Geologists: A Guide to Image Interpretation*, Gordon and Breach Science Publishers, Second edition, USA.

[2] Singhroy, V. and Molch, K., 2004, Geological Applications of RADARSAT-2, *Canadian Journal of Remote Sensing*, 30, pp. 893–902.

[3] Harris, J., 1984, Lineament mapping of Central Nova Scotia using Landsat-MSS and Seasat-SAR imagery. *Proceedings of the 9th Canadian Symposium on Remote Sensing*, 14–17 August 1984, Newfoundland, pp. 359–373.

[4] Lowman, P. D., Harris, J., Masuoka, P. M., Singhroy, V. H. and Slaney, V. R., 1987, Shuttle Imaging Radar (SIR-B) investigations of the Canadian Shield: Initial report, *IEEE Transactions on Geoscience and Remote Sensing*, GE-25, 1, pp. 55–66.

[5] Masuoka, P. M., Harris, J., Lowman, P. D. and Blodget, W., 1988, Digital processing of orbital radar data to enhance geologic structure: examples from the Canadian Shield, *Photogrammetric Engineering & Remote Sensing*, 54, pp. 621–632.

[6] Pal, S. K., Majumdar, T. J. and Bhattacharya, A. K., 2006, Extraction of linear and anomalous features using ERS SAR data over Singhbhum Shear Zone, Jharkhand using fast Fourier transform. *International Journal of RemoteSensing*, 27 (20), pp. 4513-4528.

[7] Merh, S.S., *The Geology of Gujarat.* Geological Society of India, 1995, 223 p.

[8] Mathur, U.B., 2005, *Quarternery Geology - Indian Perspective*. Geological Society of India, Memoir No. 63.

[9] Maurya, D.M., Thakkar, M.J. and Chamyal, L.S., 2003, Quaternary geology of the arid zones of

Kachchh: terra incognita. *Proceedings of Indian National Science Academy*, 69, pp. 23-135.

[10] Thakkar, M.J., Maurya, D.M., Raj, R. and Chamyal, L.S., 1999, Quartenery tectonic history and terrain evolution of the area around Bhuj, mainland Kachchh, western India. *Journal of Geological Society of India*, 53, pp. 601-610.

[11] Biswas, S. K., 1974, Landscape of Kutch-a morphotectonic analysis. Indian Journal of Earth Sciences, 1, pp. 177-190.

[12] Biswas, S. K., 1987, Regional tectonic framework, structure and evolution of the Western marginal basins of India. Tectonophysics, 135, pp. 307-327.

[13] Biswas, S. K., 1982, Rift basins in Western India and their hydrocarbon prospects with special reference to Kutch basin. American Association of Petroleum Geologists Bulletin, 66, pp. 1467-1513.

[14] Gupta, H. K., Harinarayana, T., Kousalya, M., Mishra, D.C., Mohan, I., Purnachandra Rao, N., Raju, P. S., Rastogi, B. K., Reddy, P. R. and Sarkar, D., 2001, Bhuj earthquake of 26 January. Journal of Geological Society of India, 57, pp. 275– 278.

[15] Graham, L. C., 1974, Synthetic interferometric radar for topographic mapping, Proceedings IEEE, 62, pp. 763-768.

[16] Biegert, E. K., Berry, J. L. and Oakley, S. D., 1998, Oil field subsidence monitoring using spaceborne interferometric SAR: A Belridge 4-D case history. International Center for Remote Sensing and Potential Field Studies, pp. 1-19.

[17] Gahalaut, V. K., 2006, Need for crustal deformation studies in Kachchh region. Extended Abstract presented at 'Seminar on Paleoseismology and Active faults', 2006, Institute of Seismological Research (ISR), Gandhinagar.

[18] Nasipuri, P., Mitra, D. S. and Majumdar, T. J., 2005, Generation of thermal inertia image over a part of Gujarat: a new tool for geological mapping. International Journal of Applied Earth Observation & Geo-information, 7, pp. 129-139.

[19] Satyabala, S. P., 2004, Coseismic ground deformation due to an intraplate earthquake using synthetic aperture radar interferometry: The Mw6.1 Killari, India, earthquake of 29 September 1993. Journal of Geophysical Research, 111; B02302.

[20] Rosenqvist, A., Shimada, M. and Watanabe, M., 2004, ALOS PALSAR: Technical outline and mission concepts, 4th international symposium on retrieval of Bio-and Geophysical parameters from SAR data for land applications, Austria, November 16-19, 2004.

[21] ALOS website: http://www.eorc.jaxa.jp/ ALOS/en /about/ palsar.htm

[22] Biswas, S. K. and Khattri, K. N., 2002, A geological study of earthquakes in Kutch, Gujarat, India, Journal of Geological. Society of India, 60, pp. 131-142.

[23] Biswas, S. K. and Deshpande, S.V., 1970, Geological and tectonic maps of Kutch. Bulletin of Oil & Natural Gas Commission, 7, pp. 115-116.

Call for Articles

Readers are requested to contribute short articles for publication in the forthcoming issues in their own words, preferably as per the editorial calendar given on page-3, either as a brief survey of state of the art or as articles on specific work carried out by them, or as novel concepts related to the specific theme(s). The deadline for inclusion in the next issue on **"Industry Contributions to Remote Sensing Activities"** is April 20, 2011.

- Editorial Team

Signatures, Newsletter of the ISRS–AC, Vol. 22, No.4, Nov-Dec 2010

Potential of Microwave Remote Sensing for Snow and Glacier Studies

Sushil Kumar Singh, SAC, Ahmedabad, Email: sushil@sac.isro.gov.in

1. Introduction: Snow and glaciers are one of the largest sources of water stored in the form of snow and ice outside of Polar region and known as 'third pole' of the world. Optical data has been used extensively to understand/observe the monitoring and mapping of snow cover, glacier retreat/advance, glacier mass balance and glacier inventory (Kulkarni et al., 2006; Singh et al, 2010, Kulkarni et al, 2007). However, clouds impose a severe problem in optical region especially in Himalayan region where accumulation and ablation pattern of snow plays an important role in snow and glacier melt runoff estimation. Radars have an added advantage over visible and near infrared region. The microwave signal can pass through cloud and penetrate surface to provide information on the internal structure of the medium. Radar data are often considerably more difficult to understand and interpret rather than optical electromagnetic spectrum. Surface roughness of the material relative to radar signal, and dielectric constant of the medium (moisture state), sensor geometry etc. need to be taken into consideration which influences backscatter mechanism and returned radar signal. A smooth surface reflects radar energy in specular way whereas rough surface scatters the energy in all direction. However, a surface that appears rough at shorter wavelength may appear smooth at longer wavelength. Liquid water will absorb microwave radiation but snow can allow the signal to penetrate if frozen. Sensor parameters like frequency, polarization and antenna-look angle also affect the backscatter. If the wavelength is comparable to the size of scatterer, the potential for volume scattering in the medium will be increased. Shadow and layover are the major problems for the mountainous region for low antenna-look angle. Optimal antenna-look angle for the mountainous terrain was found between 40^0 and 60^0 (MacDonald and Waite, 1971; Rott, 1984).

2. Electromagnetic properties of snow and glacier: Backscattering of snow surface (Figure 1) is controlled by the angle at which the incident beam strikes the surface and the dielectric constant of snow. The real part of dielectric constant of ice is constant throughout the microwave region. The dielectric constant of dry snow depends only on the snow density and expressed numerically as equation 1 where ρ_s is the snow density in mg/m^3. (Hallikainen, Ulaby and Abdelrazik, 1986)

$$\varepsilon' = 1 + 1.9\,\rho_s \text{-----(1)}$$

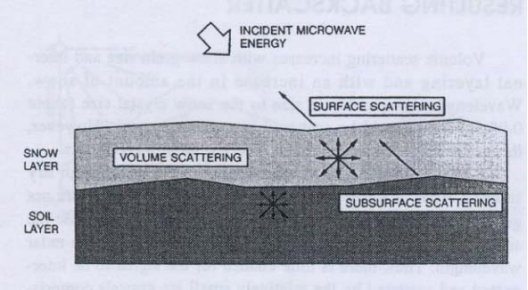

Fig 1: Scattering mechanism in snow cover surface.

The imaginary part of dielectric constant which determines the degree of absorption is very small for dry snow and exhibits some dependence on temperature. Because of low value of absorption, propagation of microwave radiation through dry snow is generally dominated by scattering.

Microwave backscattering properties of glacier depends on the time of observation. Glaciers are covered with minimum snow during summer

(ablation) season and accumulation zone is covered by generally smooth wet snow, hence showing low backscattered value. Whereas in winter, accumulation zone is covered with fresh (dry) snow over accumulation area and volume scattering dominates. Backscattering coefficients over dry-snow are generally low (typically -10 dB at C band) compared with the percolation and wet-snow zones.

3. Microwave applications for snow: Goodison et al (1980) discussed the potential of SAR for snow cover monitoring, having advantages of high spatial resolution, insensitivity to cloud and operability at night, however, complexities are linked with its interpretation. The attenuation length of dry snow is large but small percentage of moisture content (approximately 1%) can reduce this from a few meters to a few centimeters. Various studies have demonstrated wet snow discrimination (Rott and Nagler, 1995; Rees and steel, 2001; Matzler and Schanda, 1984) as shown in Figure 2 where C-band was found to be adequate over preferred X-band observations (Shi and Dozier, 1993). Baghdadi et al. (1999) proposed an algorithm to infer the presence of wet snow such as

$$\sigma_r^0 - \sigma^0 \geq a \;\; AND \;\; b \leq \sigma^0 \leq c \qquad \text{----(2)}$$

where σ^0 is the observed backscatter coefficient, σ_r^0 is the reference (snow-free or dry snow) backscatter coefficient, and a, b and c are model parameters based on incidence angle, provided that a sufficiently accurate and high resolution digital elevation model is available.

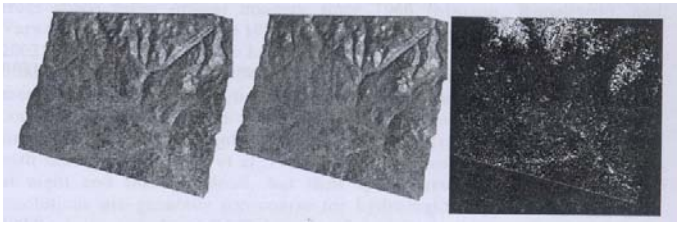

Fig 2: Detectability of wet snow using ERS-2 C(HH) SAR imagery

In most cases, the C-band co-polarized backscatter at an incidence angle of about 23^0 is typically 2 or 3 dB lower for wet snow than for snow-free terrain as shown in Figure 3 (Hallikainen et al., 1992; Rees and Steel, 2001). However, in some cases wet snow and snow-free terrain proved to be indistinguishable (Shi and Dozier, 1997) like for dense forest areas (Koskinene et al., 1997). In a study of wet snow using C-, L- and P-band polarimetric SAR of a mountainous area in Austria (Otzal), Rott et al. (1992) showed that at C-band, only the snow surface and the top few centimeters of the snowpack contributed to backscattering, while the snow volume down to a few meters on depth was sensed with the longer wavelength P-band sensor.

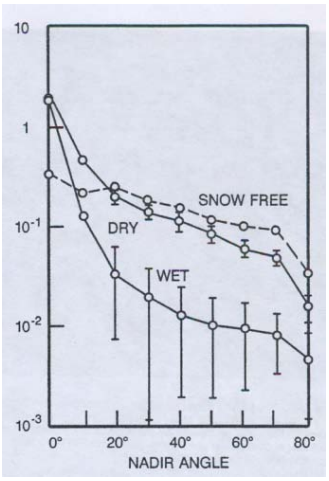

Fig 3: Backscattering coefficients for wet and dry snow

Snow Water Equivalent (SWE) showed conflicting results over radar sensitivity of SAR in (Ulaby et al., 1977) and with little or no relationship for L-band for wet snow (Goodison et al., 1980). Ulaby and stiles (1981) found a positive correlation between SWE and backscatter at 9 GHz (Figure 4) while Leconte and Pultz (1990) found an inverse relationship for C-band. ENVISAT-ASAR data was used to develop the empirical relationship between backscattering coefficient and snow physical parameters like snow wetness and density in Beas basin, Himachal Pradesh (Singh et al., 2008).

4. Microwave applications for glacier studies: Glacier can be divided into four zones namely; 1)

dry zone (where no melting takes place); 2) percolation zone (some surface melting takes place); 3) wet snow zone (current year snow fall melts and 4) superimposed zone (extensive melting which refreezes as a continuous mass of ice). The lower boundary of this superimposed ice zone is the equilibrium line. These zones show seasonal variability in backscattering behaviour.

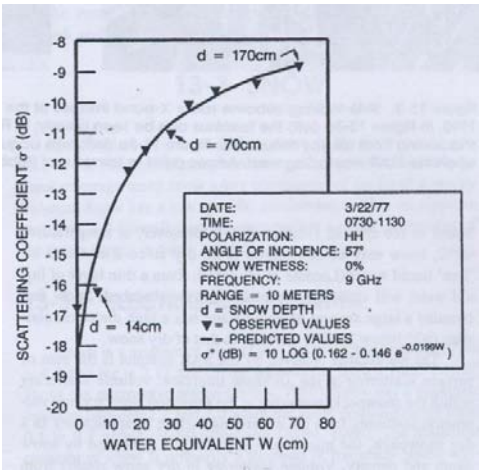

Fig 4: Scattering coefficient response to snow wetness at 9 GHz

In summer, accumulation zone is generally covered with wet snow and surface scattering dominates. Surface scattering also dominates in ablation area and is primarily controlled by surface roughness. Crevasses can give higher return of backscatter especially if oriented perpendicular to the look-direction of the radar. Volume scattering dominates in accumulation area during winter and ice grains, ice lenses and ice layers play an important role. In ablation zone, scattering is influenced by the interface between ice and overlying dry snow. Figure 5 shows the winter ASAR image of Samundra Tapu glacier (Chandra basin) and respective optical images (AWIFS) of winter and summer months.

This image shows that the backscattering of ablation zone is low in winter SAR image and accumulation zone is showing slightly high backscattering coefficient.

SAR data can provide vital information about the freeze-up and break up dates, duration of ice cover etc. of lakes which could be a key information for past climate records. The longer wavelength SAR sensor enables the study of some characteristics of subsurface conditions because of their ability to penetrate below the surface.

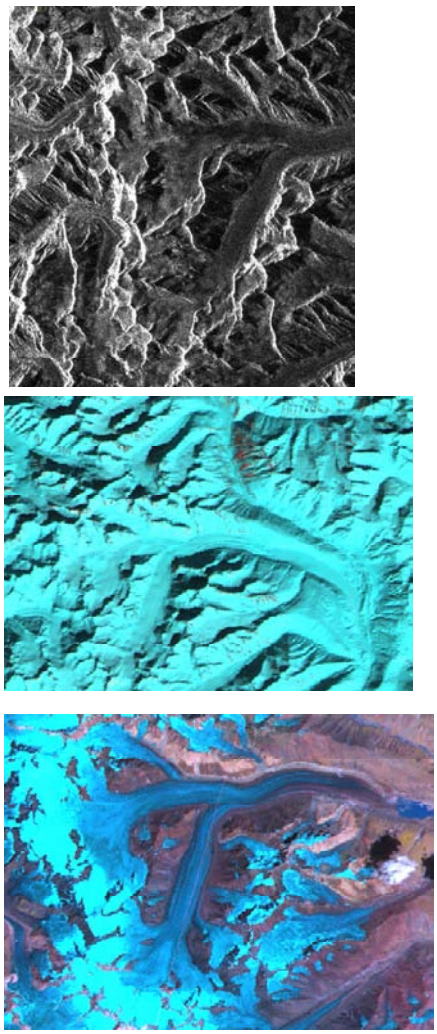

Fig 5: Behaviour of signature of Samundra Tapu glacier, Chenab basin in SAR(ENVISAT) and Optical (AWiFS, LISS-III) images

5. Conclusions: Earth sensing radars have been used since 1960s to study the cryospheric features. SAR sensors can provide vital information regarding snow physical parameters and glacier

characteristics especially in Himalayan region where cloud is a critical issue for Optical spaceborne applications. Scattering in dry snow is more dominated by volume scattering than wet snow where surface scattering dominates. Wetness within snowpack can reduce the penetration of C-band up to few cm and could provide information about onset of melting and amount of percent liquid water content of snowpack. Glacier equilibrium line, mass balance estimation, glacier velocity, subglacial topographic information, ice sheet variation, freezing-melting of lakes etc. are important issues which can be addressed with SAR technology. With the advent of SAR sensors (like ENVISAT-ASAR, RADARSAT-2, CryoSAT, TerraSAR-X, proposed Indian first SAR satellite RISAT) along with the availability of multi-frequency and multi-polarization, it will advance our understanding and the role of snow and glacier studies in global processes.

References

[1] Baghdadi, N., Fortin, J.P. and Bernier, M., 1999, Accuracy of wet snow mapping using simulated Radarsat backscattering coefficients from observed snow cover characteristics, International J. of Remote Sensing, 20(10), pp 2049-2068.

[2] Goodison, B.E, Waterman, S.E. and Langham, E.J., 1980, Application of synthetic aperture radar data to snow cover monitoring. Paper read at Sixth Canadian Symposium on Remote Sensing at Halifax, Nova Scotia.

[3] Hallikainen, M., Jaaskelainen, V.I., Kurvonen, L., Herland, E.A. and Perala, J., 1992, Applications of ERS-1 SAR data to snow mapping. Paper read at first ERS-1 symposium: Space at the service of our environment at Cannes.

[4] Hallikainen, M., Ulaby, F.T. and Abdelrazil, M., 1986, Dielectric properties of snow in the 3 to 37 GHz range, IEEE Trans. of Antenna and Propagation, AP 34, pp 1329-1340.

[5] Koskinen, J., Kurvonen, J.L., Jaaskelainen, V., and Hallikainen, M., 1994, Capability of radar and microwave radiometer to classify snow types in forested areas. Paper read at International Geoscience and Remote Sensing symposium. Surface and Atmospheric remote sensing: Technologies, Data Analysis and Interpretation, at Pasadena.

[6] Kulkarni, A.V., Bahuguna, I.M., Rathore, B.P., Singh, S.K., Randhawa, S.S., Sood, R.K. and Dhar, S., 2007, Glacial retreat in Himalayas using Indian Remote Sensing Satellite data, Current Science, Vol 92, No. 1, pp 69-74.

[7] Kulkarni, A.V., Singh, S.K., Mathur, P. and Mishra, V.D, 2006, Algorithm to monitor snow cover using AWiFS data of RESOURCESAT for the Himalayan region, *International Journal of Remote Sensing, 27(12), pp 2449-2457.*

[8] Leconte, R. and Pultz, T., 1990, Utilization of SAR data in the monitoring of snowpacks and wetlands, Proceedings of the workshop on Applications of Remote Sensing in Hydrology, 13-14 February, Saskatoon, Saskatchewan, pp 233-258.

[9] MacDonald, H.C. and Waite, W.P., 1971, Optimum radar depression angles for geological analysis, Modern Geology, 2, pp 179-193.

[10] Matzler, C. and Schanda, E., 1984, Snow mapping with active microwave sensors, International J. of Remote Sensing, 5(2), pp 409-422.

[11] Rees, W.R., 2006, Remote sensing of snow and ice, CRC press, pages 277.

[12] Rees, W.G. and Steel, A.M., 2001, Radar backscatter coefficients and snow detectability for upland terrain in Scotland. International J. of Remote Sensing, 22(15), pp 3015-3026.

[13] Rott, H., 1984 , Synthetic aperture radar capabilities for snow and glacier monitoring, Advance Space Research, 4(11), pp 241-246.

[14] Rott, H. and Nagler T., 1995, Monitoring temporal dynamics of snowmelt with ERS-1 SAR. Paper read at International Geoscience and Remote Sensing Symposium at Firenze, Italy.

[15] Rott, H., Davis, R.E. and Dozier, J., 1992, Polarimetric and multi-frequency SAR signatures of wet snow. Paper read at UGARSS'92', at Houston, Texas.

[16] Shi, J. and Dozier, J., 1995, Inferring snow wetness using C-band data from SIR-C's polarimetric synthetic aperture radar, IEEE Trans. on Geosciences and Remote Sensing, 13(4), pp 905-914.

[17] Shi, J. and Dozier, J., 1997, Mapping seasonal snow with SIR-C/X-SAR in mountainous areas. Remote Sensing Environment, 59(2), pp 294-307.

[18] Singh, G., Kumar, V., Mohite, K., Venkataraman, G. and Rao, Y.S., 2008, Snow physical parametes estimation using Envisat-ASAR data, Proceedings of International workshop on Snow, Ice, Glacier and Avalanches, January 7-9, 2008, IIT Mumbai, pp 49-56.

[19] Singh, S. K., Kulkarni, A. V. and Chaudhary, B. S., 2010, Hyperspectral analysis of snow reflectance to understand the effects of contamination and grain size, Annals of Glaciology, 54(44), pp 83-88.

[20] Ulaby, F.T., Stiles, W.H., Dellwig, L.F. and Hanson, B.C., 1977, Experiments on the radar backscatter of snow, IEEE Trans. on Geoscience Electronics, GE-15(4), pp 185-189.

[21] Ulaby, F.T. and Stiles, W.H., 1981, Microwave response of snow, Advanced Space Research, 1, pp 131-149.

Forthcoming RS related Conferences in India	
Mumbai Jan 07-09, 2011	International Conference on Environmental Science and Development, Visit: http://www.icesd.org/
Kolkata Jan 14, 2011	GWIWR-2011: National Seminar on Global Warming and Its Impact on Water Resources, Visit: http://iahwbrc.org.in/registration.htm
Hyderabad Jan 18-21, 2011	Geospatial Map Forum, Visit: http://www.geospatialworldforum.org/2011/conference/submitabstract.htm
Bhopal Mar 12-13, 2011	National Conference on Water & Environment, Visit: http://www.mp.gov.in/highereducationmp/SeminarWorkshop/MVM_Seminar.pdf
Modinager Mar 12, 2011	NCMA-2011: National conference on Microwave &it's Application, Visit: http://ksjiet.org
Port Blair Mar 23-26, 2011	International Conference on Tropical Island Ecosystems: issues related to Livelihood, Sustainable Development and Climate Change, Visit: http://tiecon2011.indianscholars.org
Dehradun Apr 7-8, 2011	ISPRS WG VI/4 - ISRS Joint International Workshop, Visit: http://www.isrsindia.in/isprs6wg4/index.html
Hyderabad Dec 10-13, 2011	11th Asian Urbanization Conference, Visit: http://osmania.ac.in

Signatures, Newsletter of the ISRS–AC, Vol. 22, No.4, Nov-Dec 2010

Microwave Remote Sensing for Land Subsidence Studies: Differential Interferometry Technique

Shweta Sharma, SAC , Ahmedabad, Email: shweta@sac.isro.gov.in

1. Introduction: Synthetic Aperture Radar (SAR) is an active remote sensing system, operating in the microwave region of the electromagnetic spectrum. It emits a series of coherent, pulsed electromagnetic waves from an antenna mounted on an airborne or spaceborne vehicle, and records amplitude and phase of backscattered signals from objects on the ground. In this sense, SAR systems acquire complex images.

Land subsidence is a gradual settling or sudden sinking of the Earth's surface owing to subsurface movement of earth materials. The principal causes of subsidence are aquifer-system compaction, drainage of organic soils, underground mining, hydro compaction, natural compaction, and sinkholes (National Research Council, 1991). Excessive extraction of groundwater, oi1 and gas resu1ts in decreased pore pressure and increased effective stress in unconsolidated sediments. That leads to the compression of aquifers and the confining aquifers and gradual land surface subsidence. Spatial variety of land-surface subsidence often leads to a specific pattern of ground deformation. Buildings and underground infrastructures are under higher risks of damage in locations with greater differential ground deformation. Land subsidence has been regarded as a human- induced hazard affecting many cities and regions in the world.

Traditionally, leveling is used for measuring vertical deformation, i.e. subsidence and uplift, at a spatially discrete set of locations along trajectories. It is followed by interpolation to get a continuous two-dimensional coverage. The accuracy is high at measurement points, but may be low at non-measured points. Besides, for a non-homogeneous deformation pattern, point-wise leveling measurements may not always be effective to represent deformation, unless points are measured at a very high density. Surveying and geotechnical monitoring systems are usually established in areas where the likelihood of deformation is very high. The main advantage of the conventional monitoring techniques used for deformation control is the high accuracy of measurements. However, the major disadvantages are a complicated and costly instrumentation, high influence of field and weather conditions, discrete character of observations and high cost of frequent surveys.

A powerful new mapping tool (InSAR) is a critical element in assessing land mitigation of subsidence. InSAR is capable of remotely sensing small changes in land surface elevation at an unprecedented level of spatial detail (see Table-1). The new displacement maps enhance our capabilities to monitor and manage subsidence caused by the compaction of susceptible aquifer systems, and reveal new insights into the controlling physical processes. Interferometric Synthetic Aperture Radar (InSAR) uses radar signals to measure deformation of the Earth's crust at an unprecedented level of spatial detail and high degree of measurement resolution. If there is a natural depression in the area, then it will be common in all the three satellite passes and hence that will be subtracted and we will get phase difference only due to land subsidence. From mapping the area coverage and magnitude of ground motions following cataclysmic earthquakes, to measuring discrete subsidence displacements over several years, InSAR has a wide variety of uses in ground movement surveying applications. SAR interferometry makes use of this phase information by subtracting the phase value in one image from that of the other, for the same point on the ground. This is, in effect, generating the interference between

the two phase signals and is the basis of interferometry. The two images over same area are called the master & the slave. First acquisition is the master and second is the slave. After co-registration, we find the difference between its phases (interferometric phase) ($\Delta\Phi_{Int}$):

$$\Delta\Phi_{Int} = \Phi_S - \Phi_M = \Phi_{Topo} + \Phi_{Mov} + \Phi_{Atm} + \Phi_{Noise} \quad \text{Eq. (1)}$$

where:

ΦTopo is the phase difference cause of topographic distortion

ΦMov is the phase difference cause of ground deformation

ΦAtm is the phase difference cause of atmospheric effects

ΦNoise is the phase difference cause of interferometric noise

There are two applications from this technique:

Digital Elevation Model (DEM) Generation: Is essential to have a null ground deformation between master and slave. With depreciable noise and atmosphere, topographic component gives us terrain topography.

Deformation estimation: Use DInSAR. The deformation of the ground surface, such as earthquake displacements, land subsidence caused by groundwater, natural gas, or oil extraction, can be quantified by comparing the phase information of two complex SAR images of which the first is recorded before deformation, and the second thereafter. This is done using differential SAR interferometry (D-InSAR). In contrast to levelling that measures the deformation at a set of irregularly distributed discrete points, D-InSAR provides a deformation image on a pixel-by-pixel basis over an area of thousands of square kilometres.

Table 1: Different methods of measuring land subsidence (Source: USGS, fact sheet 051-00, April 2000)

Different methods of measuring land subsidence

METHOD	Component displacement	Resolution[1] (millimeters)	Spatial density[2] (samples/survey)	Spatial scale (elements)
Spirit level	vertical	0.1–1	10–100	line-network
Geodimeter	horizontal	1	10–100	line-network
Borehole extensometer	vertical	0.01–0.1	1–3	point
Horizontal extensometer:				
Tape	horizontal	0.3	1–10	line-array
Invar wire	horizontal	0.0001	1	line
Quartz tube	horizontal	0.00001	1	line
GPS	vertical horizontal	20 5	10–100	network
InSAR	range	5–10	100,000–10,000,000	map pixel[3]

[1]Measurement resolution attainable under optimum conditions. Values are given in metric units to conform with standard geodetic guidelines. (One inch is equal to 25.4 millimeters and 1 foot is equal to 304.8 millimeters.)

[2]Number of measurements generally attainable under good conditions to define the spatial extent of land subsidence at the scale of the survey.

[3]A pixel on an InSAR displacement map is typically 40 to 80 meters square on the ground.

In the SAR interferometric approach, two SAR images are combined to exploit the phase difference of the signals. The interferometric phase is sensitive to both surface topography and coherent displacement along the look vector occurring between the acquisitions of the interferometric image pair. The basic idea of differential SAR interferometry is to subtract the

topography related phase from the interferogram to derive a displacement map.

2. Differential Interferometry (DInSAR technique): The interferometric SAR techniques (InSAR) use the information contained in the phase of two SAR images. The InSAR phase is sensitive to the terrain topography and to relative changes in elevation occurring between two SAR antenna passes over the same area. If the terrain topography is known, i.e. a DEM (Digital Elevation Model) of the imaged scene is available; the corresponding phase component can be subtracted from the InSAR phase, leaving the component due to the terrain surface deformation. This is the so-called differential InSAR technique (DInSAR).

In the last years different types of techniques have been developed and the capabilities of DInSAR have improved considerably. The DInSAR techniques can be classified as follows:

A) Coherence based DInSAR with a single image pair;

B) Coherence based DInSAR with multiple images;

C) DInSAR based on Interest Points (IP) selected on multiple images.

DInSAR allow to detect very accuracy ground deformation (a few mm) over wide areas. It's based on study and processing of SAR images. Final result of DINSAR is deformation map of working zone.

For the deformation estimation, a phase component (ΦTopo_simu) is simulated from a previous knowledge of topography. The techniques that use an external DEM in order to derive the topographic phase component use the two-pass DInSAR configuration. There is another configuration, the three-pass interferometry, which can work without an a priori known DEM, but it requires at least three images acquired over the same scene. Then it's possible the differential interferometric phase ($\Delta\Phi_{Int}$) calculation, it is based on interferometric phase, we take topographic component away from it.

2.1 Advantages and Limitations of DInSAR technique: DInSAR offers the typical advantages of the remote sensing techniques: it provides data over inaccessible areas (three pass method is used for detecting land subsidence over inaccessible areas.) and large area coverage. Furthermore, it can (potentially) provide deformation measurements with a quality that is comparable with that of the traditional geodetic techniques. However, it is important to underline that high quality results can only be achieved by employing an adequate InSAR processing (image registration, filtering, phase unwrapping, etc.), coupled with an appropriate statistical treatment of the DInSAR observations. Another important advantage of the DInSAR technique is the availability of large time series of SAR images.

The use of the D-InSAR technique is however affected by some important limitations, like the temporal decorrelation and the effects caused by different atmospheric conditions (atmospheric effects). Furthermore, some of the DInSAR limitations are related to the temporal evolution, the extension and the magnitude of the considered deformations. On factors limiting the accuracy of the interferometric results depends on the separation of the two orbits at the acquisition time, the smaller the separation, the lower the sensitivity to topography and to DEM residual errors. A typical estimation error of the perpendicular baseline of 0.1m for a height change of 100 m results in a displacement error of 0.03 mm. A typical estimation error for the perpendicular baseline of 0.1m results in a displacement error of 2.8mm in a 10Km distance. Therefore flattening is a critical step in subsidence measurements of large areas, and the required baseline-estimation accuracy is high (*Tazio Strozzi etal., 2001)* . The slow deformation phenomena (let's say, few millimetres per year) are only detectable over large time intervals, where the SAR images usually have very low coherence. An exception occurs in the urban areas that can remain coherent even over years. For the area, which is vegetation abundant, long wavelength L and P band will give better results due to their high penetration power. The SAR resolution represents a second limitation. Using a typical 5-look azimuth compression, the ERS SAR images are characterised by a pixel footprint of about 20 by 20 m.

Since an adequate sampling of a given deformation field has to be guaranteed, a limit on the minimum size of the detectable deformations is posed. The interferometric phase noise represents a further limitation, which is critical for all applications characterized by small deformation magnitudes.

3. Available Packages: The importance that DInSAR is gaining as a deformation monitoring tool is reflected in the number of available packages that have DInSAR analysis capabilities. Some of them are listed in Table 2. Note that this list is not exhaustive and, more importantly, that the reported information comes from publicly available documentation: this software has not been tested by the authors. The table does not include the software tools developed by the research centres specialized in Advanced-DInSAR (A-DInSAR) that are not commercialized or freely distributed for non-commercial purposes.

The first two packages listed in Table 2 are freely available for non-commercial purposes: DORIS and ROI_PAC. Both of them have their source code available. The DIAPASON is a command line software developed by a research group at the French CNES, which is suitable for advanced users. Some remote sensing software tools include specific modules for standard DInSAR analysis, i.e. the analysis based on single interferograms.

This is the case of ENVI, while other packages e.g. ERDAS, seem to provide only tools for InSAR analysis. Example of A-DInSAR commercial tools are those sold by Vexcel and Gamma. This last company, which is based in Switzerland, besides selling its products, with included the possibility to buy the source code, provides A-DInSAR analysis services.

4. DInSAR for Land Subsidence Monitoring: Repeat-pass spaceborne DInSAR has been used to derive ground displacement maps. Two SAR images acquired from two slightly different positions, at different revisit times, are used to measure the phase difference, or so-called interferogram, between the two acquisitions. The interferogram consists of topographic information, surface displacement between the two acquisitions, atmospheric delay, and noise. DInSAR requires the removal of the topographic phase contribution, hence isolating the ground displacement component. The topographic phase contribution can be simulated and then eliminated by introducing DEM information. The atmospheric component is primarily due to fluctuations of water content in the atmosphere between the satellite and the ground. The atmospheric delay can be identified using the fact that its fringe structure is independent over several interferograms, or can be modelled by using a GPS network. It is also possible to reduce the atmospheric disturbance to the displacement phase by using the 'interferogram stacking' technique.

The height ambiguity for the displacement phase is given by Equation (2). A complete 2π phase change is equivalent to a height displacement of λ/2 in the slant range direction. Since the measured phases in the interferogram are wrapped in modulo of 2π, the height displacement map can be derived by 'phase unwrapping' the interferogram.

$\varphi_{displacement} = - (4\pi / \lambda) \delta R$ -----Eq. (2)

where, $\varphi_{displacement}$ = phase contribution due to ground surface displacement

δR = height displacement in the slant range direction

Electro-Chemical (EC) sensor functionality is similar to battery. The sensor life depends on electrolyte quantity and gas exposures. Such sensors consume zero power, require simple signal processing and suitable for oxygen and carbon monoxide detection. Non-dispersive Infrared (NDIR) gas sensors work on energy absorbed by gas molecules (quantized vibrating energy). CO2, CH4 have unique absorption spectrum in infra-red region (4.25um & 3.3um) which is proportional to gas concentration (Lamberts-Beer's Law). Capacitive polymer and piezo-resistive polymer sensors are used for Humidity readings along with local temperature measurements. Integrated miniature

temperature and humidity sensors with digital interface can also be used. MEMS micro-pellistor based hydrogen sensors have fast response. It consists of temperature sensor, a reference sensor for temperature and humidity compensation and a catalytic element. Hydrogen is catalytically oxidized with oxygen, creating exothermic reaction and thus heating the temperature sensor.

The change in temperature is directly proportional to Hydrogen concentration. Piezo-resistor based absolute pressure sensors generate voltage proportional to pressure due to piezo-electric effect.

The sensor system development challenges include obtaining knowledge base w.r.t sensor operation, calibration and design of high reliability miniaturized, inexpensive, low power and compact electronics. Since these are life support systems, robust performance is achieved with intelligent processing and adequate redundancy. An integrated sensor system is designed with microcontroller to provide an easy, flexible and fast method of developing a complete system with intelligence. Such sensor system configuration is shown below. Standard digital interfaces (SPI, I2C, USART) are planned to reduce development time.

The modular sensor system caters to multiple analog or digital sensors for expandability. The analog signals from sensors are amplified and digitized through multi-channel digitizer with SPI interface. Digital outputs from sensors (normally SPI interface) interfaces directly to microcontroller. Triple modular redundancy and voting logic is used (mitigation techniques) for improving reliability. Multiple sensors/ sensor systems connected to a local area network will report time-stamped measurements, change of rates and alert both the control system and the crew through LEDs and audio. The planned mechanical configuration is shown below.

4.1 Meaning of Color in Interferogram

A raw radar echo is acquired as a complex signal comprising real and imaginary components in which information about amplitude and phase is enclosed. The amount of phase equals the two-way travel path divided by the wavelength.

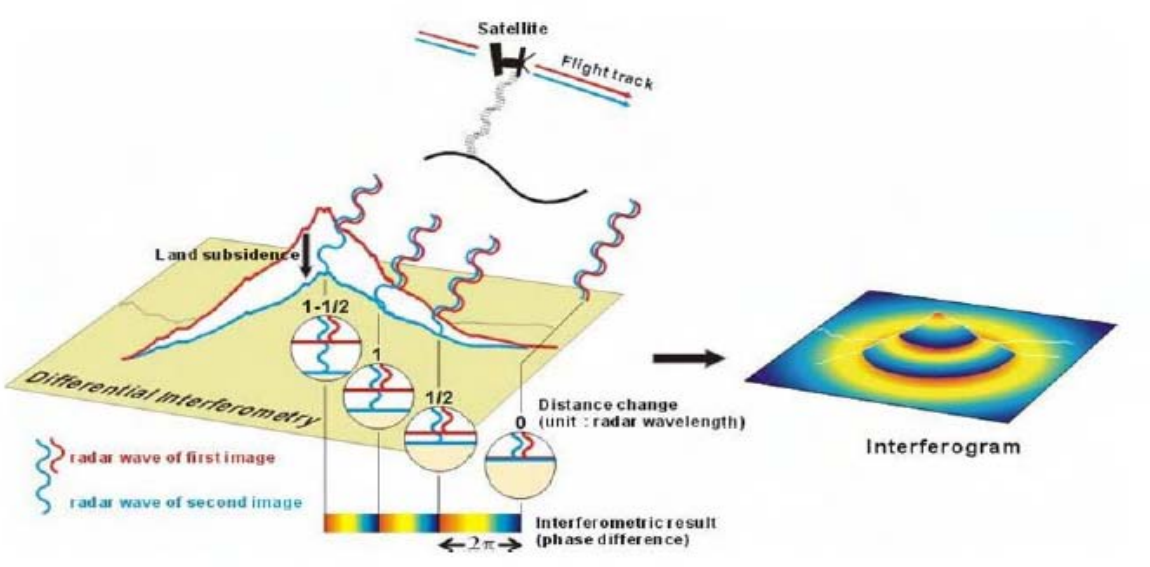

Fig 2: Schematic diagram of showing how a rainbow color of an interferogram be obtained (figure after Chang et al., 2004b).

Table 2: Available softwares with standard DInSAR or advanced DInSAR capabilities

Software name	Company/ University	Web site/ type of licence	Platform and software characteristic	DInSAR capabilities
DORIS	TU Delft	enterprise.lr.tudelft.nl/doris free license for non-commercial purposes	Unix/Linux/WinXP (C++ source code available)	Standard DInSAR with ERS1/2, RADARSAT, ENVISAT, JERS data. Additional programs for unwrapping (Snaphu) and orbit processing (Getorb) are available
ROI_PAC	Berkley University	www.openchannelfoundation.org free license for non-commercial purposes	Unix/Linux (C and F90 source code available)	Standard DInSAR with ERS1/2, JERS
DIAPASON	Developed by CNES	www.altamira-information.com commercial licence distributed by Altamira Information	Linux/Win 95, 98, NT, 2000	Standard DInSAR with ERS1/2, JERS-1, RADARSAT, ENVISAT
ENVI	Research Systems Inc. (RSI)	www.rsinc.com/envi commercial licence	Unix/Linux/Win2000 and WinXP	Module of ENVI, SARscape, standard DInSAR with ERS1/2, JERS-1, RADARSAT, ENVISAT
VEXCEL 3DSAR	Vexcel Corporation	www.vexcel.com commercial licence	Unix/Linux/Windows	Module of the EV-InSAR, CTM - Coherent Target Monitoring, with advanced DInSAR capabilities with ERS1/2, JERS-1, RADARSAT, ENVISAT
GAMMA	Gamma	www.gamma-rs.ch/ commercial licence	UNIX, Linux, Windows Modular packages in ANSI-C language, code available	Advanced DInSAR with ERS1/2, JERS-1, SIR-C X-SAR, RADARSAT, ENVISAT

The phase measurement records many different effects and that makes the image appears to be a noisy image with value uniformly distributed between 0° and 360°. By proper processing, the phase becomes meaningful only when some of these effects are isolated. A cycle of rainbow color (i.e. fringe), -пtоп or -180 to 180°, represents a λ/2 cm (λ is the wavelength used) slant-range change between the radar and the ground in an interferogram. Since the wavelength of RISAT is C-band, 5.6 cm, one-way change is thus 2.8 cm (Fig 2). So, in case of C-band radar (λ=5.6 cm), each fringe represents 28 mm radar line-of-sight displacement. As land subsidence movement is vertical in nature, the radar line-of-sight ground displacement can be converted into actual land subsidence by dividing the former value with cosine or radar incidence angle i.e. the relation between wavelength used and land subsidence derived is as follows:

$$\textit{Derived land subsidence} = \lambda / (2 \times \cos\theta) \text{----} \quad \text{(Eq. 3)}$$

where, λ=wavelength used and θ = radar incidence angle

4.2 Processing Steps for Displacement Map Generation: Following are the steps required for the quantification of the land subsidence phenomenon.

4.2.1 Baseline Estimation: Enables the user to obtain infomraiton about the baseline values and other orbital parameters of the input SAR pair.

4.2.2 Interferogram Generation: Starting with the two Single Look Complex input data, co-registered, and multi-looking interferogram, the master Intensity and slave Intensity images are generated.

4.2.3 Digital Elevation Model/Ellipsoid Interferogram Flattening: During this processing the previously generated interferogram is split into the synthetic phase and the residual phase (or differential phase).

Then the input Digital Elevation Model is re-projected onto the master SAR geometry and is re-generated as a slant range output product.

4.2.4 Adaptive Filter and Coherence Generation: The flattened interferogram (differential phase) is filtered, using the box car method, and the scene coherence is generated. The coherence data values can vary between 0 and 1, in proportion to the temporal correlation between master and slave SAR acquisitions.

4.2.5 Phase Unwrapping: The differential phase is unwrapped using a region growing algorithm. A coherence threshold is used to avoid, or minimize, unwrapping errors. Low threshold values (between 0.15 and 0.2) are suggested to limit interruptions (e.g. phase jumping) during the growing process.

4.2.6 Phase to Displacement: The phase values are converted to displacement and geocoded onto a map projection and a Ground Control Points file must be previously generated.

4.3 Sources of Errors for quantitative deformation monitoring: The key factor to achieve a quantitative DInSAR deformation monitoring is the number of available interferograms (i.e. observations). The classical DInSAR configuration is based on a single interferogram, derived from a pair of complex SAR images. This is the simplest DInSAR configuration, which often is the only one that can be implemented, due to the limited data availability: the results of most DInSAR applications are derived using a single interferometric pair. This is a zero redundancy configuration. With such a configuration it is not possible to check the presence of the different errors that may affect the interferometric observations: the deformation estimates are not reliable. Note that the same occurs for the digital elevation models derived with single InSAR pairs.

The errors associated with the DInSAR observations have different origins. Among the most important we can include the unwrapping-related errors, the residual topographic component due to DEM errors, and the atmospheric artefacts. The unwrapping-related errors usually occur in low coherence areas, where the interferometric phase noise is high. In order to avoid these areas, the phase unwrapping for sparse data can be used. However, if the coherence is too low the density of the good pixels can be not sufficient to guarantee a correct sampling of the deformation signal. The residual topographic component can represent an important error source if large baselines are used and the quality of the DEM is not known.

Finally, the atmospheric artifacts represent a very important error source, which can strongly degrade the quality of the DInSAR observations. All these error sources represent a strong limitation of the DInSAR technique based on a single interferogram. It is however important to underline that the usefulness of this simple configuration is context dependent. For instance, in all applications with strong deformations (e.g. co-seismic displacements of the order of meters) the magnitude of the above mentioned errors surely would not hide the deformation signal. Furthermore, the availability of a priori information on the phenomenon under analysis may reduce the impact of these errors. For instance, dealing with small-scale subsidences, where the location of the stable areas around the subsidence is known is it possible to reduce the influence of the atmospheric artifacts.

4.4 Results reported in literature:

- P. Damoah-Afari et al. detected ground settlement of Shanghai using InSAR techniques and found that the deformation rates obtained fall in the interval -22mm/yr and +5 mm/yr. This value is in agreement with the reported deformation rates over Shanghai during the 1990s (China Daily, 2003b) (Source: The International Archives of the Photogrammetry, Remote Sensing and Spatial Information Sciences. Vol. XXXVII. Part B7. Beijing 2008).
- H.C. Chang et al. used radar interferometry for monitoring land subsidence due to underground

water extraction and found that the total subsidence measured by DInSAR at the city region over the period of November 1992 to February 1997 was about 35cm, which was 8cm/year. This result was in agreement with the field survey data which has the subsidence rate of proximately 84mm/year in 1995. (Source: Proceedings of SSC 2005 Spatial Intelligence, Innovation and Praxis: The national biennial Conference of the Spatial Sciences Institute, September, 2005. Melbourne: Spatial Sciences Institute. ISBN 0-9581366-2-9)

- Tazio Strozzi, et al. applied Differential Interferometric method for urban areas and found that the observed maximum subsidence velocity was about 40 cm/year, which was in agreement with the results of leveling surveys and theoretical models. The reason of the subsidence is strong groundwater extraction combined with highly compressible clays over which Mexico City is built. (Source: Differential Interferometric Applications in Urban Areas: Final Report, Gamma Remote Sensing AG Thunstrasse 130 CH-3074 Muri BE, Switzerland, June 2001).
- The feasibility of surface deformation mapping with ERS differential SAR interferometry was confirmed for a wide range of deformation velocities ranging from m/year (Ruhrgebiet, Mexico City) to cm/year (Bologna) and mm/year (Eugenean Geothermal Basin) by. Urs Wegmüller et al. (Source: ERS - ENVISAT Symposium, Gothenburg, Sweden, 16-20 Oct. 2000).
- The rate of land subsidence in Calcuuta University has been found to range between 5 and 6.5 mm/yr and the subsidence fringe was observed to be located in and around Machhua Bazar, Calcuuta University and Razabajar Science College. (Source: Assessment of land subsidence phenomenon in Kolkata city, India using satellite-based D-InSAR technique", RS Chatterjee et al. Current Science, Vol.93, No.1, 10July 2007).

5. Conclusion: Since the first description of the technique, which was based on L-band SEASAT SAR data (Gabriel et al., 1989), the great potential of DInSAR for land deformation applications has been recognized. Of major interest were, in particular, some typical features of the remote sensing systems, like the wide areas covered by each image, the global coverage and the repeat observation capabilities, associated with the intrinsic high metric quality of the DInSAR observations. In fact, since the beginning, it was clear that the spaceborne DInSAR are able to measure small deformations with a high sensitivity, comparable to a small fraction of the radar wavelengths, which are in the order of centimetres to few tens of centimetres. Later on, other important characteristics were recognized. Firstly, the high spatial resolution capability of the SAR systems, which in particular cases allows the deformation monitoring of small features, like buildings or infrastructures, to be performed. Secondly, in the last years another relevant property has gained importance: the availability of large historical SAR datasets, which in the case of the ERS1/2 dataset covers almost 14 years.

Ground subsidences and uplifts due to fluid pumping, construction works, geothermal activity, etc. have been described in several papers, see e.g. Massonnet et al. (1997); Galloway et al. (1998) Amelung et al. (1999); Wicks et al. (2001) Most of the published results concern urban areas, over which DInSAR data remains coherent even with large observation periods. With the advent of the Persistent Scatterers techniques it is expected to get more and more deformation monitoring results outside the urban, suburban and industrial areas.

References

[1] Gabriel, A.K., Goldstein, R.M., and Zebker, H.A., 1989, Mapping small elevation changes over large areas—Differential radar interferometry: *Journal of Geophysical Research*, v. 94, p. 9,183–9,191.

[2] Massonnet, D., and Feigl, K.L., 1998, Radar interferometry and its application to changes in the

earth's surface: *Reviews of Geophysics*, v. 36, p. 441–500.

[3] Zebker, H.A., Rosen, P.A., Goldstein, M., Gabriel, A., and Werner, C.L., 1994, On the derivation of coseismic displacement fields, using differential radar interferometry—The Landers earthquake: *Journal of Geophysical Research*, v. 99, p. 19,617–19,634.

[4] Massonnet, D., Rossi, M., Carmona, C., Adragna, F., Peltzer, G., Feigl, K., and Rabaute, T., 1993, The displacement field of the Landers earthquake mapped by radar interferometry: *Nature*, v. 364, p. 138–142.

[5] Massonnet, D., Briole, P., and Arnaud, A., 1995, Defl ation of Mount Etna monitored by spaceborne radar interferometry: *Nature*, v. 375, p. 567–570.

[6] Rosen, P.A., Hensley, S., Zebker, H.A., Webb, F.H., and Fielding, E., 1996, Surface deformation and coherence measurements of Kilauea volcano, Hawaii, from SIR-C radar interferometry: *Journal of Geophysical Research*, v. 101, p. 23,109–23,125.

[7] National Research Council, 1991, Mitigating losses from land subsidence in the United States: Washington, D. C., National Academy Press, 58 p.

[8] Wicks, C. Jr., Thatcher, W., and Dzurisin, D., 1998, Migration of fluids beneath Yellowstone Caldera inferred from satellite radar interferometry: *Science*, v. 282, p. 458-462.

[9] R., Lewis, A.S., and Ahmadi, B., 1998, InSAR imagery reveals seasonal and longer-term land-surface elevation changes infl uenced by ground-water levels and fault alignment in Santa Clara Valley, California [abs.]: *EOS (supplement) Transactions, American Geophysical Union*, no. 45, November 10, 1998, p. F37.

[10] Amelung, F., Galloway, D.L., Bell, J.W., Zebker, H.A., and Laczniak, R.J., 1999, Sensing the ups and downs of Las Vegas—InSAR reveals structural control of land subsidence and aquifer-system deformation: *Geology*, v. 27, p. 483-486.

[11] Galloway, D.L., Hudnut, K.W., Ingebritsen, S.E., Phillips, S.P., Peltzer, G., Rogez, F., and Rosen, P.A., 1998, Detection of aquifer system compaction and land subsidence using interferometric synthetic aperture radar, Antelope Valley, Mojave Desert, *California: Water Resources Research*, v. 34, p. 2,573–2,585.

[12] Vadon, H., and Sigmundsson, F., 1997, 1992–1995 crustal deformation at Mid-Atlantic ridge, SW Iceland, mapped by radar interferometry: *Science*, v. 275, p. 193–197.

[13] Ferretti, A., C. Prati and F. Rocca (2000). Nonlinear subsidence rate estimation using the Permanent Scatterers in differential SAR interferometry. *IEEE Transactions on Geoscience and Remote Sensing*, 38(5), 2202-2012.

[14] Chang, C.P., Wang, C.T., Chang, T.Y., Chen, K.S., Liang, L.S., Pathier, E., and Angelier, J., 2004b, Application of SAR interferometry to a large thrust deformation: the 1999 M-w=7.6 Chichi earthquake in central Taiwan: *Geophysical Journal International*, v. 159, p. 9-16.

[15] Gabriel, A.K., Goldstein, R.M., Zebker, H.A., 1989. Mapping small elevation changes over large areas: differential radar interferometry. *J. Geophys. Res*., 94 (B7), pp. 9183-9191.

[16] Tazio Strozzi et al., 2001,. Land subsidence monitoring with Differential SAR interferometry. *Photogrammetric Engineering and Remote Sensing*, November 2001, pp. 1261-1270.

Applications of SAR Interferometry in Crustal Deformation Studies

K. M. Sreejith & A. S. Rajawat, SAC, Ahmedabad, Email: {sreejith, asrajawat}@sac.isro.gov.in

Active microwave remote sensing using synthetic aperture radar (SAR) sensors has become an important tool for a wide variety of earth observations. Geophysical applications of SAR interferometry (InSAR) to measure changes in the Earth's surface have been explored since the last two decades. InSAR is a method to combine the phases of two different radar images gathered simultaneously or at different times with slightly different looking angles from the satellites. This technique calculates the interference pattern caused by the difference in phase between these images. The resulting interferogram is a contour map of the change in distance between the ground and the radar instrument. The measured phase difference shows an ambiguity cycle of 2π that corresponds to a 2-way travel path difference of the radar wavelength (λ) along with phase terms proportional to the target motion caused by deformation during that time interval. Thus, if the phases due to topography are removed from the interferogram the residual fringes correspond to the ground surface motion along the sensor-target Line of Sight (LOS) direction. This technique is generally known as Differential InSAR (DInSAR) and has been used to measure surface deformations caused by a variety of sources like earthquakes, landslides, mining etc. The principle of measuring surface deformation using InSAR technique is described in Fig. 1.

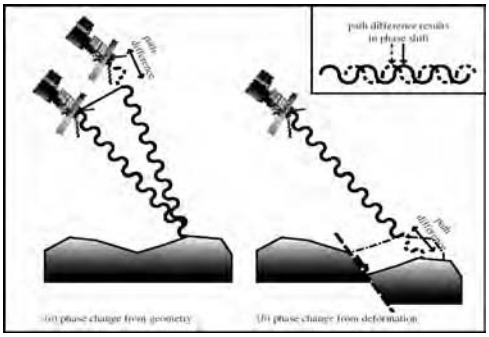

Fig 1: Graphics showing the mapping of surface deformation using InSAR technique

Apart from conventional seismological methods, Geodetic GPS are nowadays used to study the deformations caused by earthquakes. Though the level of accuracy is very high, these studies have limited spatial coverage. Further, these methods are terrain dependent and accessibility to the area may be difficult. InSAR has become a better alternative which can provide highly accurate deformation values covering a large area with accuracy in terms of a fraction of radar wavelength. This was first demonstrated by Massonnet et al. in a classic paper which graced the front cover of *Nature* (Massonnet *et al.* 1993). Their interferogram generated from ERS-1 SAR data sets could successfully capture the surface movements produced by the 1992 Landers earthquake (Fig. 2).

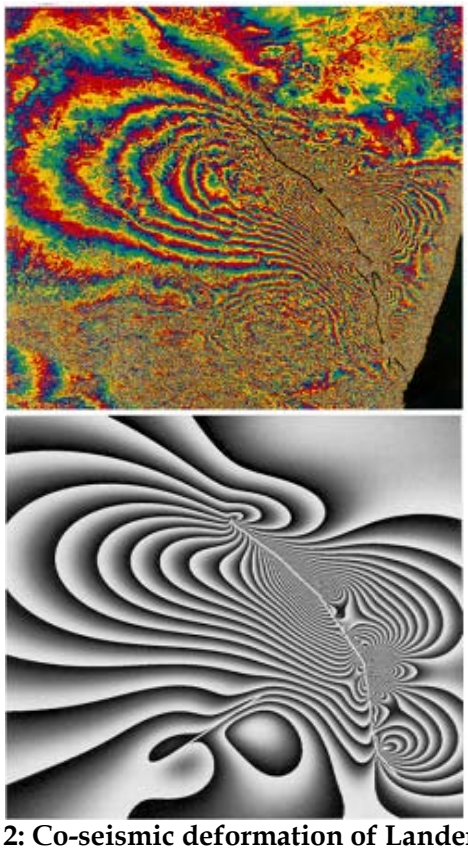

Fig 2: Co-seismic deformation of Landers earthquake (left) with modeled interferogram from fault geometry (right) (Massonnet et al., 1993)

Further, it has been proved that InSAR could be used as an alternative tool to obtain location, magnitude and type of an earthquake which otherwise could be only possible with seismological observations. Since then, several studies have been attempted demonstrating the application of InSAR for earthquake deformation studies (Prati et al., 2010 and references therein). Lack of data availability and loss of coherence produced by various decorrelation effects provides constraints in using InSAR techniques in certain areas. Nevertheless, recently developed techniques like Persistent Scatterers (PS) technique has given promising results for monitoring long term surface deformation as it is independent of overall phase decorrelation.

In India, InSAR studies for seismic deformation mapping have achieved limited success. Though Killari earthquake of 30 September, 1993 was mapped using InSAR technique (Satyabala et al., 2003), the Bhuj earthquake of 26 January, 2001 of magnitude 7.8 could not be effectively mapped due to loss of coherence. This earthquake was one of the largest intraplate events ever reported casing wide spread destruction. According to Gujarat government records, more than 20,000 people died, 166,000 injured and more than 370, 000 houses were collapsed leaving 600,000 people homeless.

Kachchh region falls in Zone-V (most prone to earthquakes) of the Seismic Zonation map of India. Recent studies reveal intense seismic activity around the epicentral area of 2001, Bhuj earthquake. Space Applications Centre (SAC), Ahmedabad and Institute of Seismological Research, Gandhinagar have recently initiated studies to map the on-going deformation using seismological geodetic and SAR datasets as part of the R&D support to the Disaster Management Support Program (DMSP) of Department of Space. The analysis of SAR data for the period 2007-2009 resulted in mapping the surface deformation of about 0-50 mm along the line of sight of the satellite over a part of Kachchh region. These results were validated using DGPS based field surveys, which showed comparable deformation rates. However, the deformation map generated in this study is limited to the areas where coherence is high.

The study reveals that InSAR technique can be an effective tool for understanding the crustal deformation in Kachchh. More SAR data analysis at regular time intervals may further improve the results. The currently operating SAR sensors like ENVISAT- ASAR, ALOS- PALSAR have very limited data availability over India. Launch of ISRO's planned RISAT Mission may improve the data availability.

References

[1] Massonnet, D., Rossi, M., Carmona, C., Adragna, F., Peltzer, G., Feigl, K. and Rabaute, T., The displacement field of the Landers earthquake mapped by radar interferometry. *Nature*, 1993, 364, 138–142.

[2] Prati, C., Ferretti, A., and Perissin, D., Recent advances on surface ground deformation measurement by means of repeated space-borne SAR observations. *J. Geodynamics*, 2010, 49, 161–170.

[3] Satyabala, S. P., Coseismic ground deformation due to an intraplate earthquake using synthetic aperture radar interferometry: The Mw6.1 Killari, India, earthquake of 29 September 1993. *J. Geophy. Res.*, 2006, 111, B02302.

[4] Schmidt, D. A., and Burgmann, R., InSAR constraints on the source parameters of the 2001 Bhuj earthquake. *Geophy. Res. Lett.*, 2006, 33, L02315.

Signatures, Newsletter of the ISRS–AC, Vol. 22, No.4, Nov-Dec 2010

Ocean Observations System for India Using Active Microwave Remote Sensing Techniques

Raj Kumar & Abhisek Chakraborty, SAC, Ahmedabad, Email: rksharma@sac.isro.gov.in

1. Introduction: India's exclusive economic zone, stretching 200 nautical miles into the Indian Ocean, encompasses more than 2 million square kilometres and the total coastline stretches to approximately 7500 km including the islands. Since Independence, the special efforts made to modernize coastal fisheries, and encourage deep-sea fishing through joint ventures led to a more than fourfold increase in coastal fish production. Most of the livelihood of coastal population depends upon the ocean living resources. In addition to the fishing skills of these fishermen, they also consider the physical state of the ocean as part of their daily routine. Most of them still use folklore to make their own predictions, but ocean predictions based on scientific understanding also made inroads for their consideration before venturing into the seas. In addition to these, the other users of the Indian ocean region are offshore industries, ports and harbours and shipping industries which are most technology savvy. They are strongly dependent on weather and require marine weather forecasting extending to the limit of 5-10 days. An important component of marine weather forecast is sea state and therefore wave forecasting, using surface level wind forecast is of prime importance (Janssen, 2004). Department of Space and Ministry of Earth Sciences have already initiated the work in this direction and predictions of a few parameters are being provided on an operational basis. The present efforts are still not able to generate satisfactory predictions; hence more extensive efforts are needed to generate more accurate observation and prediction systems.

The ocean state means knowledge of different parameters of surface and deeper parts of the oceans, such as sea level, temperature, salinity, surface winds and waves. The present state of the ocean can be determined by in-situ observations as well as observations from space platforms. The best possible ocean state can be generated using the in-situ measurements at a specific location. Recently ARGO Floats have become major source of sub-surface information, however due to vast extent of oceans; it is next to impossible to deploy in-situ instruments at each and every location. The deployment and their regular maintenance has been the major constraint to have observations especially in the Southern Ocean region, which is far away from any continent. Hence these observations are mainly concentrated in the Northern Hemisphere region. In view of the above, the spaceborne sensors are crucial for integrated ocean observation system. The major advantage of spaceborne observations is their high temporal repetivity and global coverage. Even with the combination of in-situ and spaceborne observations, the information about ocean state may not be possible at desired temporal and spatial intervals, whereas, the numerical models provide ocean state parameters at regular grids. By having combinations of ocean observation systems and numerical models, one can obtain the improved ocean state information, which is not available by either of them alone. Ocean is responsible for about 50% of heat transport from low to high latitudes and its release into the atmosphere. The variations in the heat budget and transport lead to climate variations. The major thrust area in ocean research is therefore towards observations, process monitoring and prediction of these variabilites by having optimum combination of observations and numerical models (Detlef and Chassignet, 2000). In the field of Ocean State Forecast, ocean surface winds and waves play a dominant role. The significant impact of ocean surface waves on atmospheric and oceanic circulation has been observed through wave induced stress. Towards the observation of these parameters, various remote sensing instruments have been launched and are also being planned in near future.

India has recently launched its own Scatterometer (Oceansat-2) for global monitoring of Ocean Surface Winds last year. To generate higher resolution information of our coastal and deep ocean regions, a high resolution Synthetic Aperture Radar (SAR), Radar Imaging SATellite (RISAT), is scheduled for next year. Satellite with ARgos and ALtika (SARAL), an ISRO-CNES satellite Altimeter system will be launched sometime next year with ISRO's launch vehicle.

This write-up mainly focuses the studies on physical state of the ocean and efforts being made to derive the surface and deeper layer information about the oceans using spaceborne sensors and utilisation of these data for improved ocean state prediction.

2. Observations Systems: Satellite based ocean observations in combination with numerical models have revolutionised the way of obtaining ocean wave information for operational purposes. Satellite observations are contributing to improve short term wave forecasts through data assimilation in operational numerical models. The two spaceborne systems which are predominantly used for physical oceanographic parameters are satellite radar altimeter and Synthetic Aperture Radar (SAR). Scatterometers are primarily used to retrieve surface winds, the prime source for ocean waves and currents generation.

2.1 Radar Altimeter: The feasibility of measuring ocean wave heights and wind speeds from space was demonstrated more than thirty years ago with the launch of GEOS3 and the SEASAT in 1970s. Since then, algorithms have been refined, and extensively validated against in-situ data. However, the routinely processed data provided by the space agencies have to be carefully quality controlled and calibrated. The other important parameters related to the surface waves are wave period and swell height. Swells are the long period waves generated due to winds, which propagate to the other oceanic regions without the influence of local winds. Since these parameters are not directly available from the satellite data, efforts have been made to derive the swell height and wave period from the satellite altimeter data using different techniques (Jignesh et al, 2005; Remya et al, 2010). The climatology of all these parameters have also been generated using 10 years of Satellite altimeter data, which is useful for offshore engineering as well as ship routing studies (Abhijit Sarkar et al, 1993, Vethamony et al, 1999).

For normal wave heights, all satellite derived calibration relations give almost the same correction, whereas for large wave heights, such as 10 m or so, there may be difference of 0.5m in calibration. This emphasises the importance of validation against large set of in-situ data before extreme wave analysis. Extreme wave analysis is important for offshore industries and ship routing. Probabilistic forecast of extreme waves are being tried using ensemble prediction. Using the TOPEX altimeter data of 10 years, extreme wave analysis has been carried out to predict 50 and 100 years wave heights using distribution function. The results indicate that the wind speed ranges up to 50 m/s, whereas wave height in the Indian Ocean regime could occasionally go beyond 13 meters. It also shows the higher waves in the Arabian Sea region than the Bay of Bengal region. Such an extreme condition could cause serious hazards in the Indian coastal areas. Similar study was also performed using wave model hindcast experiments by forcing the model with atmospheric model winds for 10 years. Both the satellite data and model analysed results show similar trends (Raj Kumar et al, 2009).

One of the major applications of satellite altimeter is to provide sea surface height. Altimeter measures the time taken between pulses sent by the altimeter and returned back from the ocean surface. For derivation of sea surface height (SSH) within a few cms accuracy, accurate measurements of time difference as well as different atmospheric and other sea state corrections are needed. The electro-magnetic (EM) bias correction is believed to be the source of one of the largest uncertainties in altimetric SSH observations. Earlier, EM bias correction algorithms were derived from the altimeter data as a function of wind speed and wave height through variance minimization techniques. The

efforts were made to characterize the impact of such corrections on the altimeter data and compare it with an empirical algorithm based on tower observations of wave slopes and wave age, and with theoretical predictions of EM bias. A significant correlation has been found between high-frequency ocean signals with the TOPEX operational EM bias correction. This suggests that an EM bias algorithm cannot be estimated from altimeter data alone through variance minimization techniques. Since the EM bias depends on parameters that cannot be measured by an altimeter (e.g., wave slope), improved theoretical corrections appear to be preferable to altimetry-based empirical estimates. Using wave buoy and wave model (WAM) data, a good agreement has been found between existing theoretical correction and empirical corrections based on wave slope and wave age information over a significant range of parameters (Raj Kumar et al, 2003).

2.2 Scatterometer: As the winds are major forcing for all ocean models, the accurate observations and prediction of surface winds is quite important. The frequency of spaceborne observations of surface winds had increased tremendously after the availability of Quikscat as well as ASCAT scatterometer data. After the 10 years of regular availability of wind vectors by QuikSCAT, there was a sudden gap due to problem in QuikSCAT. However with the ISRO's launch of Oceansat-2 Scatterometer on September 23, 2009 with repetivity of 2 days and swath of ~1800 km, the surface wind data availability has been continued. The Oceansat-2 scatterometer is a Ku-band pencil beam radar, capable of measuring backscattering coefficients at vertical and horizontal polarizations in swaths of 1800 and 1400 km. Surface Wind Vectors over global oceans are retrieved from backscattering coefficients data The algorithms for monitoring ocean surface wind vector have been developed for Seasat, ERS-1 and Oceansat-2 scatterometers (Gohil & Pandey, 1985; Gohil et al 2008). The near real time, ocean surface winds at 50 x 50 km or better spatial resolution are available using Oceansat-2 scatterometer for major atmospheric and ocean applications. A System Definition study using scattering theory and wave spectrum was also performed to study the sensitivity of ocean radar backscatter for frequency selection of scatterometer (Raj Kumar et al, 1988; Abhijit Sarkar et al, 1986, 1987). At present Calibration and validation exercises for the Oceansat-2 scatterometer are being carried out. The preliminary calibration and validation experiments show that the ocean surface wind data being made available by the Oceansat-2 Scatterometer is well within the mission specifications.

With Scatterometer observations of ocean surface wind vectors over global oceans, the strength and movement of cyclones can be monitored right from early stages of its formation till its landfall. Assimilation of surface wind vectors is known to have significant impact on accuracy of the weather forecast models. The in-house assimilation experiments have shown the positive impact of Oceansat-2 scatterometer on the weather predictions. Winds thus forecast, feed into ocean state forecast models, with which continuous monitoring and prediction of ocean surface waves and circulations, the major applications of Oceansat – 2 Scatterometer are being pursued for improved predictions.

2.3 Synthetic Aperture Radar: A thorough estimate of the sea state is obtained through two dimensional distribution of wave energy in frequency and direction domain. A directional wave spectrum is a compact means of presenting the important physical characteristics of a given wave field. It gives a more complete description of the waves generated at a particular place and time than integrated parameters such as significant wave height and the predominant wave direction. Synthetic Aperture Radar (SAR) onboard satellites such as ERS-1/2, ENVISAT, RADARSAT and forthcoming RISAT are capable to provide higher resolution ocean surface data, on a global and continuous basis, which can be Fourier analysed digitally to provide directional spectra. Various SAR datasets have been analysed using quasi-linear modulation transfer function approach to derive

2-Dimensional ocean wave spectra. For the analysis, the SAR image is divided into frames of smaller sizes and analysis has been performed for each sub area (Raj Kumar et al, 1995). For the precise measurement of ocean wave spectra, scientists have successfully utilised single-look complex images from ENVISAT and RADARSAT to produce cross-spectra among multiple looks and inverted the cross-spectra to get directional spectra (Engen and Johnsen,1995; Johnsen and Desnos,1999).

Coastal bathymetry is one of the most important parameters for the coastal ocean state predictions. In general, the bathymetric feature does not vary much in the rocky ocean bottom regions, however in the area of sandy bottom, the depths vary from season to season and in the harbour area continuous dredging is required to maintain the required depths for ships movements. Accurate measurement of bathymetry can be obtained by ship based hydrographic measurements over the entire area of study, however these are found to be expensive and inadequate. These in-situ measurements can be synergistically complemented with those by remote sensing techniques, which have the advantage of being area-extensive. The spaceborne techniques have limitations of retrieval of depth information only in particular environmental conditions. As the surface waves approach coastal regions, they start influenced by the sea floor approximately at the point where the depth equals half the deep water wavelength. Using refraction process and dispersion relationship, the depths at coastal waters can be estimated with a reasonably good accuracy. Efforts have been made to estimate the depths using ERS-1 SAR images for west and east coastal regions of India (Raj Kumar et al, 1999). The other technique is based on interaction between bottom, currents, surface waves and backscatter interaction. It has been seen that this technique also provides the depth in sandy bottom regions with a very good accuracy in favourable environmental conditions.

Calibrated backscattered values over oceans obtained from SAR images are directly proportional to surface winds. Wind directions can be computed from the peaks in Fourier transformed images. These peaks signify the growth of wind streaks due to roll of atmospheric boundary layer over ocean surfaces (Wackerman et. al., 1996). Once the directions are known, backscattered values can be simulated using specific geophysical model function (CMOD) (Horstmann et. al., 2000). On using these simulated values, the original calibrated SAR images are then inverted utilising a Bayesian approach (popularly known as Maximum Likelihood Estimator, MLE) to produce high resolution wind fields over ocean surfaces. SAR derived winds contain various features which cannot be captured in winds observed by scatterometer because of its poor resolution.

High Resolution SAR images are used to detect ships in open oceans as well as coastal regions. The intensity histograms over background and target (ship) regions show an overlap area for the higher intensity values, signifying possibility of false detection. Such possibilities are minimised for the operational purposes by using a moving window type approach. Within such a window target pixels are isolated from the background by setting a particular threshold (Eldhuset, 1996). In order to automate the system, an adaptive threshold setting is preferred. The isolated ship pixels thus obtained are grouped to identify original ships.

Pollution of the sea surface by mineral or petroleum oil is a major environmental problem. In addition to mineral oil, natural surface film floating on the sea surface, produced by marine plants and oceans (biogenic slicks), refineries, oil terminals, industrial plants, oil platforms and seepage of natural oil from the sea bottom also damp the short gravity-capillary waves. These slicks often make it difficult to decide whether the dark patches are due to the mineral oil spills or from biogenic slicks. To make things even worse, dark patches are also found due to the rain impinging on the sea surface. Synthetic aperture radar data acquired by the ERS, ENVSAT and RADARSAT satellites have been used for obtaining statistical

information on oil pollution. SAR images are very useful in locating the preferred areas where tankers are washed and effluents are discharged. SAR imagery has been successfully adopted in an operational oil spill monitoring in Norway. It can also be used for monitoring oil pollution in coastal waters.

References

[1] Abhijit Sarkar and Raj Kumar, 1986, International Journal of Remote Sensing, 7, 10, 1369-1375.

[2] Abhijit Sarkar, Raj Kumar, R M Gairola, B S Gohil, L V G Rao, P Vethamony, K Santanam, A M Almeida and R Vaithiyanathan, 1993, ISRO Scientific Report.

[3] Alpers W and H E Espedal, 2005, *Oils and Surfactants*, Synthetic Aperture Radar Marine User's Manual, (ed) by C R Jackson, J R Apel, NOAA Chapter 11, 263-275.

[4] Detlef Stammer and E. Chassignet, 2000, Oceanography, Vol. 13, No2, 51-56.

[5] Eldhuset K,1996, IEEE Trans. Geosciences & Remote Sensing, Vol. 34, No 4,July,1996.

[6] Engen G and Johnsen H, 1995, IEEE Trans. Geoscience and Remote Sens, Vol 33 No 4, 1047-1056.

[7] Gohil B S and P C Pandey, 1985, J. Geophysical research, 90(C4), 7307-7311.

[8] Gohil BS, Abhijit Sarkar, Vijay K Agarwal, 2008, IEEE Geosciences and Remote Sensing Letters, Vol. 5, July 2008, 387-391.

[9] Jignesh Kshatriya, Abhijit Sarkar and Raj Kumar, 2005, Marine Geodesy, Vol. 28, No 1, 71-79, 2005.

[10] Janssen P 2004, Cambridge University Press, 300pp.

[11] Johnsen, H. and Desnos, Y.-L., 1999, Proceedings IGARSS '99 , Vol 1, pp 378 – 380. Raj Kumar and Abhijit Sarkar, 1988, ESA SP-284, IEEE88CH2496-6, Published by ESA Publication Division.

[12] Raj Kumar, Abhijit Sarkar and P C Pandey, 1995, Proc. Of the 7th URSI Symposium, pp. 69-72.

[13] Raj Kumar, A Sarkar and P C Pandey, 1999, Continental Shelf Research, Vol. 19, No.2, 171-181.

[14] Raj Kumar, Detlef Stammer, W. Kendall Melville and P Janssen, 2003, Journal of Geophysical Research, Vol. 108, No. C11, 3351.

[15] Raj Kumar, SA Bhowmick, S Ray, V Bhatt, S Surendran, Sujit Basu, A Sarkar and V K Agarwal, 2009, Natural Hazards, Volume 49, Issue 2, 275-291, doi:10.100/s11069-008-9310-y.

[16] Remya G, Raj Kumar, Sujit Basu, and Abhijit Sarkar, 2010, IEEE Geoscience and Remote Sensing Letters, Vol. 8, No. 2 (published online).

[17] Ruchi Kalra, M C Deo, Raj Kumar and V K Agarwal, 2005, Journal of Marine Systems, Vol. 18, 289-300.

[18] Vethamony P, K Sudeesh, B P Kumar, CSR Reddy, LVG Rao, Raj Kumar, A Sarkar, M Mohan and S Karthikeyan, 1999, NIO Report, NIO/TR-3/2000.

[19] C.C. Wackerman, C.L.Rufenach, R.A. Schuman, J.A. Johannessen, K.L. Davidson, IEEE Geosciences & Remote Sensing, Vol. 34, No 6, November,1996.

[20] J. Horstmann, W. Koch, S. Lehner, R. Tonboe, IEEE Geosciences & Remote Sensing, Vol. 38, No 5, September,2000.

[21] Ulaby F T, R K Moore, and A K Fung, 1981,82, 86, Microwave Remote Sensing: Active and Passive, Vol.I, II and III, Artech House, Norwood MA.

Active and Passive Microwave Remote Sensing of Polar Ice

Sandip R. Oza, R. K. K. Singh, N. K. Vyas & Abhijit Sarkar, SAC , Ahmedabad, Email: sandipoza@sac.isro.gov.in

1. Introduction: The Arctic and the Antarctic polar icy regions play a critical role in the Earth's climate system. The polar ice comprises of sea ice, ice sheet, ice-shelf and polynyas. The changes observed in sea ice extent of the polar regions in the recent past are alarming. Sea ice is one of the most varying geophysical features on Earth; it covers 7% of the Earth's surface at the minimum and 13% at the maximum level. Sea ice forms a blanket over polar ocean during winter that melts in summer. During the winter, this blanket acts as a thermal (thermally) insulating barrier between the underlying ocean and the overlying atmosphere. Hence, sea ice is having a profound effect on the oceanic and atmospheric circulations.

The Greenland and the Antarctic ice sheet-ice shelf system is also playing an important role in the climate system. The concept of slow changes in the Antarctic ice sheet predicted by climate models has been challenged by recent observations from satellite (Rignot 2006). Understanding of the mass balance and surface dynamics of the Earth's major ice sheets in Greenland and Antarctica are of fundamental importance in accurate prediction of sea-level rise (Quincey and Lackman 2009). These large scale changes observed over the icy surface of the polar regions demand a constant monitoring and the modelling of ice processes. The present article briefly summarizes the polar ice studies carried out at Space Applications Centre.

2. Assessment of the changes observed in sea ice cover: Since 1978, the space-borne passive microwave data is available for the polar region. These data were extensively used at SAC for sea ice mapping of the Antarctic and the Arctic (Bhandari et al. 2005, Vyas et al., 2003). The Oceansat-1 MSMR multi-frequency passive microwave radiometer derived brightness temperature maps for winter maximum and summer minimum sea ice cover over the Arctic region for the year 2000.

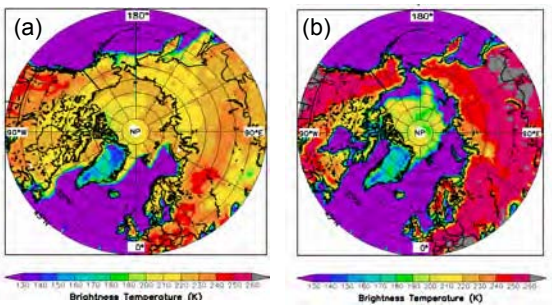

Fig 1: Oceansat-1 MSMR Brightness temperature maps showing (a) winter maximum and (b) summer minimum sea ice cover in the Arctic.

An atlas of Antarctic Sea ice from Oceansat-1 MSMR data (June 1999- September 2001) was also published in 2004 (Vyas et al., 2004). The changes that have taken place over the recent decade, investigated using QuikSCAT scatterometer data are shown in the Figure 2. In the Arctic region, a significant negative trend is observed in sea ice area during summer time, whereas in the Antarctic a mix of positive and negative trend is seen.

The operational data from the QuikSCAT is available only up to November 1999. However, the data from the Oceansat-2 OSCAT Ku-band scatterometer launched by ISRO in September 1999 is providing the Sigma-0 data that has a potential to study the polar ice variations. A preliminary study for the Antarctic region carried out using OSCAT Level2A data (Version 1) is shown in Figure 3. The observed sea ice area is higher in November as compared to February. This is due to the melting of sea ice in the summer period, (mainly during December and January). It is also observed that the sea ice area (observed) in November, that is, the sea ice area that exists at the end of winter, is also significantly reduced from the climatological maximum sea ice extent (1978-2002).

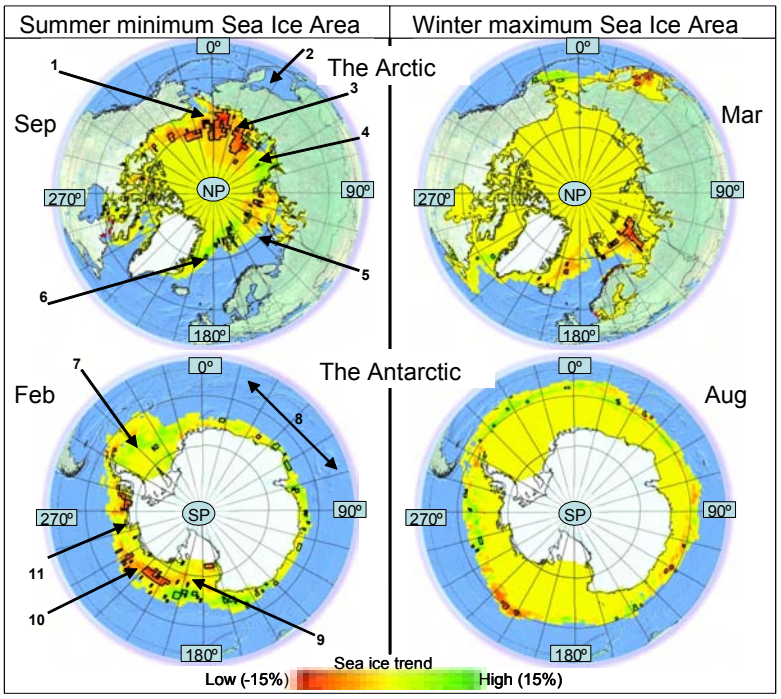

Fig 2: Recent trends in the summer minimum and the winter-maximum sea ice area (1) Chukchi, (2) Okhotsk, (3) East Siberian, (4) Laptev, (5) Barents, (6) East Greenland, (7) Weddell, (8) Indian Ocean sector, (9) Ross, (10) Amundsen, (11) Bellingshausen

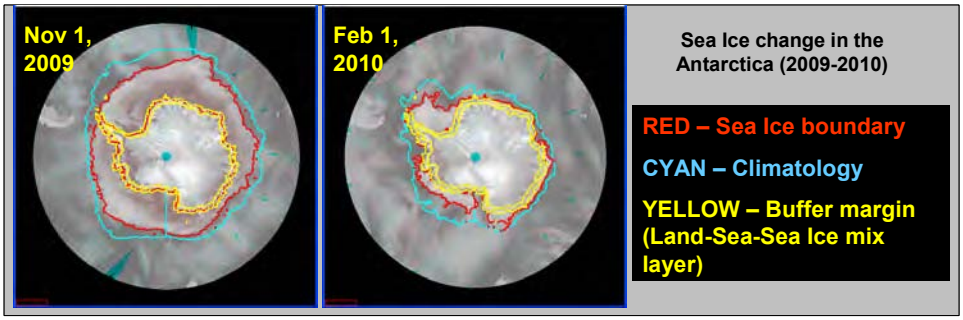

Fig 3: Sea ice cover as observed from Oceansat-2 OSCAT scatterometer data

3. Investigation of surface variations observed over Amery Ice-shelf, East Antarctica: The Amery Ice Shelf is the third largest embayed shelf in Antarctica. Moreover, the Amery Ice Shelf (AIS) is the largest ice shelf within East Antarctica and is near to the proposed site (69.33°-69.50° S, 75.92°-76.50° E) of the third Indian Antarctic station (http://www.ncaor.gov.in). It drains the grounded ice from the interior of the Lambert Glacier drainage basin, which covers 16% mass of the East Antarctic ice sheet and is the world's largest glacier by volume. The geometry of the cavity beneath the AIS is thought to have a strong influence on the thermohaline circulations (Willians *et al* 1998). Longer melt-season and the presence of surface melt ponds on Antarctic ice shelves have been linked to shelf break-up (Scambos *et al* 2000). Thus, monitoring surface melt conditions is critical for evaluating the stability of Antarctic ice shelves (Kunz and Long 2006).

A study of inter-annual variations in surface melting over Amery Ice Shelf, East Antarctica has been recently carried out by Oza et al. (2010) using QuikSCAT scatterometer data (1999-2009). The Sigma-0 values

during summer period show lower values than those during winter due to increase in wetness. This fact has been utilised to derive the Melting Index (MI) as shown in figure 4. The (derived) melting index thus derived has also been compared with the melting index derived by Picard and Fily (2006) using passive microwave radiometer (PMR) data and with the air temperatures recorded by Australian Antarctic Station 'Davis' (http://data.aad.gov.au/aadc) (Figure 3). Picard and Fily (2006) have derived CMS using the PMR data. CMS is defined as the sum over all the pixels of the number of melting days detected during the summer season multiplied by pixel surface area. It is observed that the scatterometer derived MI is highly correlated with the passive microwave derived cumulative melting surface (CMS). The data available from Oceansat-2 OSCAT scatterometer, will provide continuity of QuikSCAT data and generate a long time series for the study of polar sea ice, ice sheet and ice-shelf area.

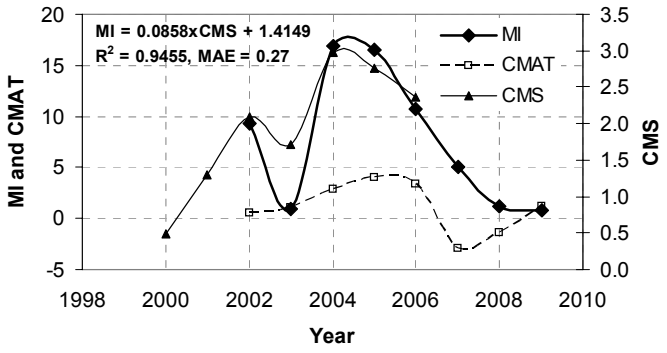

Fig 4: Inter-annual variations of Melting Index (MI), Cumulative Melting Surface (CMS), and Cumulative monthly Mean Air Temperature (CMAT)

References:

[1] Bhandari, S. M., Vyas, N. K., Dash, M., Khanolkar, A., Sharma, N., Khare, N. and Pande, P. C., 2005. Simultaneous MSMR and SSM/I observations and analysis of sea-ice characteristics over the Antarctic region. Int. J. Remote Sens., 26:3123-3136.

[2] Kunz, L. B. and Long., D., 2006. Melt Detection in Antarctic Ice-Shelves using scatterometers and microwave radiometers; *IEEE Trans. on Geosci. and Remote Sensing* **44** 2461-2469.

[3] Oza S. R, Singh R. K. K., Vyas, N. K., and Sarkar, Abhijit, 2010. Study of inter-annual variations in surface melting over Amery Ice Shelf, East Antarctica using space-borne scatterometer data. Journal of Earth System Science (Accepted for the publication).

[4] Picard, C. and Fily, M., 2006. Surface melting observations in Antarctica by microwave radiometers: Corrcting 26-year time series from changes in acquision hours; *Rem. Sensing of Environ.* **104** 325-336.

[5] Quiencey, D. G., and Lackman, A., 2009. Progress in satellite remote sensing of ice sheets. Progress in Physical Geography, 33:547-567.

[6] Rignot, E., 2006. Changes in ice dynamics and mass balance of the Antarctic ice sheet. Phil. Trans. R. Soc. A., 364:1637-1655.

[7] Scambos, T., Hulbe, C., Fahnestock, M. and Bohlander, J., 2000. The link between climate warming and break-up of ice shelves in the Antarctic Peninsula; *J. Glaciol*. **46** 510-530.

[8] Vyas, N. K., Bhanderi, S. M., Dash, M. K., Pandey, P. C., Khare, N., Khanolkar, A. and Sharma, N., 2004. An Atlas of Antarctic Sea Ice from OCEANSAT-1 MSMRSAC-NCAOR-01-2004, National Centre for Antarctic and Ocean Research (DOD), Goa, India.

[9] Vyas, N. K., Dash, M. K., Bhandari, S. M., Khare, N., Mitra, A. and Pande, P. C., 2003. On the secular trend in sea ice extent over the Antarctic region based on OCEANSAT-1 MSMR Observations. Int. J. Remote Sens., 24:2277-2287.

[10] Willians, M. J. M., Jenkins, A. and Determann, J., 1998. Physical control on ocean circulation beneath ice shelves revealed by numerical models. In Jacobs S S and R R Weiss, eds Ocean, ice and atmosphere interactions at the Antarctic continental margin, Antarctic Research Series 75, (Washington DC: American Geophysical Union) pp 285-300.

Chapter News

Glimpses from Environmental Educational Excursion to Udaipur

The Environmental Educational Excursion to Udaipur and Environs jointly organised by Indian Society of Remote Sensing - Ahmedabad Chapter (ISRS-AC), Indian Meteorological Society - Ahmedabad Chapter (IMSA), Indian Society of Geomatics-Ahmedabad Chapter (ISG-AC) and Indian National Cartographic Association-Gujarat Branch (INCA-GB) for their members and their families during Dec 16–18, 2010. Total 83 members including their families participated in the educational excursion. The places of interest visited during the excursion include: City Place, Fateh Sagar, Solar Observatory, Pratap Smarak, Saheliyon ki Bari. Participants trekked to Sajjan Garh, where Geology/Geomorphology of Aravali hill ranges was explained by Shri A.K. Sharma. A space science quiz was also organised for children by Shri K.P. Bharucha. All children participated with great enthusiasm and prizes were distributed to winners.

A Brief Report on 11th Prof. Pisharoty Memorial Lecture by Prof. A K Singhvi, PRL

The 11th lecture in the P.R. Pisharoty Memorial lecture series was delivered by the eminent geologist Prof. A.K. Singhvi, Outstanding Scientist, Physical Research laboratory, Ahmedabad on December 07, 2010. The lecture was titled, '*The Role of Retrospective Science in Planning the Planet's Future*'. In his lecture, Prof. Singhvi talked about important aspects of paleo-science relevant to Indian sub-continent and the new techniques like Luminescence dating as an important tool in paleo-climate studies. The lecture also included new results from recent studies on the erosion of mountains and human impacts thereof and the relevance of retrospective science for future planning of the planet. In his concluding remarks he stressed for a proper institutional framework where such studies can be taken up in a mission mode. He emphasized that remote sensing can play an important role in it. Around 150 participants attended the lecture. Printed lecture notes were distributed to participants. The lecture was well received by the audience. Following are a few glimpses of the 11th P R Pisharoty memorial lecture.

Signing Off

Dear Reader,

We, the Editorial Team, have compiled a series of articles on the chosen theme for this issue from a mix of sensor designers, data processing team and application scientists.

Even though there is a small amount of redundancy of topics covered by several authors, the reported application techniques used are apparently different. The size of the Newsletter has been gradually increasing and is about to hit a century, thanks to all members for their active contributions. In fact, we couldn't include all the articles that were submitted for publication.

Each member of the Editorial Team has contributed in some way or other in bringing out this Issue. We thank all contributing authors, the ISRS-AC office bearers for their support and particularly thank our Secretary Smt. Parul Patel and Chairman **Shri. DRM Samudraiah** for useful suggestions.

We thank those of you who cared to convey your views on our past issue.

Please send in your contributions for future issues and any feedbacks on the current issue to the email: **nandakumar@sac.isro.gov.in.** Theme for the forthcoming issue is listed in page-3 of this issue.

For the Editorial Team,

R. Nandakumar

ISRS

Editorial Team

ISRS-Ahmedabad Chapter
Room No-4372
Space Applications Centre (SAC)
Indian Space Research Organisation (ISRO)
Ahmedabad-380015, Gujarat
Phone: +91 79 2691 4372

R. Nandakumar, SAC
Subodh Kachhela, SAC
Shweta Sharma, SAC
Amit Shukla, SAC
Yogesh Verma, SAC